

INFORMATION TO USERS

This manuscript has been reproduced from the microfilm master. UMI films the text directly from the original or copy submitted. Thus, some thesis and dissertation copies are in typewriter face, while others may be from any type of computer printer.

The quality of this reproduction is dependent upon the quality of the copy submitted. Broken or indistinct print, colored or poor quality illustrations and photographs, print bleedthrough, substandard margins, and improper alignment can adversely affect reproduction.

In the unlikely event that the author did not send UMI a complete manuscript and there are missing pages, these will be noted. Also, if unauthorized copyright material had to be removed, a note will indicate the deletion.

Oversize materials (e.g., maps, drawings, charts) are reproduced by sectioning the original, beginning at the upper left-hand corner and continuing from left to right in equal sections with small overlaps.

Photographs included in the original manuscript have been reproduced xerographically in this copy. Higher quality 6" x 9" black and white photographic prints are available for any photographs or illustrations appearing in this copy for an additional charge. Contact UMI directly to order.

**Bell & Howell Information and Learning
300 North Zeeb Road, Ann Arbor, MI 48106-1346 USA
800-521-0600**

UMI[®]

Novel Tools for Studying Electron Densities:

Investigation and Design of Exchange-Correlation Functionals for Density
Functional Theory

by

S. Kent Worsnop

Submitted in partial fulfilment of the requirements for the degree of
Doctor of Philosophy

at

Dalhousie University

Halifax, NS

October, 1998

©Copyright by S. Kent Worsnop, 1998.



**National Library
of Canada**

**Acquisitions and
Bibliographic Services**

395 Wellington Street
Ottawa ON K1A 0N4
Canada

**Bibliothèque nationale
du Canada**

**Acquisitions et
services bibliographiques**

395, rue Wellington
Ottawa ON K1A 0N4
Canada

Your file Votre référence

Our file Notre référence

The author has granted a non-exclusive licence allowing the National Library of Canada to reproduce, loan, distribute or sell copies of this thesis in microform, paper or electronic formats.

The author retains ownership of the copyright in this thesis. Neither the thesis nor substantial extracts from it may be printed or otherwise reproduced without the author's permission.

L'auteur a accordé une licence non exclusive permettant à la Bibliothèque nationale du Canada de reproduire, prêter, distribuer ou vendre des copies de cette thèse sous la forme de microfiche/film, de reproduction sur papier ou sur format électronique.

L'auteur conserve la propriété du droit d'auteur qui protège cette thèse. Ni la thèse ni des extraits substantiels de celle-ci ne doivent être imprimés ou autrement reproduits sans son autorisation.

0-612-49300-8

Canada

DALHOUSIE UNIVERSITY

FACULTY OF GRADUATE STUDIES

The undersigned hereby certify that they have read and recommend to the Faculty of Graduate Studies for acceptance a thesis entitled "Novel Tools for Studying Electron Densities: Investigation and Design of Exchange-Correlation Functionals for Density Functional Theory"

by Stephen Kent Worsnop

in partial fulfillment of the requirements for the degree of Doctor of Philosophy.

Dated: December 7, 1998

External Examiner
Research Supervisor
Examining Committee



DALHOUSIE UNIVERSITY

Date: December 16, 1998

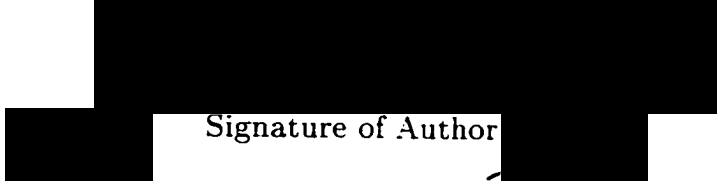
Author: S. Kent Worsnop

Title: Novel Tools for Studying Electron Densities:
Investigation and Design of Exchange-Correlation Functionals
for Density Functional Theory

Department or School: Department of Chemistry

Degree: Ph. D. Convocation: May Year: 1999

Permission is herewith granted to Dalhousie University to circulate and to have copied for non-commercial purposes, at its discretion, the above title upon the request of individuals or institutions.

 Signature of Author

The author reserves other publication rights, and neither the thesis nor extensive extracts from it may be printed or otherwise reproduced without the author's written permission.

The author attests that permission has been obtained for the use of any copyrighted material appearing in this thesis (other than brief excerpts requiring only proper acknowledgement in scholarly writing), and that all such use is clearly acknowledged.

*To John and Meghan my mentors and my guardians.
To Mom and Dad my supporters and my inspiration.
To Renéé my love and my life.*

Contents

List of Figures	x
List of Tables	xii
Abstract	xiii
List of Abbreviations	xiv
List of Symbols	xvi
Acknowledgements	xix
1. Introduction	1
2. Theoretical Background	5
2.1 Schrödinger Equation	5
2.2 Born-Oppenheimer Approximation	7
2.3 The Independent Particle Model (Hartree-Fock (HF) Theory)	8
2.4 Basis Sets	12
2.5 Correlation Energy	14
2.5.1 Configuration Interaction (CI) Method	16
2.5.2 Many-Body Perturbation Theory (MBPT)	18
2.5.3 The Coupled Cluster Approximation	20
2.5.4 Quadratic Configuration Interaction	21
2.6 Density Functional Theory	21
2.7 The Exchange-Correlation Energy Functional	25

2.7.1	The Local (Spin) Density Approximation	26
2.7.2	The Exchange-Correlation Hole	28
2.7.3	Post Local Spin Density Approximation	31
3.	Comparison of Electron Densities	43
3.1	Obtaining Electron Densities from Wavefunctions	44
3.2	Density Difference Plots	45
3.2.1	An Illustrative Example: Density Difference Plots for C_2H_n , n=2,4,6 and C_6H_6	46
3.3	Expanding on the Density Difference Plot: Reoptimising the Becke Three-Parameter Expression	58
3.4	Results and Discussion	60
3.5	Conclusions	64
4.	An Orbital-Based Density Difference Index	68
4.1	Orbital-Based Density Difference Index	69
4.2	Computational Details	72
4.3	Results and Discussion	73
4.4	Conclusions	82
5.	A Spin-Polarisation Index	87
5.1	Spin-Density Polarisation Index	88
5.2	Computational Details	90
5.3	Results and Discussion	91
5.4	Conclusions	105

6. Radial Moments of the Electron Density	110
6.1 Analytical Calculation of the Radial Moments of the Electron Density	112
6.2 Computational Details	116
6.3 Results and Discussion	118
6.4 The Effects of Solvation on the Radial Moments of the Density	131
6.5 Conclusions	141
7. Reoptimisation of the Becke Three-Parameter Hybrid Functional	146
7.1 Details of Optimisation	147
7.2 Results and Discussion	149
7.3 Conclusion	165
8. Conclusion and Future Work	169

List of Figures

2.1	Enhancement factors for the LSDA	35
2.2	Enhancement factors for LGC	36
2.3	Enhancement factors for BP86	37
3.1	QCISD-BLYP density difference plots for C ₂ H ₂ (a), C ₂ H ₄ (b), C ₆ H ₆ (c) and C ₂ H ₆ (d).	48
3.2	QCISD-BP86 density difference plots for C ₂ H ₂ (a), C ₂ H ₄ (b), C ₆ H ₆ (c) and C ₂ H ₆ (d).	49
3.3	QCISD-SVWN density difference plots for C ₂ H ₂ (a), C ₂ H ₄ (b), C ₆ H ₆ (c) and C ₂ H ₆ (d).	50
3.4	QCISD-B3LYP density difference plots for C ₂ H ₂ (a), C ₂ H ₄ (b), C ₆ H ₆ (c) and C ₂ H ₆ (d).	53
3.5	QCISD-B3P86 density difference plots for C ₂ H ₂ (a), C ₂ H ₄ (b), C ₆ H ₆ (c) and C ₂ H ₆ (d).	54
3.6	QCISD-HF density difference plots for C ₂ H ₂ (a), C ₂ H ₄ (b), C ₆ H ₆ (c) and C ₂ H ₆ (d).	56
3.7	QCISD-MP2 density difference plots for C ₂ H ₂ (a), C ₂ H ₄ (b), C ₆ H ₆ (c) and C ₂ H ₆ (d).	57
3.8	QCISD-B3P86 density difference plots for HF.	62
3.9	QCISD-new hybrid functional density difference plots for HF.	63
4.1	Functional and basis set dependence of QCISD-DFT DDIs for H ₂ : ● 6-31++G**, ■ aug-CC-PVDZ, and ▲ aug-CC-PVTZ.	75

4.2	Functional dependence of the QCISD-DFT DDIs obtained with the aug-CC-PVDZ basis set: ● N ₂ , ▲ O ₂ , and ■ F ₂	76
4.3	Functional and basis set dependence of MP2-DFT DDIs for H ₂ : ● 6-31++G**, ■ aug-CC-PVDZ, and ▲ aug-CC-PVTZ.	77
4.4	Functional dependence of the MP2-DFT DDIs obtained with the aug-CC-PVDZ basis set: ● N ₂ , ■ O ₂ , and ▲ F ₂	79
5.1	Plot of the radial distribution of the spherically averaged spin-density difference for wave function based methods using the aug-CC-PVDZ basis set for O ₂	95
5.2	Plot of the radial distribution of the spherically averaged spin-density difference for DFT based methods using the aug-CC-PVDZ basis set for O ₂	96
5.3	Graph of the spherically averaged QCISD densities using the aug-CC-PVDZ basis set for O ₂	98
5.4	Plot of the spherically averaged β densities for the wave function based methods using the aug-CC-PVDZ basis set for O ₂	99
5.5	Plot of the spherically averaged β densities for the DFT based methods using the aug-CC-PVDZ basis set for O ₂	101
5.6	Plot of the spherically averaged β density calculated with the Hartree-Fock method using a variety of basis sets for O ₂	102
6.1	The effect of additional polarisation functions for N ₂ using both the QCISD and MP2 methods. (● MP2 with the 6-311G basis set, ■ MP2 with the 6-311+G basis set, ○ QCISD with the 6-311G basis set and □ QCISD with the 6-311+G basis set)	121

6.2	The effect of additional polarisation functions for H ₂ O using both the QCISD and MP2 methods. (● MP2 with the 6-311G basis set, ■ MP2 with the 6-311+G basis set, ○ QCISD with the 6-311G basis set and □ QCISD with the 6-311+G basis set)	122
7.1	Density difference plot for BeH. a) MP2-B3PW91 and MP2-B3P[MP2] b) QCISD-B3PW91 and QCISD-B3P[QCI]	152
7.2	Density difference plot for LiH. a) MP2-B3PW91 and MP2-B3P[MP2] b) QCISD-B3PW91 and QCISD-B3P[QCI]	153
7.3	Density difference plot for CO. a) MP2-B3PW91 and MP2-B3P[MP2] b) QCISD-B3PW91 and QCISD-B3P[QCI]	154
7.4	Density difference plot for CO ₂ . a) MP2-B3PW91 and MP2-B3P[MP2] b) QCISD-B3PW91 and QCISD-B3P[QCI]	156
7.5	Density difference plot for HCN. a) MP2-B3PW91 and MP2-B3P[MP2] b) QCISD-B3PW91 and QCISD-B3P[QCI]	157
7.6	Density difference plot for C ₂ H ₂ . a) MP2-B3PW91 and MP2-B3P[MP2] b) QCISD-B3PW91 and QCISD-B3P[QCI]	158
7.7	Density difference plot for C ₂ H ₄ . a) MP2-B3PW91 and MP2-B3P[MP2] b) QCISD-B3PW91 and QCISD-B3P[QCI]	159

List of Tables

3.1	Optimised parameters for H ₂ , N ₂ , O ₂ , F ₂ , CO and HF.	60
3.2	Comparison of results obtained using optimised values of <i>A</i> , <i>B</i> and <i>C</i> with B3P86, QCISD and experimental results.	61
3.3	Comparison of total energies calculated at the experimental geometries.	64
4.1	QCISD-DFT values for the density difference index.	74
4.2	MP2-DFT values for the density difference index.	78
4.3	Values for the density difference index for a variety of molecules using the aug-CC-PVDZ basis set.	81
4.4	Values for the density difference index for C ₂ H _{<i>n</i>} , <i>n</i> = 2, 4, 6 using the aug-CC-PVDZ basis set and C ₆ H ₆ using the CC-PVDZ basis set. . .	82
5.1	Spin-density polarisation index values for ³ Σ ⁻ O ₂	93
5.2	Atomisation energies (in a.u.) for O ₂ using the aug-CC-PVDZ basis set	97
5.3	Spin density polarisation index values for selected molecules calculated by use of the aug-CC-PVDZ basis set	100
5.4	<i>Z</i> values for selected molecules calculated by use of the aug-CC-PVDZ basis set	104
6.1	Radial moments of the electron density for N ₂ and H ₂ O calculated using the MP2 and QCISD methods with a variety of basis sets. . . .	118
6.2	Radial moments of the density calculated at the centre of mass using the 6-311G(2df,p) basis set and a variety of methods.	124

6.3	The difference between the solvated and gas phase r^{-1} and r moments as calculated at the centre of mass using the 6-311G(2df,p) basis set and the Onsager solvation model.	132
6.4	The difference between the solvated and gas phase r^2 and r^3 moments as calculated at the centre of mass using the 6-311G(2df,p) basis set and the Onsager solvation model.	134
6.5	The difference between the solvated and gas phase r^{-1} and r moments as calculated at the centre of mass using the 6-311G(2df,p) basis set and the SCI-PCM solvation model.	137
6.6	The difference between the solvated and gas phase r^2 and r^3 moments as calculated at the centre of mass using the 6-311G(2df,p) basis set and the SCI-PCM solvation model.	139
7.1	The DDI/electron for all molecules given by B3PW91 and the optimised functionals and the differences between these two values.	149
7.2	Comparison of molecular properties for fourteen different molecules.	160
7.3	Calculated geometric parameters and frequencies. Bond lengths are in Å and frequencies are in cm^{-1}	163
7.4	Mean of the absolute differences between DFT and high-level <i>ab initio</i> or experimental geometric parameters. Maximum absolute differences are given in the brackets.	164
7.5	Calculated SPIs for molecules in doublet or triplet states.	165

Abstract

The accuracy of electron densities calculated using density functional theory (DFT) is assessed by comparison with results obtained from conventional *ab initio* methods based upon the Hartree-Fock (HF) ground state wavefunction. To simplify the comparisons new methods are introduced and are combined with other established tools. The information gained with these various methods is then used to determine parameters for two hybrid functionals.

Previously density difference plots have given good qualitative results for many molecules. An example of this method, with plots for C_2H_n , $n=2,4,6$ and C_6H_6 , assesses the accuracy of a few DFT functionals. Generally all functionals are reasonably accurate but also show some large differences when compared to conventional *ab initio* densities. To improve upon these results the parameters of a new hybrid functional are optimised using a method inspired by the density difference plots. This functional exhibits some encouraging results but also shows many problems.

The problems involved with the optimisation of the new functional lead to the development of the density difference index (DDI) to facilitate the comparison of two electron densities. Results indicate that the DDI yields a semi-quantitative measure of the distance between two electron densities. Also, the DDI values reveal a qualitative difference between DFT and conventional *ab initio* electron densities.

The spin polarisation index (SPI) extends the results obtained by the DDI by quantitatively comparing the α and β electron densities in open-shell species. Generally the SPIs calculated with DFT are quite similar to conventional *ab initio* results. A few exceptions are found, though, where DFT substantially underestimates the SPI.

The radial moments of the electron density are related to many different molecular properties and can be determined experimentally while also giving information on the spatial properties of different electron densities. Using a new analytical method for calculating these moments it is found that the DFT moments compare well with both experimental and QCISD results. The solvation effects for all methods are generally quite similar and there is evidence of rearrangement of the electron distributions upon dissolution.

The results of the investigations of DFT electron densities indicate that improvements can be made. A reoptimisation of the parameters from Becke's three-parameter hybrid functional is carried out to improve the calculated electron density. The optimised parameters are found by fitting the DFT electron densities to MP2 and QCISD densities using the DDI. A selection of molecular properties, including the radial moments of the electron density and the SPIs of some open-shell species, calculated using the new functionals are compared to conventional *ab initio* results with only fair results. However, there are indications that the electron densities of the new functionals gave a reasonable approximation of the two reference electron densities.

List of Abbreviations

AO	atomic orbital
Bx ¹	Becke's 1988 gradient-corrected exchange functional
B3x ¹	Becke's three-parameter hybrid functional
CC, CCD	coupled cluster (including double excitations only)
CI, CISD	configuration interaction (including single and double excitations only)
DDI	density difference index
DFT	density functional theory
DZ	double zeta
G2	Gaussian 2
GGA	generalised-gradient approximation
GTO	Gaussian-type orbital
HF	Hartree-Fock
LDA, LSDA	local (spin) density approximation
xLYP ¹	Lee, Yang and Parr's gradient-corrected correlation functional
MBPT	many-body perturbation theory
MO	molecular orbital
MPn	nth order Møller-Plesset perturbation theory
xP86 ¹	Perdew's 1986 gradient-corrected correlation functional

¹ x is used as a placeholder. In the hybrid functional and gradient-corrected exchange functional x represents the correlation functional used while in for the gradient-corrected correlation functionals x represents the exchange functional used.

xPW91 ¹	Perdew and Wang's 1991 gradient-corrected correlation functional
QCI, QCISD	quadratic configuration interaction (including single and double excitations only)
QMSM	quantum molecular similarity measure
RHF, ROHF	restricted (open-shell) Hartree-Fock
SPI	spin polarisation index
STO	Slater-type orbital
SVWN	the local spin density approximation using Vosko, Wilk and Nusair's parameterisation of the correlation functional
TZ	triple zeta
UHF	unrestricted Hartree-Fock

List of Symbols

Ψ	determinantal wavefunction
ψ_i	molecular orbital
ϕ_μ	atomic orbital
χ_i	Kohn-Sham orbital
\hat{H}	Hamiltonian operator
\hat{T}	kinetic energy operator
\hat{V}	potential energy operator
$\mathbf{S}, S_{\mu\nu}$	overlap matrix (element)
$\mathbf{F}, F_{\mu\nu}$	Fock matrix (element)
$\mathbf{P}, P_{\mu\nu}$	density matrix (element)
$h(i)$	one-electron Hamiltonian operator
δ_{ij}	Kronecker delta
$(\mu\nu \gamma\lambda)$	two-electron integral
ϵ_a	molecular orbital energy
α	alpha electron
β	beta electron
T	excitation operator

$E[\rho]$	energy functional
$T[\rho]$	kinetic energy functional
$V_{ee}[\rho]$	interelectronic potential energy functional
$J[\rho]$	Coulomb repulsion energy functional
$E_{xc}[\rho]$	exchange-correlation energy functional
$v(\mathbf{r})$	external potential
$v_{xc}(\mathbf{r})$	exchange-correlation potential
ϵ_{xc}	exchange-correlation energy per particle
ϵ_x	exchange energy per particle
ϵ_c	correlation energy per particle
$\rho(\mathbf{r})$	electron density
$\rho_1(\mathbf{r}; \mathbf{r}')$	single-particle electron density
$\rho_2(\mathbf{r}; \mathbf{r}')$	diagonal elements of second-order density matrix
n_{xc}	exchange-correlation hole
$F_{xc}(r_s, s)$	exchange-correlation enhancement factor
T_s	kinetic energy of the Kohn-Sham non-interacting reference density
$\langle S^2 \rangle$	expectation value of the square of the spin operator
$\langle r^n \rangle$	n^{th} radial moment of the electron density

Acknowledgements

The research presented in this thesis was completed under the supervision of Dr. Russell J. Boyd, who, throughout my four years at Dalhousie, has assisted and helped to guide my work. Also, special thanks go to Drs. Jesus Ugalde, Cecilia Sarasola and Jiahu Wang whose ideas have influenced and shaped my work.

I would also like to thank Drs. Jesus Ugalde and Cecilia Sarasola for the use of their computational programs and for their hospitality during my stay in Spain. Without them I would not have had the chance to share in another culture or have gained the experience of working with another research group.

The many members of Dr. Boyd's group have been a pillar of strength during my studies. In particular, I would like to thank Dr. George Heard for his input and generosity and for afternoon frolics to the Graduate House. Also I would like to thank Stacey Wetmore and Jian Wang, especially, who have been of great support throughout my work. Finally, I wish to thank the other members of the group throughout the years, Jaime Martell, Mimi Lam, Jing Kong, Nelaine Mora-Diaz, Fuqiang Ban and the person who helped to addict me to coffee Kathryn Rankin, for their ideas and friendship.

It would have been impossible for this work to have been completed without support from those inside and outside of the department. First I would like to thank Dr. Charles Warren, Mr. Chris Wright and Mrs. Adele Evans for all of their input and help whenever a problem occurred with one of the computers. I am also grateful to Ms. Sharon Barkhouse for many discussions about teaching within the first year laboratories.

A Dalhousie graduate fellowship and Sumner awards are acknowledged for their financial support of my work.

The role of my family has been one of support and encouragement. I thank my father and mother, who have always been there for me, and my brother and my sister who have helped me to stay grounded. Finally, sincere thanks to Renée Masching whose support has helped me through many tough times and whose love has been a beacon during some of the darkest nights.

1. Introduction

Advances in both theoretical techniques and computer hardware have increased the influence of quantum chemical calculations on chemical research. Many of the improved techniques, though, are very costly in terms of calculation time and hardware storage and a highly accurate calculation on systems with only five to ten non-hydrogen atoms can tax even today's resources. This has limited the chemical systems which can be effectively studied using these techniques. With the advent of density functional theory (DFT)^{1,2} many of these restrictions are relieved and the efficiency of DFT has allowed calculations on much larger systems with reasonably accurate results.

The accuracy of DFT calculations is wholly dependent upon the calculated densities which are in turn dependent on the approximate exchange-correlation functionals used within the Kohn-Sham equations.² Many different methods have been used in the design of these functionals with mixed results³ and today many more methods are being investigated. The design and assessment of these new functionals has usually been dependent upon comparing calculated molecular properties with known accurate values. This procedure, though, is limited since the molecular properties can only give an indirect measurement of the accuracy of the electron density. A more appealing method for design and assessment of exchange-correlation functionals is

through the direct comparison of electron densities.

This work focusses upon the comparison of electron densities to reveal the similarities and dissimilarities between densities calculated with various methods. The results from these comparisons are then used to design a new functional to try and yield more accurate DFT electron densities. However, before this can be accomplished a brief outline of the computational methods used throughout this work will be presented in chapter 2. Short explanations of conventional *ab initio* methods are given first followed by a more in-depth analysis of DFT. The DFT section's main focus is upon the relationship of the exchange-correlation functional within DFT and the design of some of the more popular functionals.

The tools used in this thesis to compare electron densities are presented in the following four chapters. Chapter 3 presents the density difference plot which has been used previously to compare different electron densities.⁴⁻⁶ The usefulness of this technique is explained through an illustrative example with encouraging results. The focus of this chapter then shifts to modifying the density difference plots to yield quantitative results. These values are then used in a preliminary study in the design of a new functional with poor results.

The tools presented in chapter 4 and 5 were developed to try and give better quantitative results when comparing electron densities. The density difference index (DDI), in chapter 4, gives a direct comparison between DFT electron densities and electron densities from methods known to be accurate. Results from a series of small molecules confirm that DFT gives reasonably accurate results and some connections are made with the density difference plots of chapter 3. The second tool, the spin polarisation index (SPI), compares the α and β electron densities in open-shell species. Again the results from various molecules are given with some interesting conclusions.

The investigation of the spin polarisations given in chapter 5 also lead to some interesting observations about the radially averaged α and β electron densities of O_2 .

The radial moments of the electron density can yield spatial information about electron densities and can also be determined experimentally. Although these characteristics make the moments a good tool for comparison of densities, little work has been done on them lately. Chapter 6 presents a relatively new analytical method for calculating the radial moments of the electron density and then gives comparisons with various molecules. Also presented is a study on the effects of solvation upon the calculation of the radial moments.

Although the establishment of these methods has revealed much about DFT electron densities, methods must be developed so that they can be used in the design of functionals. Chapter 7 reinvestigates the simple method of optimising functional parameters. Again a direct comparison of electron densities will be used to optimised the parameters, however, this time this will be accomplished through the use of the DDI. The results of this optimisation are presented through various methods comparing the new functional with one that is already well established. This is only one avenue for using these new tools and after giving global conclusions the final chapter presents some other avenues for the use of the tools presented in this thesis.

References

- [1] P. Hohenberg and W. Kohn, *Phys. Rev.* **136**, 864 (1964).
- [2] W. Kohn and L. J. Sham, *Phys. Rev.* **140**, A1133 (1965).
- [3] J. M. Seminario and P. Politzer, editors, *Modern Density Functional Theory: A Tool for Chemistry*, Elsevier, 1995.

-
- [4] J. Wang, L. A. Eriksson, B. G. Johnson, and R. J. Boyd, *J. Phys. Chem.* **100**, 5274 (1996).
- [5] J. Wang, B. G. Johnson, R. J. Boyd, and L. A. Eriksson, *J. Phys. Chem.* **100**, 6317 (1996).
- [6] J. Wang, Z. Shi, R. J. Boyd, and C. A. Gonzalez, *J. Phys. Chem.* **98**, 6988 (1994).

2. Theoretical Background

Theoretical chemistry was set in motion many years ago with the introduction of Niels Bohr's model of the atom and was the foundation for the many theories of today. Like all aspects of science, though, theoretical chemistry has advanced; from Bohr's model of the atom to Erwin Schrödinger's equation and beyond. One must have a thorough understanding of these fundamental tools which have been developed before being able to advance in theoretical chemistry.

2.1 Schrödinger Equation

The most fundamental theory of quantum chemistry is that a stationary state of a molecule can be described by a wavefunction, Ψ , which contains both the spin and spatial variables and satisfies the time-independent Schrödinger equation,¹

$$\hat{H}\Psi = E\Psi. \tag{2.1}$$

Here \hat{H} is the Hamiltonian operator, and E is the energy corresponding to the stationary state. The wavefunction found from the solution of this equation contains all information about the stationary state. This allows for the calculation of any

observable quantity of the state such as the probability distribution of the electrons, $|\Psi|^2$, also known as the electron density.

Examining the equation more closely reveals that the Hamiltonian operator for nonrelativistic systems can be expressed as the sum of two operators, the kinetic and potential energy operators,

$$\hat{H} = \hat{T} + \hat{V} \quad (2.2)$$

The kinetic energy operator is given by the expression,

$$\hat{T} = - \sum_i \frac{h^2}{8\pi^2 m_i} \nabla_i^2 \quad (2.3)$$

while the potential energy operator is of the form,

$$\hat{V} = \sum_{i < j} \frac{Q_i Q_j e'^2}{r_{ij}} \quad (2.4)$$

The sums given are over all particles, nuclei and electrons, m_i is the mass of particle i , h is Planck's constant, $e' = e/\sqrt{4\pi\epsilon_0}$ and r_{ij} is the distance between particles i and j . The values of Q_i and Q_j vary with the type of particle. $Q_i = -1$ if the particle is an electron and $Q_i = Z_i$ for a nucleus with atomic number Z_i .

Although, in theory the Schrödinger equation yields the exact wavefunction of a stationary state, in practice it is found that for almost all systems the equation is insoluble. Consequently theoretical chemists have had to devise a series of approximations which allow for the solution of the equation.

2.2 Born-Oppenheimer Approximation

The Born-Oppenheimer approximation^{1,2} is one of the most common approximations used to simplify the solution of the Schrödinger equation. Born and Oppenheimer postulated that considering the mass of a nucleus is on the order of 10 000 times heavier than that of the electron the mass of the nucleus can be assumed to be infinite. This means that the nuclear kinetic terms in equation 2.2 can be neglected and the internuclear repulsion, V_{NN} , can be treated as a constant.

To show the effect of this approximation on \hat{H} the atomic units, used throughout this thesis, must first be defined. The unit for length is given by the Bohr radius, a_o , which is,

$$a_o = \frac{\hbar^2}{4\pi^2 m e^2} \quad (2.5)$$

while the unit of energy, the hartree, is given by

$$E_H = \frac{e^2}{a_o} \quad (2.6)$$

These definitions allows the terms in \hat{H} to be gathered into the electronic Hamiltonian using one- and two-electron terms,

$$\hat{H}_{elec} = \sum_{i=1}^N h(i) + v(r_{ij}) \quad (2.7)$$

where N is the number of electrons in the system. The one-electron Hamiltonian, $h(i)$, is defined as,

$$h(i) = -\frac{1}{2} \nabla_i^2 - \sum_{A=1}^M \frac{Z_A}{r_{iA}} \quad (2.8)$$

whereas the two-electron potential term $v(r_{ij})$ is defined as,

$$v(r_{ij}) = \frac{1}{2} \sum_{i=1}^N \sum_{j \neq i}^N \frac{1}{r_{ij}} \quad (2.9)$$

The corresponding electronic Schrödinger equation,

$$\hat{H}_{elec} \Psi_n = E_n \Psi_n \quad (2.10)$$

with,

$$\langle \Psi_n | \Psi_m \rangle = \delta_{nm} \quad (2.11)$$

defines the potential energy hypersurfaces that govern the dynamics of nuclear motion within the Born-Oppenheimer approximation. The total energy for fixed nuclei can then be expressed as,

$$E(R) = E_n(R) + \sum_{A < B} \frac{Q_A Q_B}{R_{AB}} \quad (2.12)$$

This approximation usually gives satisfactory results for the ground states of neutral molecules but there are some practical limitations to this approximation which have been exposed through various spectroscopic experiments.³ Also its failure in the excited electronic states of polyatomic molecules and ions is common and new theoretical methods are needed to deal with this and other problems.⁴

2.3 The Independent Particle Model (Hartree-Fock (HF) Theory)

Even though the Hamiltonian has been simplified through the use of the Born-Oppenheimer approximation the Schrödinger equation is still not separable. This is due to the presence of the Coulomb repulsion between two electrons, represented by the $\frac{1}{r_{ij}}$ term in the Hamiltonian. The introduction of one-electron wavefunctions,

also called molecular orbitals (MOs), allows for the handling of these interelectronic repulsion terms. Using MOs allows each electron to be treated separately and the dynamics of the electron can be thought of being that of a free electron moving over the whole molecule in some appropriate 'effective' potential field.^{1,2}

One way to express the wavefunction Ψ , in terms of MOs is by simply multiplying all the occupied MOs together. However, in 1930 Slater noted that since electrons are fermions with spin $\frac{1}{2}$ the overall molecular wavefunction would have to be antisymmetric. Unfortunately the basic product of MOs does not produce an antisymmetric wavefunction thus to keep the wavefunction antisymmetric it should be written as the normalised determinant,

$$\Psi(x_1, x_2, \dots, x_N) = (N!)^{-\frac{1}{2}} \det|\psi_1(x_1)\psi_2(x_2) \cdots \psi_N(x_N)| \quad (2.13)$$

where x_i includes both the spatial and spin coordinates for electron i and $\psi_i(x_i)$ is the i th occupied MO.

Usually a linear combination of atomic orbitals (LCAO), $\sum_{\mu=1}^n \phi_{\mu}$, centred at each atom is used to expand the MO such that,

$$\psi_i = \sum_{\nu=1}^n c_{\nu i} \phi_{\nu} \quad (2.14)$$

The calculation of the coefficients, $c_{\nu i}$, is accomplished using a self consistent set of equations known as the Hartree-Fock-Roothaan (HFR) equations:

$$\sum_{\nu=1}^n c_{\nu i} (F_{\mu\nu} - \epsilon_i S_{\mu\nu}) = 0 \quad \mu = 1, 2, \dots, n \quad (2.15)$$

where the $F_{\mu\nu}$ are the elements of the Fock matrix obtained using the expression,

$$F_{\mu\nu} = H_{\mu\nu} + \sum_{\gamma} \sum_{\lambda} P_{\gamma\lambda} [(\mu\nu|\gamma\lambda) - \frac{1}{2}(\mu\gamma|\nu\lambda)] \quad (2.16)$$

and the $S_{\mu\nu}$ are the overlap matrix elements given by,

$$S_{\mu\nu} = \int \phi_{\mu}^* \phi_{\nu} d\tau \quad (2.17)$$

The evaluation of the Fock matrix depends on three mathematical objects the Hamiltonian matrix, \mathbf{H} , the density matrix, \mathbf{P} , and the two-electron integrals, $(\mu\nu|\gamma\lambda)$. The Hamiltonian matrix is made up of the single electron integrals,

$$H_{\mu\nu} = \int \phi_{\mu}^*(1) \left(-\frac{1}{2} \nabla^2 - \sum_A \frac{Z_A}{R_{1A}} \right) \phi_{\nu}(1) d\tau_1 \quad (2.18)$$

while the density matrix is defined as,

$$P_{\gamma\lambda} = 2 \sum_{i=1}^{occ} c_{\gamma i} c_{\lambda i} \quad (2.19)$$

and the two-electron integrals are given by,

$$(\mu\nu|\gamma\lambda) = \int \int \phi_{\mu}^*(1) \phi_{\nu}(1) \frac{1}{r_{12}} \phi_{\gamma}^*(2) \phi_{\lambda}(2) d\tau_1 d\tau_2 \quad (2.20)$$

From this it is apparent that to calculate \mathbf{P} the atomic orbital coefficients, $c_{\gamma i}$, must be known. This means that prior knowledge of the values of the coefficients is needed to solve for the MO energies, ϵ_{ν} and vice versa. Thus to solve the HFR equations an iterative approach is taken with an initial guess for the atomic orbital coefficients.

The most time consuming part of the solution of the HFR equations is the cal-

calculation of the two-electron integrals. This time can be easily reduced if the inherent symmetry of the two-electron integrals is accounted for. It can easily be shown that for complex one-electron functions,⁵

$$(\mu\nu|\gamma\lambda) = (\gamma\lambda|\mu\nu) = (\nu\mu|\lambda\gamma) = (\lambda\gamma|\nu\mu) \quad (2.21)$$

while for one-electron functions that are real there are further symmetries,

$$(\mu\nu|\gamma\lambda) = (\mu\nu|\lambda\gamma) = (\nu\mu|\gamma\lambda) = (\nu\mu|\lambda\gamma) = (\gamma\lambda|\mu\nu) = (\gamma\lambda|\nu\mu) = (\lambda\gamma|\mu\nu) = (\lambda\gamma|\nu\mu) \quad (2.22)$$

From these expressions the ground state energy of the system can be calculated easily. From the HFR equations above the calculated MO energy is,

$$\epsilon_a = \langle \psi_a | h(1) | \psi_a \rangle + \sum_b^N (aa|bb) - (ab|ba) \quad (2.23)$$

Using this expression in the Schrödinger equation then gives the Hartree-Fock energy as,

$$E_{HF} = 2 \sum_{a=1}^{\frac{N}{2}} \epsilon_a - \sum_{a,b=1}^{\frac{N}{2}} [(aa|bb) - (ab|ba)] + V_{N,N} \quad (2.24)$$

for a system of doubly occupied MOs, also referred to as a ‘closed shell’ system.

A single Slater determinant of doubly occupied MOs represents this singlet ground state quite well. Problems can arise, though, with this model when the spin multiplicity is greater than 1, also known as open-shell states. Many different ways have been used to help deal with these open-shell states. Two of these will be described below.

The restricted Hartree-Fock (RHF) approximation is used on a state with multiplicity $(p - q + 1)$, where p and q are the number of electrons with α and β spin

respectively and $p > q$. The wavefunction used is given by:

$$\Psi_{RHF}(1, 2, \dots, n) = \det|\psi_1(1)\alpha(1)\psi_1(2)\beta(2)\dots$$

$$\psi_q(2q)\alpha(2q)\psi_q(2q+1)\beta(2q+1)\dots\psi_{p+q}\alpha(p+q)| \quad (2.25)$$

The assumption of the equivalence of the spatial functions in the RHF method is not reasonable since there are an unequal number of open shells with β spin than with α spin. A more general approximation, which does not assume the equivalence of the spatial functions, is represented in the unrestricted Hartree-Fock (UHF) method. For each electron with spin α or β a different spatial orbital is assigned so that the single determinantal wavefunction is written as

$$\Psi_{UHF} = \det|\psi_1^\alpha(1)\psi_2^\alpha(2)\dots\psi_p^\alpha(p)\psi_1^\beta(p+1)\psi_2^\beta(p+2)\dots\psi_q^\beta(p+q)| \quad (2.26)$$

The choice of which method to use is still problematic. In general, the UHF method yields a lower total energy and a more accurate spin distribution than the RHF method. Yet, unlike the RHF approximation, the UHF wavefunctions are not always eigenfunctions of the total spin operator and thus do not correspond to pure electronic states.

2.4 Basis Sets

As was previously stated the molecular orbitals are constructed using a linear combination of atomic orbitals which in turn are mathematically modelled using a basis set. The first basis set introduced was formulated based on the atomic orbitals of hydrogen. These orbitals, called Slater-type orbitals (STO), have the normalised

form:

$$\frac{[2\xi/a_o]^{n+\frac{1}{2}}}{[(2n)!]^{\frac{1}{2}}} r^{n-1} \exp\left[\frac{\xi r}{a_o}\right] Y_l^m(\theta, \phi) \quad (2.27)$$

n , l and m are integers and ξ is the orbital exponent. This model reproduces most of the spatial properties of the atomic orbitals, like the cusp condition at the nucleus, but integration problems arise when dealing with multicentre integrals.

A more practical approach can be supplied from the use of Gaussian-type orbitals (GTOs) which have the normalised form,

$$r^{n-l} \exp\left[\frac{-\xi r^2}{a_o}\right] Y_l^m(\theta, \phi) \quad (2.28)$$

again n , l , and m are integers and ξ the orbital exponent. Integrals involving GTOs are much more tractable since the product of two Gaussians centred at different points is a third Gaussian centred at a third point.⁶ The description of the wavefunction attained through the use of GTOs is not the same as that provided by STOs and thus accuracy is sacrificed for practicality when using GTOs in a basis set. A method which tries to achieve a compromise between the accuracy of the STOs and the computational efficiency of the GTOs is to use several GTOs to model an STO, i. e.

$$STO = \sum_i c_i g_i \quad (2.29)$$

The coefficients c_i are optimised to give the best possible fit of the GTOs, g_i 's, to the STO and are held fixed during the calculation.

An infinite number of STOs or GTOs, usually referred to as a complete basis set, would be needed to perfectly represent the atomic orbitals (AOs) within a basis set expansion. This, of course, is not feasible and so different size expansions can be used. The minimal expansion uses just one basis function for each AO while the

double-zeta (DZ) and triple-zeta (TZ) basis sets have two and three basis functions for each AO, respectively. Split-valence basis sets try to model the valence region of an atom more accurately while giving a minimal description of the core. To do this the basis set uses one basis function to describe the core-shells and two or three basis functions to describe the valence shells. This description tends to yield results which are superior to the minimal basis set and as good as or inferior to the double or triple zeta basis sets.

Geometric concerns can also be taken into account by the use of polarisation and diffuse basis functions. Polarisation functions add extra p, d or f functions to the basis set which allows for more angular flexibility during a calculation. Diffuse functions have small exponents and thus allow for larger AOs which is important for anionic calculations.

The efficiency of theoretical calculations are dependent on the number of basis functions used. This indicates that minimal basis sets will have the lowest computational cost but they will also give the lowest accuracy. The double and triple zeta basis sets will increase the accuracy of the calculations but also increase the computational cost dramatically. Care should be taken to choose the correct basis set so that the desired accuracy is achieved with the smallest basis set thus making the calculation as computationally efficient as possible.⁷

2.5 Correlation Energy

At the heart of the Hartree-Fock-Roothaan equations is the assumption that each electron is independent of all other electrons. In reality, though, electrons interact with each other and so the Hartree-Fock energy is only an approximation. However, the normalised Hartree-Fock wavefunction, Ψ_{HF} , satisfies the variation principle so

that,

$$\langle \Psi_{HF} | \hat{H} | \Psi_{HF} \rangle = \mathcal{E} \quad (2.30)$$

where \mathcal{E} is the correct total energy. From this it is trivial to show that the Hartree-Fock energy can only provide an upper bound to the correct total energy even in the limit of a complete basis set. The difference between the true energy and the Hartree-Fock energy is then defined as the correlation energy,^{2,8} i. e.

$$E_{corr} = \mathcal{E} - E_{HF} \quad (2.31)$$

Many different methods have been created to deal with the problem of electron correlation. Most of these methods are based on one of three different modifications made to the wavefunction before solving the Schrödinger equation. The configuration interaction (CI) wavefunction observes that the excited states of the wavefunction contribute to the ground state energy of a molecule. These excited wavefunctions must therefore be included when solving for the energy of a molecule. The second method, many-body perturbation theory (MBPT) uses the fact that the effects of electron correlation are small and can be treated as a slight perturbation to the independent particle Hamiltonian. The last method, referred to as the coupled cluster method, uses an exponential expansion of excitation operators to yield excited wavefunctions similar to CI.

2.5.1 Configuration Interaction (CI) Method

The configuration interaction wavefunction introduces the excited electronic configurations through a linear combination of Slater determinants:^{2,8}

$$\Phi = d_o \Psi_o + \sum_{ar} d_a^r \Psi_a^r + \sum_{\substack{a < b \\ r < s}} d_{ab}^{rs} \Psi_{ab}^{rs} + \sum_{\substack{a < b < c \\ r < s < t}} d_{abc}^{rst} \Psi_{abc}^{rst} + \dots \quad (2.32)$$

The ground state Slater determinant, Ψ_o , is equivalent to the Hartree-Fock wavefunction while Ψ_i^r corresponds to a Slater determinant with one excited electron, Ψ_{ij}^{rs} corresponds to a Slater determinant with two excited electrons, and so on. The expansion coefficients are given by d_i^r , d_{ij}^{rs} , etc.

This new formulation of the wavefunction allows for new definitions of Hamiltonian and overlap matrices such that,

$$H_{ij} = \langle \Psi_i | \hat{H} | \Psi_j \rangle, \quad S_{ij} = \langle \Psi_i | \Psi_j \rangle \quad (2.33)$$

where for simplicity Ψ_i and Ψ_j are used to represent any state with 0 to n excited electrons and \hat{H} is the Hartree-Fock Hamiltonian. By using the variational principle with the new Hamiltonian matrix, an equation analogous to 2.16 can be obtained.

$$\sum_k A_{ik} (H_{jk} - E_i S_{jk}) = 0 \quad (2.34)$$

The lowest eigenvalue, E_0 is an upper bound to the ground state energy while the higher eigenvalues are upper bounds for the excited state energies.

The accuracy of the ground state energy increases with the number of excited configurations included in the calculation. If all possible excitations are included, referred to as full CI, equation 2.34 will yield the most accurate approximation to the

ground state energy within a given basis set. This energy is invariant to the nature of the orbitals used and hence gives the best result under the LCAO approximation. However, as the number of electrons increases, full CI becomes too expensive computationally to calculate and so other approximate methods attempt to achieve the full CI results at reduced computational cost.

The simplest approximation to make is to truncate the CI expansion after a fixed number of excitations. Truncation after only single and double excitations (CISD) can account for most of the correlation energy. Ignoring higher terms in the CI series, though, introduces a few problems, the most severe of these being the lack of size-consistency. For any method to be size-consistent the relative errors involved in any calculation should increase in proportion to the size of the molecule. While it is generally impossible for any approximate theory to achieve this condition it is normally required for the model to be size-consistent at infinite separation.

Size-consistency can be attained with a truncated CI scheme in two ways, include higher-level excitations or increase the size of the reference space used. Both of these methods greatly increases the computational effort of a CI calculations. Methods have been derived to approximate the inclusion of higher-level excitations by using the lower-level excited determinants. One example of this type of approximation is the Davidson correction. Techniques have also been created to make using a larger reference space more efficient. These usually focus on using the orbitals from a multi-configurational Hartree-Fock calculation to enhance the convergence of the CI expansion.

2.5.2 Many-Body Perturbation Theory (MBPT)

Perturbation theory allows for the refinement of both the Hartree-Fock wavefunction and energy. This is achieved by treating the correlation energy as a perturbation of the Hartree-Fock Hamiltonian, i.e.

$$H = H_{HF} + H' \quad (2.35)$$

Splitting up the Hamiltonian in this way creates a mathematical relationship between the energy and wavefunction of the unperturbed system and the energies and wavefunctions of the perturbed system. This means that the perturbed state can be solved using the energies and wavefunction of the unperturbed state. The mathematical relationship is established by linking the unperturbed state to the fully perturbed state by the introduction of a continuum of slightly perturbed states. Mathematically this is the same as introducing a coupling constant, λ , into the Hamiltonian such that,

$$H = H_{HF} + \lambda H' \quad (2.36)$$

Two special cases are immediately apparent, the unperturbed state $\lambda = 0$ and the fully perturbed state $\lambda = 1$.

Due to the λ dependence now introduced into the Hamiltonian it is easily shown that the wavefunction and energy will now also be dependent on λ . To introduce this λ dependency expand both the energy and the wavefunction in a Taylor series about λ ,

$$\Psi_i = \Psi_i^{(0)} + \lambda \Psi_i^{(1)} + \lambda^2 \Psi_i^{(2)} + \dots \quad i = 1, 2, \dots, n \quad (2.37)$$

$$E_i = E_i^{(0)} + \lambda E_i^{(1)} + \lambda^2 E_i^{(2)} + \dots \quad i = 1, 2, \dots, n \quad (2.38)$$

Here $E_i^{(0)}$ and $\Psi_i^{(0)}$ are the unperturbed wavefunction and energy while $E_i^{(k)}$ and $\Psi_i^{(k)}$ can be thought of the k th order correction to the energy and wavefunction, respectively. Substituting these expressions for H , E_i and Ψ_i into the Schrödinger equation and collecting like powers of λ will then give the perturbation expressions,

$$\begin{aligned} H_{HF}\Psi_i^{(0)} &= E_i^{(0)}\Psi_i^{(0)} \\ H'\Psi_i^{(0)} + H_{HF}\Psi_i^{(1)} &= E_i^{(0)}\Psi_i^{(1)} + E_i^{(1)}\Psi_i^{(0)} \\ &\vdots \end{aligned} \tag{2.39}$$

Moller and Plesset introduced a perturbation of the Hartree-Fock Hamiltonian to approximate the correlation energy excluded from the Hartree-Fock energy. This method uses the Hartree-Fock wavefunction as the unperturbed wavefunction for the basis of the calculation. Thus using the single determinantal wavefunction it was shown that the zeroth-, first- and second-order energy corrections are given by,

$$E_0^{(0)} = \sum_a^N \epsilon_a \tag{2.40}$$

$$E_0^{(1)} = -\frac{1}{2} \sum_{a,b=1}^N (aa|bb) - (ab|ba) \tag{2.41}$$

$$E_0^{(2)} = \sum_{\substack{a < b \\ r < s}} \frac{|(ar|bs) - (as|br)|^2}{\epsilon_a + \epsilon_b - \epsilon_r - \epsilon_s} \tag{2.42}$$

The energies, ϵ_i , are just the MO energies previously defined for the Hartree-Fock MOs. As seen above the Hartree-Fock energy is just the sum of the zeroth- and first-order corrections and thus to get any correction to the energy the perturbation needs to be taken to at least second order. This method can also be used to find corrections to the wavefunction using only the Hartree-Fock wavefunction.

2.5.3 The Coupled Cluster Approximation

The coupled cluster approximation (CC),^{2,9} like the configuration interaction method, includes excited electronic configurations in its wavefunction in order to calculate the correlation energy. The CC wavefunction though is usually expressed in a different manner than the CI wavefunction and is usually expressed as,

$$\Psi^{CC} = \exp(T)|\Psi_0 \rangle \quad (2.43)$$

The operator T is a combination of excitation operators, T_n , which excite n electrons from n molecular orbitals and when the operator T includes all electronic excitations the coupled cluster approximation is indistinguishable from the full CI approximation. However, due to many constraints T cannot include all electronic excitations and is usually approximated.

One of the first approximations made by J. Čížek⁹ was to only include excitations of pairs of electrons, that is $T \approx T_2$. This approximation allows for the derivation of the closed coupled cluster equations,

$$\sum_{\substack{c < d \\ i < u}} \langle \Psi_0 | H | \Psi_{cd}^{tu} \rangle d_{cd}^{tu} = E_{corr} \quad (2.44)$$

$$\langle \Psi_{ab}^{rs} | H | \Psi_0 \rangle + \sum_{\substack{c < d \\ i < u}} \langle \Psi_{ab}^{rs} | H - E_0 | \Psi_{cd}^{tu} \rangle d_{cd}^{tu} + \sum_{\substack{c < d \\ i < u}} \langle \Psi_0 | H | \Psi_{cd}^{tu} \rangle (d_{ab}^{rs} * d_{cd}^{tu}) = E_{corr} d_{ab}^{rs} \quad (2.45)$$

Two points should be made about these equations, the first is that if $d_{ab}^{rs} * d_{cd}^{tu}$ was set equal to zero then these equations reduce to the configuration interaction method which includes only double excitations. The second point is that the $d_{ab}^{rs} * d_{cd}^{tu}$ value

is a complex product of the double excitation coefficients given by

$$\begin{aligned}
d_{ab}^{rs} * d_{cd}^{tu} &= d_{ab}^{rs} d_{cd}^{tu} - d_{ac}^{rs} d_{bd}^{tu} + d_{ad}^{rs} d_{bc}^{tu} - d_{ab}^{rt} d_{cd}^{su} + d_{ac}^{rt} d_{bd}^{su} - d_{ad}^{rt} d_{bc}^{su} \\
&+ d_{ab}^{ru} d_{cd}^{st} - d_{ac}^{ru} d_{bd}^{st} + d_{ad}^{ru} d_{bc}^{st} + d_{ab}^{tu} d_{cd}^{rs} - d_{ac}^{tu} d_{bd}^{rs} + d_{ad}^{tu} d_{bc}^{rs} \\
&- d_{ab}^{su} d_{cd}^{rt} + d_{ac}^{su} d_{bd}^{rt} - d_{ad}^{su} d_{bc}^{rt} + d_{ab}^{st} d_{cd}^{ru} - d_{ac}^{st} d_{bd}^{ru} + d_{ad}^{st} d_{bc}^{ru}
\end{aligned} \tag{2.46}$$

which is an approximation to the quadruple excitation coefficients, d_{abcd}^{rstu} . By approximating the quadruple excitation coefficients in this way the coupled cluster method retains size consistency.

2.5.4 Quadratic Configuration Interaction

The quadratic configuration interaction (QCI) method also uses lower excitation coefficients to approximate higher excitation coefficients to create a set of closed equations from a truncated configuration interaction (CI) wavefunction. Doing so the QCI method creates a new wavefunction which not only retains size consistency but also improves the truncated CI results. Closer examination of the QCI wavefunction reveals that it is very similar to the coupled cluster wavefunction and as such results obtained with QCI can be viewed as an approximation of the coupled cluster results.

2.6 Density Functional Theory

In 1964 the foundations for another method to solve the Schrödinger equation were introduced.^{10,11} Two theorems, put forth by Hohenberg and Kohn,¹² revealed that one could obtain all the information about a system using only the electron density of a molecule, $\rho(\mathbf{r})$. More specifically, the first theorem demonstrated that the electron density of a molecule, $\rho(\mathbf{r})$, uniquely determines the external potential, $v(\mathbf{r})$, of the

system. This indicates that the energy of the system can be represented as a functional of the density,

$$E[\rho] = \int \rho(\mathbf{r})v(\mathbf{r})d\mathbf{r} + T[\rho] + V_{ee}[\rho] \quad (2.47)$$

Note that this expression for the energy contains both the kinetic energy functional, $T[\rho]$, and the interelectronic repulsion energy functional, $V_{ee}[\rho]$. In a less formal sense this theorem states that given any electron density, $\bar{\rho}$, there is a unique wavefunction, $\tilde{\Psi}$, associated with it.

The variational principle is then the basis of the second theorem given by Hohenberg and Kohn.¹² This implies that the energy associated with a density for a molecule, $\bar{\rho}$, will always be greater than or equal to the energy associated with the exact density of the molecule, ρ_0 . Stated symbolically,

$$E[\bar{\rho}] = \langle \tilde{\Psi} | H | \tilde{\Psi} \rangle \geq E[\rho_0] \quad (2.48)$$

Also, the variational principle maintains that the equality holds if and only if $\bar{\rho} = \rho_0$. The use of the variational principle, however, limits density functional theory to calculations on the ground states of molecules only.

To solve for the density of a molecule the energy of the molecular system must be stationary with respect to the calculated density. To meet this condition the following equation must hold,

$$\delta E[\rho] - \xi \delta \left[\int \rho(\mathbf{r})d\mathbf{r} - N \right] = 0 \quad (2.49)$$

where ξ is a Euler-Lagrange multiplier. Also, the density must be subject to the constraint,

$$\int \rho(\mathbf{r})d\mathbf{r} = N \quad (2.50)$$

The Euler-Lagrange equation can then be formulated,

$$\xi = v(\mathbf{r}) + \frac{\delta T[\rho]}{\delta \rho(\mathbf{r})} + \frac{\delta V_{ee}[\rho]}{\delta \rho(\mathbf{r})} \quad (2.51)$$

In the above equation both $\frac{\delta T[\rho]}{\delta \rho(\mathbf{r})}$ and $\frac{\delta V_{ee}[\rho]}{\delta \rho(\mathbf{r})}$ are functional derivatives.

The Euler-Lagrange multiplier cannot be calculated directly without the knowledge of the exact kinetic and electron-electron repulsion energy functionals. However, an indirect method for solving the Euler-Lagrange equation was introduced by Kohn and Sham.¹³ Using a noninteracting reference system Kohn and Sham introduced a determinantal wavefunction made up of N noninteracting electrons in N orbitals, χ_i . This allowed for the exact calculation of the kinetic energy.

$$T_s = \sum_i^N \eta_i \langle \chi_i | -\frac{1}{2} \nabla^2 | \chi_i \rangle \quad (2.52)$$

for this noninteracting system. Also by using this method the electron density was simplified to,

$$\rho(\mathbf{r}) = \sum_i^N \eta_i |\chi_i(\mathbf{r})|^2 \quad (2.53)$$

It should be noted that for pure state DFT $\eta_i = 0$ or 1 . This creates an effective potential, v_s , on the system and the orbitals obey the equation,

$$\left[-\frac{1}{2} \nabla^2 + v_s(\mathbf{r})\right] \chi_i = \epsilon_i \chi_i \quad (2.54)$$

From this a simple expression for the energy of the noninteracting system can be obtained,

$$E[\rho] = T_s[\rho] + \int v_s(\mathbf{r}) \rho(\mathbf{r}) d\mathbf{r} \quad (2.55)$$

Returning to an interacting system it can be shown that the energy can be written

as:

$$E[\rho] = \int v(\mathbf{r})\rho(\mathbf{r})d\mathbf{r} + T_s[\rho] + (T[\rho] - T_s[\rho]) + V_{ee}[\rho] \quad (2.56)$$

The largest contribution to the interelectronic repulsion term is the Coulomb repulsion energy,

$$J[\rho] = \frac{1}{2} \int \int \frac{1}{r_{12}} \rho(\mathbf{r}_1)\rho(\mathbf{r}_2)d\mathbf{r}_1d\mathbf{r}_2 \quad (2.57)$$

which is easily calculated within the Kohn-Sham noninteracting reference space. Using this expression the exchange-correlation energy functional can be defined as,

$$E_{xc}[\rho] = T[\rho] - T_s[\rho] + V_{ee}[\rho] - J[\rho] \quad (2.58)$$

This expression for E_{xc} will reduce the expression for the total energy to,

$$E[\rho] = \int v(\mathbf{r})\rho(\mathbf{r})d\mathbf{r} + T_s[\rho] + J[\rho] + E_{xc}[\rho] \quad (2.59)$$

This energy expression demonstrates that the interacting electron problem can be recast into a system involving noninteracting electrons. More specifically, the N noninteracting one-electron orbitals will obey the set of equations,

$$\left[-\frac{1}{2}\nabla^2 + v(\mathbf{r}) + \int \frac{\rho(\mathbf{r}')}{|\mathbf{r} - \mathbf{r}'|}d\mathbf{r}' + v_{xc}(\mathbf{r})\right]\chi_i(\mathbf{r}) = \epsilon_i\chi_i(\mathbf{r}) \quad (2.60)$$

given that $v_{xc} = \delta E_{xc}[\rho]/\delta\rho(\mathbf{r})$. Proceeding as in the Hartree-Fock procedure and representing the orbitals with a basis set,

$$\chi_i = \sum_{\mu} c_{\mu i}\phi_{\mu} \quad (2.61)$$

produces what are known as the Kohn-Sham equations,

$$\sum_{\nu} \left\langle \phi_{\mu} \left| -\frac{1}{2}\nabla^2 + v(\mathbf{r}) + \int \frac{\rho(\mathbf{r}')}{|\mathbf{r}-\mathbf{r}'|} d\mathbf{r}' + v_{xc}(\mathbf{r}) - \epsilon_i \right| \phi_{\nu} \right\rangle c_{\nu i} = 0 \quad (2.62)$$

The Kohn-Sham equations imply that if $E_{xc}[\rho]$ is known, and hence $v_{xc}(\mathbf{r})$ then the Schrödinger equation can be solve as accurately as the basis set used allows. Unfortunately, $E_{xc}[\rho]$ is unknown and only a few approximations have been proposed. However, due to the computational efficiency of DFT, which is as efficient as a HF calculation, there is much interest in creating better and better approximations to $E_{xc}[\rho]$. Within time accurate exchange-correlation functionals will be created and calculations including correlation energies can be done without the computational drawbacks of CI, MBPT and CC.

2.7 The Exchange-Correlation Energy Functional

The computational efficiency of DFT has spawned much research in the design and refinement of exchange-correlation energy functionals. As shown above the Kohn-Sham equations, 2.62, require an explicit form of E_{xc} for their solution. Although E_{xc} must exist the search for E_{xc} has encountered many difficulties and still a systematic way for calculating E_{xc} has not been found. Thus many different and varying models have been used to approximate E_{xc} and solve the Kohn-Sham equations.

The simplest of these models is based on a uniform electron gas and has been studied extensively. More accurate calculations can be achieved by using different models or through a modification to the electron gas model. An in depth look at these models will help to shed light on how accurate current functionals are and what has been done to date.

2.7.1 The Local (Spin) Density Approximation

The local density approximation (LDA) was one of the first approximations of the exchange-correlation energy functional. This simple model used a uniform-electron-gas to model the electron correlations within a molecule.¹⁰ The exchange-correlation functional produced by the LDA then has the form,

$$E_{xc}^{LDA}[\rho] = \int e_{xc}(\rho) d\mathbf{r} \quad (2.63)$$

This functional is merely the integral of exchange-correlation energy density per unit volume, e_{xc} . Taking the functional derivative will then yield the exchange-correlation potential,

$$v_{xc}^{\sigma LDA}(\mathbf{r}) = \frac{\delta E_{xc}^{LDA}}{\delta \rho_{\sigma}(\mathbf{r})} = \frac{\delta e_{xc}^{LDA}}{\delta \rho_{\sigma}(\mathbf{r})} \quad (2.64)$$

which when substituted into the Kohn-Sham equations defines the Kohn-Sham local-density approximation.

In any system the exchange and correlation energy per particle, ϵ_{xc} , are separately and uniquely defined. This allows ϵ_{xc} to be split into separate exchange and correlation contributions, that is $\epsilon_{xc} = \epsilon_x + \epsilon_c$. An explicit formulation of the exchange-energy per particle was formulated even before the creation of DFT and was given by Dirac in 1930,¹⁴

$$\epsilon_x(\rho) = -C_x \rho(\mathbf{r})^{1/3}, \quad C_x = \frac{3}{4} \left(\frac{3}{\pi} \right)^{1/3} \quad (2.65)$$

This approximation is only valid for the spin compensated case where $\rho^{\alpha}(\mathbf{r}) = \rho^{\beta}(\mathbf{r}) = \frac{1}{2}\rho(\mathbf{r})$, but complete spin pairing is not present in all cases. For functionals involving incomplete spin pairing, otherwise known as spin polarisation, the exchange

energy functional must be expressed as a functional of two different spin-densities,

$$E_x^{LSDA}[\rho^\alpha, \rho^\beta] = 2^{1/2} C_x \int [(\rho^\alpha)^{4/3} + (\rho^\beta)^{4/3}] d\mathbf{r} \quad (2.66)$$

This is known as the local spin density approximation (LSDA) since it accounts for differences in spin polarisation.

To show that this definition of the exchange energy functional is of the form represented in equation 2.63 a spin polarisation parameter, ξ , must be defined,

$$\xi = \frac{\rho^\alpha - \rho^\beta}{\rho} = \frac{\rho^\alpha - \rho^\beta}{\rho^\alpha + \rho^\beta} \quad (2.67)$$

The exchange energy per particle, ϵ_x , can then be given by the expression,

$$\epsilon_x(\rho, \xi) = \epsilon_x^0(\rho) + [\epsilon_x^1(\rho) - \epsilon_x^0(\rho)]f(\xi) \quad (2.68)$$

where, $\epsilon_x^0 = C_x \rho^{1/3}$, is the spin-compensated exchange density, $\epsilon_x^1 = 2^{1/3} C_x \rho^{1/3}$ is the spin-completely-polarised exchange density. Using this definition of $\epsilon_x(\rho)$ again puts the exchange energy functional in the form,

$$E_x^{LSDA}[\rho^\alpha, \rho^\beta] = \int \rho \epsilon_x(\rho, \xi) d\mathbf{r} \quad (2.69)$$

Unlike the exchange energy functional the correlation energy functional, $E_c[\rho^\alpha, \rho^\beta]$, cannot be broken into the sum of two different spin contributions since correlation energy affects both like- and unlike-spin electron-electron interactions. It is not surprising, then, that a closed form for the correlation energy for the homogeneous electron gas has not been found. Some approximate forms for ϵ_c have been found, one such is given by Vosko, Wilk and Nusair,¹⁵ and coupling them with ϵ_x gives the

local spin-density approximation to the Kohn-Sham Equations.

2.7.2 The Exchange-Correlation Hole

The results obtained from the LSDA were encouraging but indicated that improvements still could be made.¹⁶⁻¹⁹ Investigations of the exchange-correlation hole found connections between it and the exchange-correlation energy functional. Most important were the conditions that the exchange-correlation hole imposed upon the energy functional.

Put in the simplest of terms the exchange-correlation hole is the region of space around an electron where the probability of finding another electron is 0. This can be defined by decomposing the second-order density matrix into,^{20,21}

$$\rho_2(\mathbf{r}_\sigma, \mathbf{r}'_{\sigma'}) \equiv n_\sigma(\mathbf{r})n_2(\mathbf{r}_\sigma, \mathbf{r}'_{\sigma'}), \quad (2.70)$$

so that $n_2(\mathbf{r}_\sigma, \mathbf{r}'_{\sigma'})d^3\mathbf{r}'$ is the probability of finding an electron in a volume $d^3\mathbf{r}'$ centred at \mathbf{r}' with spin σ' given that there is an electron of spin σ in a volume d^3r centred at \mathbf{r} . From this the spin-decomposed exchange-correlation hole around an electron of spin σ can then be given by the relation,

$$n_2(\mathbf{r}_\sigma, \mathbf{r}'_{\sigma'}) \equiv n_{\sigma'}(\mathbf{r}') + n_{xc}(\mathbf{r}_\sigma, \mathbf{r}'_{\sigma'}) \quad (2.71)$$

For closed-shell species the spins can be summed to give the non-spin decomposed hole,

$$n_{xc}(\mathbf{r}, \mathbf{r}') = \sum_{\sigma, \sigma'} \frac{n_\sigma(\mathbf{r})}{n(\mathbf{r})} n_{xc}(\mathbf{r}_\sigma, \mathbf{r}'_{\sigma'}) \quad (2.72)$$

which then can be related to the spin-summed second-order density matrix.

The use of the Hellmann-Feynman theorem connects the exchange-correlation hole to the exchange correlation energy by treating E_{xc} as the electrostatic interaction between the density and the hole averaged over a coupling constant, λ . Thus,

$$E_{xc} = \int_0^1 d\lambda E_{xc,\lambda}[n] = \frac{1}{2} \int d^3r n(\mathbf{r}) \int d^3u \frac{\bar{n}_{xc}(\mathbf{r}, \mathbf{r} + \mathbf{u})}{u} \quad (2.73)$$

where \bar{n}_{xc} is the exchange-correlation hole averaged over the coupling constant,

$$\bar{n}_{xc}(\mathbf{r}, \mathbf{r}') = \int_0^1 n_{xc,\lambda}(\mathbf{r}, \mathbf{r}') d\lambda \quad (2.74)$$

The exchange-correlation hole can be approximated by the sum of two linearly independent holes, although in real systems this is not always the case. Thus, the hole can be decomposed into the sum of the exchange hole, $n_x(r)$, and the correlation hole, $n_c(r)$. This approach simplifies the exchange correlation hole since each of these two holes have well known conditions. The exchange, or Fermi, hole is due to the Pauli exclusion principle, and obeys the conditions:

$$n_x(\mathbf{r}_\sigma, \mathbf{r}'_{\sigma'}) \leq 0, \quad (2.75)$$

and

$$\int d^3r n_x(\mathbf{r}_\sigma, \mathbf{r}'_{\sigma'}) = -\delta_{\sigma,\sigma'} \quad (2.76)$$

While the correlation hole obeys the condition:

$$\int d^3r' n_c(\mathbf{r}_\sigma, \mathbf{r}'_{\sigma'}) = 0 \quad (2.77)$$

The two conditions on the exchange hole can be accounted for by the fact that the

wavefunction is a non-interacting Slater determinant while the integral condition on the correlation hole arises from the normalisation of the second-order density matrix.

Another condition arises when the separation between two electrons tends to zero. At this point the Coulomb interaction dominates and leads to a cusp in the exchange-correlation hole at zero separation.²² The pair distribution function allows for a simple formulation of this subtle condition and like the exchange-correlation hole it can be related to the second-order density matrix,

$$g(\mathbf{r}_\sigma, \mathbf{r}'_{\sigma'}) = \frac{\rho_2(\mathbf{r}_\sigma, \mathbf{r}'_{\sigma'})}{[n_\sigma(\mathbf{r})n_{\sigma'}(\mathbf{r}')]} \quad (2.78)$$

Defining the spherically-averaged derivative of the pair distribution at zero separation as,

$$g'(\mathbf{r}, \mathbf{r}) = \left[\frac{\partial}{\partial u} \right]_{u=0} \int \frac{d\Omega_{\mathbf{u}}}{4\pi} g(\mathbf{r}, \mathbf{r} + \mathbf{u}), \quad (2.79)$$

then the cusp condition can be shown to be,²³

$$g'(\mathbf{r}, \mathbf{r}) = g(\mathbf{r}, \mathbf{r}) \quad (2.80)$$

Like the exchange-correlation hole the pair distribution function can be split into exchange and correlation contributions. Using the above derivative and the Pauli exclusion principle it is known that only antiparallel spins can have zero separation and thus the non-vanishing derivative must be a pure correlation effect. From this it can be shown that,

$$g'_x(\mathbf{r}_\sigma, \mathbf{r}_{\sigma'}) = 0 \quad (2.81)$$

and,

$$g'_c(\mathbf{r}_\sigma, \mathbf{r}_{\sigma'}) = (1 - \delta_{\sigma, \sigma'}) g(\mathbf{r}_\sigma, \mathbf{r}_{\sigma'}) \quad (2.82)$$

2.7.3 Post Local Spin Density Approximation

Although the exchange and correlation holes can place specific conditions upon $E_{xc}[\rho]$ it is quite difficult to create an actual functional from them. Different methods have been used to create functionals which improve upon LSDA. The accuracy of these newer functionals has helped to push DFT to the forefront of theoretical chemistry.

Generalised-Gradient Approximations

The generalised-gradient approximation was one of the first methods used to go beyond the local spin density approximation and has produced many different functionals with varying results.²⁴⁻²⁸ To improve upon the local spin density approximation the generalised-gradient approach introduces a dependence on the gradient of the density into the exchange and correlation energy,

$$E_{xc}^{GGA}[\rho^\alpha, \rho^\beta] = \int d^3r f(\rho^\alpha(\mathbf{r}), \rho^\beta(\mathbf{r}), \nabla\rho^\alpha, \nabla\rho^\beta) \quad (2.83)$$

The lowest-order gradient correction (LGC) gives the simplest correction to the LSDA.¹³ It can be uniquely determined by dimensional analysis.

$$E_x^{LGC} = E_x^{LDA} - \beta \sum_\sigma \int \frac{(\nabla\rho_\sigma)^2}{\rho_\sigma^{4/3}} d^3r \quad (2.84)$$

where β is a constant. This functional, sometimes called the $X\alpha\beta$ functional has some severe problems: the exchange potential will diverge asymptotically in atomic and molecular systems, the value of the constant β has been the subject of much confusion and the value of β has some Z dependence and hence the $X\alpha\beta$ model isn't universal.

As a consequence of these problems Becke derived a semi-empirical correction

to the $X\alpha\beta$ model. To better understand the changes presented by this model the reduced density gradient, x_σ , is introduced,

$$x_\sigma = \frac{|\nabla\rho_\sigma|}{\rho_\sigma^{4/3}} \quad (2.85)$$

As previously stated the $X\alpha\beta$ potential diverges as this reduced density gradient increases. To compensate Becke added another term into the model,

$$E_{x\alpha\beta\gamma} = E_x^{LDA} - \beta \sum_\sigma \int (\nabla\rho_\sigma) x_\sigma [1 + \gamma x_{sigma}^2]^{-1} d^3r \quad (2.86)$$

This increased the number of parameters in the expression to two, β and γ . When $\gamma = 0$ this expression just reduces to the $X\alpha\beta$ expression but assumes a $\rho^{4/3}$ integrand with large values of γ . The integrand will reduce to $\rho^{4/3}$ also when the reduced density gradient is large or within the exponential tail of atomic or molecular charge distributions. The parameters, β and γ , were determined empirically and found to have values of 0.0036 and 0.004, respectively. These values do not seem to exhibit any Z dependence and hence give the $X\alpha\beta\gamma$ model universality.²⁹

The $X\alpha\beta\gamma$ model uses a somewhat arbitrary choice of large gradient behaviour to fix the divergent behaviour of the $X\alpha\beta$ model. Improved theoretical models for the large reduced density gradient behaviour have been given by Perdew,²⁶ Becke³⁰ and others.³¹ In 1988, Becke then proposed a further modification which took into account the exact asymptotic behaviour of the exchange-energy density.²⁵

It is well known that as the distance between two charged particles tends to infinity, the Coulomb potential, $U(r)$, tends to $\frac{1}{r}$. The exchange-hole potential,

$$U_x^\sigma = \int \frac{n_{xc}(\mathbf{r}_\sigma, \mathbf{r}'_{\sigma'})}{|\mathbf{r} - \mathbf{r}'|} d^3\mathbf{r}' \quad (2.87)$$

will then exhibit this same asymptotic behaviour due to its Coulombic nature, that is

$$\lim_{r \rightarrow \infty} U_x^\sigma = -\frac{1}{r} \quad (2.88)$$

This potential can easily be related to the exchange energy of the molecule through the simple expression,

$$E_x = \frac{1}{2} \sum_{\sigma} \int \rho_{\sigma} U_x^{\sigma} d^3r \quad (2.89)$$

This equation shows that the behaviour of ρ must also be known as r tends to infinity. It is easy to show that the asymptotic behaviour of the spin density is given by,

$$\lim_{r \rightarrow \infty} \rho_{\sigma} = e^{-b_{\sigma} r} \quad (2.90)$$

where b_{σ} is related to the ionisation potential of the system.

In 1988, Becke introduced a functional of the form,

$$E_x = E_x^{LDA} - \beta \sum_{\sigma} \int \rho_{\sigma}^{4/3} \frac{x_{\sigma}^2}{(1 + 6\beta x_{\sigma} \sinh^{-1} x_{\sigma})} d^3r, \quad (2.91)$$

which is commonly referred to as the B88 functional. This formulation exhibits the correct asymptotic behaviour for the exchange-energy density under substitution of the asymptotic spin density. This system reproduces the LSDA values for a homogeneous electron gas and for systems which have smooth slowly varying densities, that is a system with low density gradients, this functional reduces to the LGC expression.

Since Becke introduced this functional in 1988 many other expressions for exchange and correlation energy densities have been devised using the generalised-gradient approximation. The expressions for these are as complicated, if not more so, as the B88 expression and are excluded from this thesis. The methods of design may

vary from using a Taylor expansion of the exchange-correlation functional to fitting very-accurate correlation data for He and finally to designing a functional from first principles. All of these functionals fit the GGA model.

With a large number of GGA functionals to date and more being added a tool to analyse the performance of these functionals was designed by Perdew and co-workers.³² If a dimensionless measure of the gradient is given by,

$$s = \frac{|\nabla\rho|}{2k_F\rho} \quad (2.92)$$

with the local Fermi wavevector, k_F , defined as

$$k_F = (3\pi^2\rho)^{1/3} \quad (2.93)$$

and given that the local Wigner-Seitz radius, r_s , is

$$r_s = \left(\frac{4\pi\rho}{3}\right)^{-1/3} \quad (2.94)$$

then an exchange-correlation enhancement factor, $F_{xc}(r_s, s)$, can be defined as,

$$E_{xc}^{GGA}[\rho/2, \rho/2] = \int \rho(\mathbf{r})\epsilon_x[\rho(\mathbf{r})]F_{xc}[r_s(\mathbf{r}), s(\mathbf{r})]d^3r \quad (2.95)$$

Then using the exchange energy per particle for a uniform gas, $\epsilon_x(\rho) = -3k_F/4\pi$, a calculation of the enhancement factor for each functional was completed.

The enhancement factor, $F_{xc}(r_s, s)$, is a measure of the enhancement in the energy per particle over local exchange. For real systems the energies can contain significant contributions up to about $s = 3$ and $r_s = 18$. Some values for real systems are $s \leq 2$ and $1 \leq r_s \leq 6$ for the valence electrons in solid metals and $s \leq 1$ and $r_s \leq 1$ in the

core of an atom. In the limit of $r \rightarrow \infty$ the values of s and r_s grow exponentially.²⁰

A look at the enhancement factors for the LSDA approximation, figure 2.1,²⁰ shows curves that are horizontal lines since the approximation is gradient independent by definition. When at the high density limit, $r_s = 0$, $F_{xc} = 1$, while when r_s is greater than 1, F_{xc} increases beyond 1 due to the correlation contribution to the exchange-correlation energy. The LGC approximation on the other hand gives parabolic curves, figure 2.2²⁰ for the enhancement factors due to including only second-order gradient contributions. While the LGC approximation improves LSDA results in systems

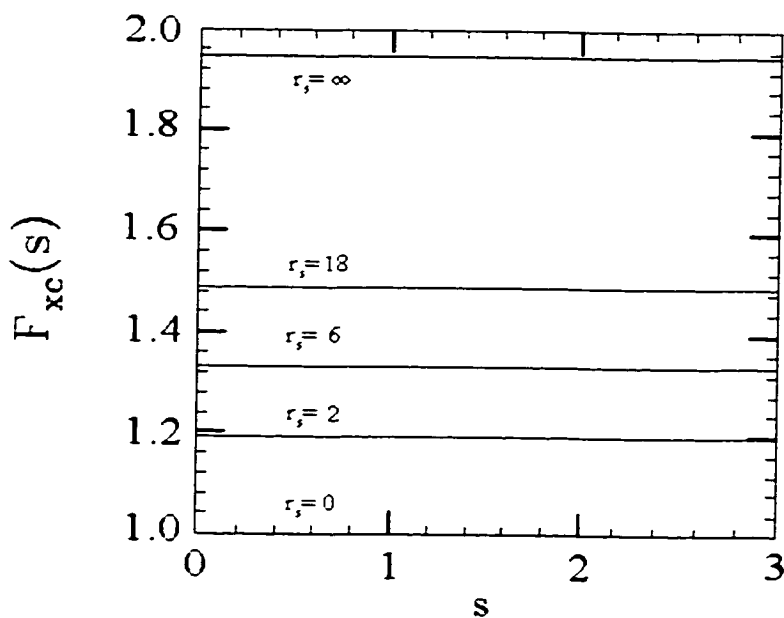


Figure 2.1: Enhancement factors for the LSDA

with slowly varying densities it typically gives worse results for real electronic systems which contain regions of rapidly varying densities.

This type of analysis is carried out upon the GGAs to give an indication of whether or not a GGA obeys known conditions on the true exchange-correlation functional. One example of this is found using the exchange functional by Becke, as derived above, combined with the 1986 correlation functional of Perdew and Wang.²⁶

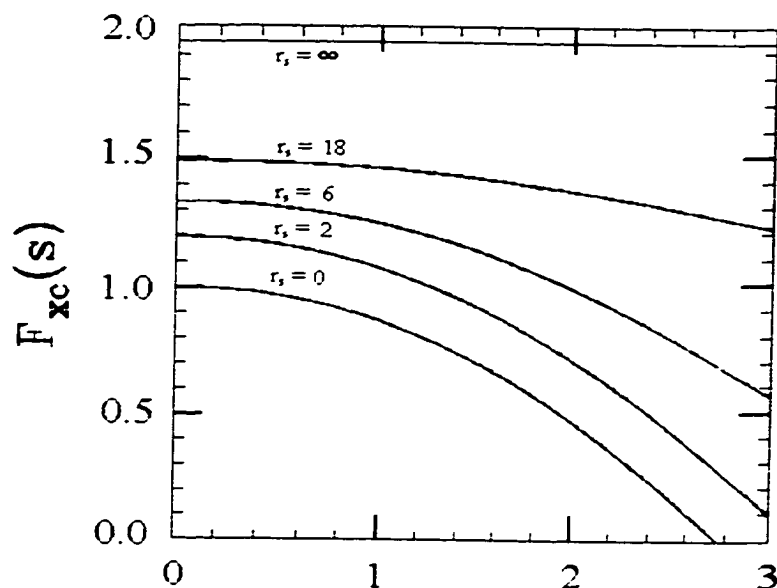


Figure 2.2: Enhancement factors for LGC

This functional includes the uniform gas limit and the LGC by having the correct s^2 dependence, as seen in figure 2.3.²⁰ However, it still violates uniform scaling and the Lieb-Oxford bound which states,³³

$$F_{xc}(r_s, s) \leq 2.27 \quad (2.96)$$

Although, this method sheds light upon the inherent problems for each functional it does not reveal how accurate these functionals are in terms of calculated molecular properties. A study of molecular properties is the only indication of this type of accuracy for a newly designed functional. Many of these types of calculations have been done, comparing and contrasting the accuracy of GGA functionals.^{16,32,34-36} The final results of these studies show that GGAs give a marked improvement over LSDA and that some functionals are comparable to other high level calculations.

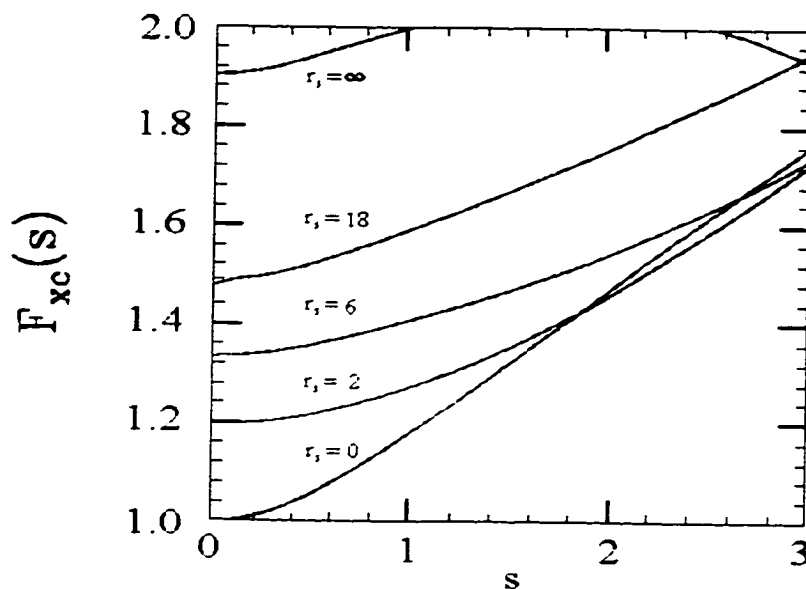


Figure 2.3: Enhancement factors for BP86

Hybrid Functionals

The accuracy attained by the GGAs is still not satisfactory, generally being within 3 to 5 kcal/mol of experiment for many thermochemical properties, and the limits of the GGA model may soon be reached.^{16, 18, 19, 37} Hybrid functionals were introduced to try and increase the accuracy of DFT by introducing a small amount of exact exchange energy into the exchange energy functional. Why this was done is most easily explained using the adiabatic connection method.

In the adiabatic connection method the exchange-correlation energy may be given by,

$$E_{xc} = \int_0^1 U_{xc}^\lambda d\lambda \quad (2.97)$$

The coupling-strength parameter, λ , controls the Coulomb interaction between electrons, and U_{xc}^λ is the potential energy of the exchange-correlation at the coupling strength λ . This essentially sums over a continuum of partially interacting systems,

$0 \leq \lambda \leq 1$, from the noninteracting Kohn-Sham reference, $\lambda = 0$, to the fully interacting real system, $\lambda = 1$. The $\lambda = 0$ lower limit, corresponding to the Kohn-Sham reference system, is the limit of greatest importance. The exchange-correlation potential energy of this system, U_{xc}^0 , is the pure exchange energy of the Slater determinant of the Kohn-Sham orbitals and does not include any dynamic correlation. This suggests at $\lambda = 0$ only exchange energy is present within E_{xc} and this energy is essentially, although not exactly, equal to the Hartree-Fock exchange energy.³⁸

The LSDA model can be used to calculate U_{xc}^λ for each value of λ but this replacement is inappropriate in molecular bonds near the $\lambda = 0$ exchange-only limit. This problem can be understood by looking at the LSDA description of H_2 . The exact exchange hole of the hydrogen molecule is the negative of the σ_g orbital density and is reference-point independent. This implies that the static hole which is uniformly distributed over both centres does not have any left-right correlation. The hole generated using the electron-gas model, though, is reference-point centred and relatively localised. The effect of this is to give a crude simulation of left-right correlation which, though needed in the interacting system, misrepresents the noninteracting system. Thus, it could be argued that the LSDA approximation in the noninteracting limit, $\lambda = 0$, is the principal source of error.³⁹

These problems still occur even with the gradient corrected methods and even the most sophisticated approaches still display slight overbinding tendencies. Becke has therefore created functionals which include a mixture of exact exchange and LSDA exchange to correct for the $\lambda = 0$ or noninteracting case. The most useful of these is the Becke three-parameter expression given by,

$$E_{xc} = E_{xc}^{LSDA} + a_o(E_x^{exact} - E_x^{LSDA}) + a_x \Delta E_x^{B88} + a_c \Delta E_c^{PW91} \quad (2.98)$$

The values of the constants $a_o = 0.20$, $a_x = 0.72$, and $a_c = 0.81$ were determined semi-empirically by fitting the functional to experimental data. The gradient corrections, ΔE_x^{B88} and ΔE_c^{PW91} , are the corrections to the LSDA exchange and correlation energies, respectively.

Reasonable physical arguments can be made for the motivation of equation 2.98. The second term has some of the LSDA exchange being replaced by exact exchange and the amount replaced is controlled by the coefficient a_o . Thus a_o reflects the relative importance of the independent-particle character of the model. As a first approximation this value can be thought of as a constant. The coefficients, a_x and a_c , meanwhile allow for the optimum admixture of exchange and correlation-type gradient corrections. Finally, it should be noted that the above expression is the simplest mixture of LSDA exchange and correlation, exact exchange and gradient corrections that recovers the uniform electron-gas limit.

References

- [1] I. N. Levine, *Quantum Chemistry, Third Edition*, Allyn and Bacon, Inc., 1983.
- [2] A. Szabo and N. S. Ostlund, *Modern Quantum Chemistry: Introduction to Advanced Electronic Structure Theory*, McGraw-Hill, 1982.
- [3] R. G. Wooley, *J. Mol. Structure (THEOCHEM)* **230**, 17 (1991).
- [4] H. Koppel, L. S. Cedarbaum, W. Domcke, and S. S. Shaik, *J. Chem. Phys.* **89**, 2023 (1988).
- [5] S. Wilson, editor, *Methods In Computational Chemistry*, volume 1, Plenum Press, 1987.

-
- [6] I. Shavitt, *Methods in Computational Physics*, Academic Press, 1963.
- [7] V. I. Minkin, B. Y. Simkin, and R. M. Minyaev, *Quantum Chemistry of Organic Compounds*, Springer-Verlag, 1990.
- [8] R. McWeeny, *Methods of Molecular Quantum Mechanics*. Academic Press, 1989.
- [9] J. Čížek, *J. Chem. Phys.* **45**, 4256 (1966).
- [10] R. G. Parr and W. Yang, *Density-Functional Theory of Atoms and Molecules*, Oxford University Press, 1989.
- [11] B. O. Roos, editor, *Lecture Notes in Quantum Chemistry II*, Springer-Verlag, 1994.
- [12] P. Hohenberg and W. Kohn, *Phys. Rev.* **136**, 864 (1964).
- [13] W. Kohn and L. J. Sham, *Phys. Rev.* **140**, A1133 (1965).
- [14] P. A. M. Dirac, *Proc. Cambridge Phil. Soc.* **36**, 376 (1930).
- [15] S. H. Vosko, L. Wilk, and M. Nusair, *Can. J. Phys.* **58**, 1200 (1980).
- [16] B. G. Johnson, P. M. W. Gill, and J. A. Pople, *J. Chem. Phys.* **98**, 5612 (1993).
- [17] J. Andzelm and E. Wimmer, *J. Chem. Phys.* **96**, 1280 (1992).
- [18] L. Fan and T. Ziegler, *J. Chem. Phys.* **95**, 7401 (1991).
- [19] C. W. Murray, N. C. Handy, and R. D. Amos, *J. Chem. Phys.* **98**, 7145 (1993).
- [20] J. M. Seminario and P. Politzer, editors, *Modern Density Functional Theory: A Tool for Chemistry*, Elsevier, 1995.
- [21] R. McWeeny, *Rev. Mod. Phys.* **32**, 335 (1960).

- [22] J. C. Kimball, *Phys. Rev. A* **7**, 1648 (1973).
- [23] E. R. Davidson, *Reduced Density Matrices in Quantum Chemistry*, Academic Press, 1976.
- [24] C. Lee, W. Yang, and R. G. Parr, *Phys. Rev. B* **37**, 785 (1988).
- [25] A. D. Becke, *Phys. Rev. A* **38**, 3098 (1988).
- [26] J. P. Perdew and W. Yue, *Phys. Rev. B* **33**, 8800 (1986).
- [27] H. Lee, C. Lee, and R. G. Parr, *Phys. Rev. A* **44**, 768 (1991).
- [28] G. J. Laming, V. Termath, and N. C. Handy, *J. Chem. Phys.* **99**, 8765 (1993).
- [29] A. D. Becke, *J. Chem. Phys.* **84**, 4524 (1986).
- [30] A. D. Becke, *J. Chem. Phys.* **85**, 7184 (1986).
- [31] A. E. DePristo and J. D. Kress, *J. Chem. Phys.* **86**, 1425 (1987).
- [32] J. P. Perdew, J. A. Chevary, S. H. Vosko, K. A. Jackson, M. R. Pederson, D. J. Singh, and C. Fiolhais, *Phys. Rev. B* **46**, 6671 (1992).
- [33] M. Levy and J. P. Perdew, *Phys. Rev. B* **48**, 11638 (1993).
- [34] A. D. Becke, *J. Chem. Phys.* **97**, 9173 (1992).
- [35] B. Meihlich, A. Savin, H. Stoll, and H. Preuss, *Chem. Phys. Lett.* **157**, 200 (1989).
- [36] P. Csavinszky, *Int. J. Quant. Chem.* **33**, 265 (1988).
- [37] C. Lee, G. Fitzgerald, and W. Yang, *J. Chem. Phys.* **98**, 2971 (1993).

[38] A. D. Becke, J. Chem. Phys. **98**, 1372 (1993).

[39] A. D. Becke, J. Chem. Phys. **98**, 5648 (1993).

3. Comparison of Electron Densities

The use of computational chemistry to research new aspects of chemistry or to support experimental work has increased dramatically. A significant factor for this increase is the recent advances within density functional theory (DFT) which yield results comparable with other high-level theories.^{1,2} This coupled with the computational efficiency of DFT calculations has increased the number of systems which can now be studied.

Even though many improvements have been made to DFT, it is still thought to be in its infancy and new functionals are constantly being proposed. The molecular properties found using any functional, though, is dependent upon the calculated electron densities and thus it is imperative that they yield an accurate density. Therefore, any information which can be used to improve the electron densities calculated using approximate DFT functionals is valuable. One method of obtaining information about the DFT electron densities is to compare calculated DFT densities with the electron density of a method which is known to give accurate molecular properties.³ However, comparison of electron densities is not straightforward which makes the process of assessing the functional's accuracy difficult.

A simple, yet limited, way to compare electron densities, the density difference

plot, has previously been shown to give good qualitative results when comparing densities.⁴⁻⁶ Through the use of an illustrative example the use of these plots is studied and the results explained. These results indicate that with a small modification a quantitative measure of the density differences can be calculated. This quantitative value can then be used to optimise a new exchange-correlation functional and hopefully to improve the calculated DFT density. A preliminary investigation of this modification and a study of a new functional is presented after the density difference plots.

3.1 Obtaining Electron Densities from Wavefunctions

Before any comparison of electron densities can be accomplished, the method used to obtain electron densities from the various calculations must be described. The DFT electron density can be calculated using the Kohn-Sham orbitals⁷ (see section 2.6) with the expression,

$$\rho(\mathbf{x}_1) = \sum_i^N \eta_i |\chi_i(\mathbf{x}_1)|^2 \quad (3.1)$$

Here η_i is the occupation number and N is the number of orbitals. For methods based on the HF ground-state wavefunction, though, the electron density is a function of the electronic wavefunction.^{8,9} Given an overall wavefunction, $\Psi(\mathbf{x}_1, \mathbf{x}_2, \dots, \mathbf{x}_N)$, the electron density is obtained using the expression,

$$\rho(\mathbf{x}_1) = N \int \Psi(\mathbf{x}_1, \mathbf{x}_2, \dots, \mathbf{x}_N) \Psi^*(\mathbf{x}_1, \mathbf{x}_2, \dots, \mathbf{x}_N) d\mathbf{x}_2 d\mathbf{x}_3 \dots d\mathbf{x}_N \quad (3.2)$$

A more generalised version of this function has been developed since the above function proves problematic for the calculation of one-electron properties.^{7,10} This single-

particle density function is given by:

$$\rho_1(\mathbf{x}_1; \mathbf{x}'_1) = N \int \Psi(\mathbf{x}_1, \mathbf{x}_2, \dots, \mathbf{x}_N) \Psi^*(\mathbf{x}'_1, \mathbf{x}_2, \dots, \mathbf{x}_N) d\mathbf{x}_2 d\mathbf{x}_3 \dots d\mathbf{x}_N \quad (3.3)$$

Obviously the single-particle density function reduces to the electron density function when $\mathbf{x}'_1 = \mathbf{x}_1$.

Calculation of the single-particle density for multi-determinant wavefunctions is quite difficult. For these methods a unitary transform is applied to the molecular orbitals such that the resulting orbitals have the property,

$$\rho_1(\mathbf{x}_1; \mathbf{x}'_1) = \sum_{i=1}^M \lambda_i \psi_i(\mathbf{x}_1) \psi_i^*(\mathbf{x}'_1) \quad (3.4)$$

where M is the number of transformed orbitals. This new set of molecular orbitals, called the natural orbitals, are then used to calculate the single-particle electron density.

3.2 Density Difference Plots

One of the simplest methods to contrast electron densities is to compare them visually with density difference plots.⁴⁻⁶ To create these graphs wavefunctions or the DFT Kohn-Sham orbitals for a molecule are obtained and the corresponding electron densities are calculated. Then a one- or two-dimensional grid is set up and the electron densities are evaluated at every point on the grid. Finally, at each point on the grid the difference between two electron densities is calculated and the results are plotted.

To simplify the comparison of many methods a single method's electron density is used as a standard against which all other methods are compared. However, theoretical results are usually compared to available experimental data to determine their

accuracy. Since, experimental electron densities are not available the chosen standard method should be known to yield a good approximation of other experimental results. The quadratic configuration interaction method including single and double excitations (QCISD)¹¹ is one such method and was chosen as the standard in the following example.

3.2.1 An Illustrative Example: Density Difference Plots for C_2H_n , $n=2,4,6$ and C_6H_6

The Gaussian 94¹² computational package was used to calculate the densities for each of the four molecules at the experimental geometries. The aug-CC-PVDZ¹³ basis set was employed for the calculation of ethyne, ethene and ethane but due to computational restraints the smaller CC-PVDZ¹³ basis set was used for the benzene calculations. A regular rectangular grid with 200 points in both the x and y directions was then positioned to include a carbon-carbon bond midpoint in each molecule and two hydrogen atomic centres. Electron densities were calculated at each point on the grid sampling a 10 a.u. by 10 a.u. area centred at the chosen carbon-carbon bond midpoint. Density differences were then calculated at each point on the grid and contour plots of the results were obtained. A second plot was also obtained along the carbon-carbon bond axis by calculating the density differences at regular intervals 5 a.u. in either direction from the bond midpoint.

The first plots examined were those from the non-hybrid functionals used in the study, the local spin density exchange and correlation functional, using the Vosko, Wilk and Nusair parameterisation of the correlation energy, SVWN,^{14,15} the Becke 1988 gradient-corrected exchange functional¹⁶ combined with the Lee, Yang and Parr gradient-corrected correlation functional,¹⁷ BLYP, and finally the Becke 1988

gradient-corrected exchange functional combined with the Perdew 1986 gradient-corrected correlation functional,¹⁸ BP86. All of the density difference plots along the carbon-carbon bonds, seen in figures 3.1, 3.2 and 3.3, have a similar outline for these functionals. Negative density differences are observed close to the carbon atoms and then from this minimum value the density differences increase to a maximum value at the bond midpoint. Although the plots are similar in shape, differences are observed both between functionals and between molecules. The density differences given by the SVWN functional near the carbon atoms are the most negative of all three functionals and also yield the largest maximum values at the bond midpoint. For BLYP and BP86 the density difference ranges are much smaller than the SVWN case but only small differences near the carbon atoms and the bond midpoint are seen between the two functionals. For the four molecules studied the density difference plots are organised with respect to increasing bond length and therefore with respect to decreasing electron density within the bond. Ethyne, which has the shortest bond length and thus the most electron density within the bond, exhibits the largest negative density differences near the carbon atoms and a substantial negative density difference at the bond midpoint for all methods. As the bond length increases and the electron density within the bonding region decreases the density differences near the carbon atoms and at the bond midpoint both increase. The magnitude of these increases are dependent upon which functional is used but positive density differences are observed at the bond midpoint of ethane for all methods. Positive density differences are also observed at the bond midpoint of ethene, with SVWN only, and benzene, with SVWN and BP86. This may suggest that these functionals underestimate the electron density in the carbon-carbon σ bond but overestimate the π bond electron density. The magnitude of this overestimation and underestimation,

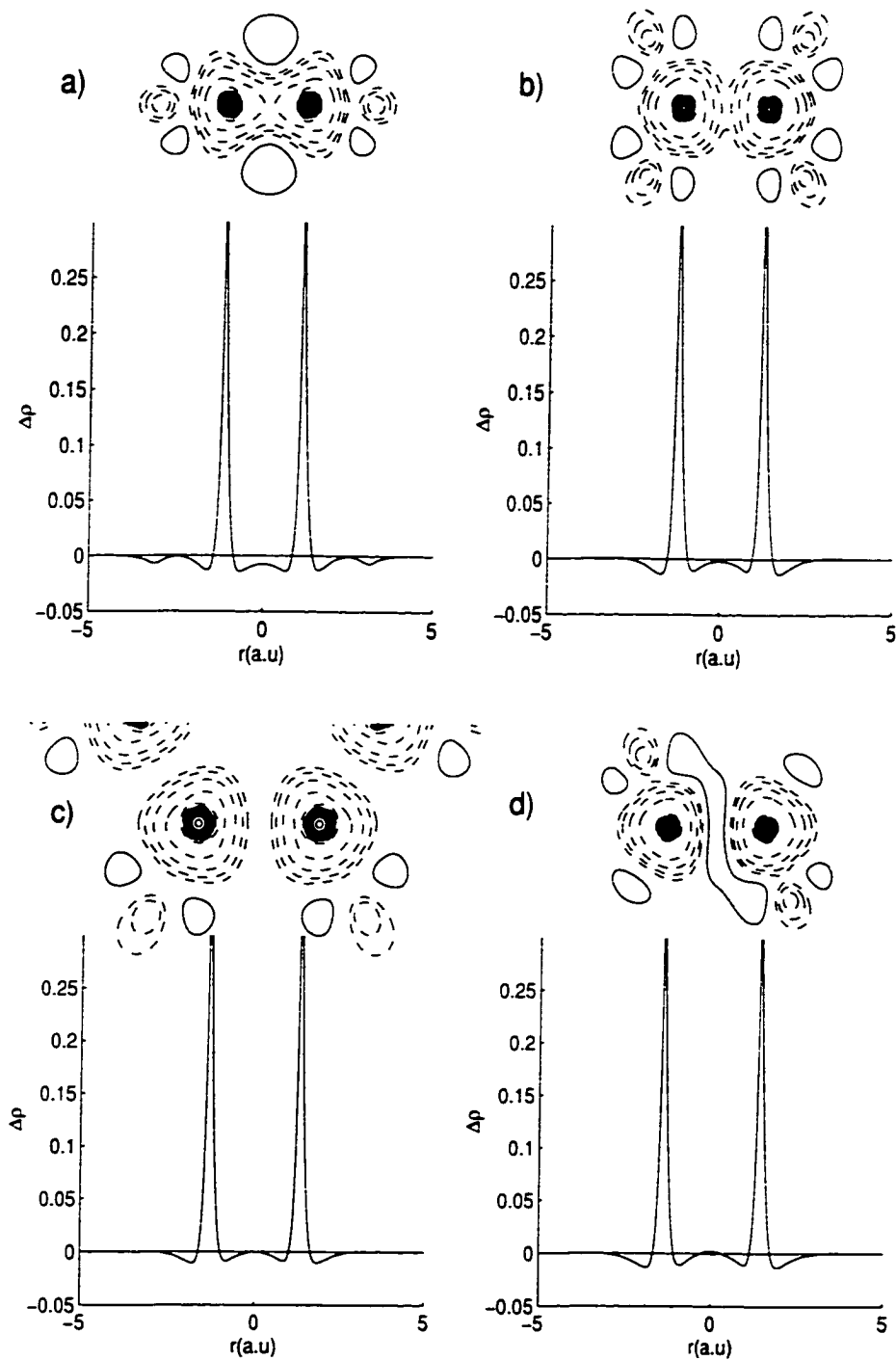


Figure 3.1: QCISD-BLYP density difference plots for C_2H_2 (a), C_2H_4 (b), C_6H_6 (c) and C_2H_6 (d).

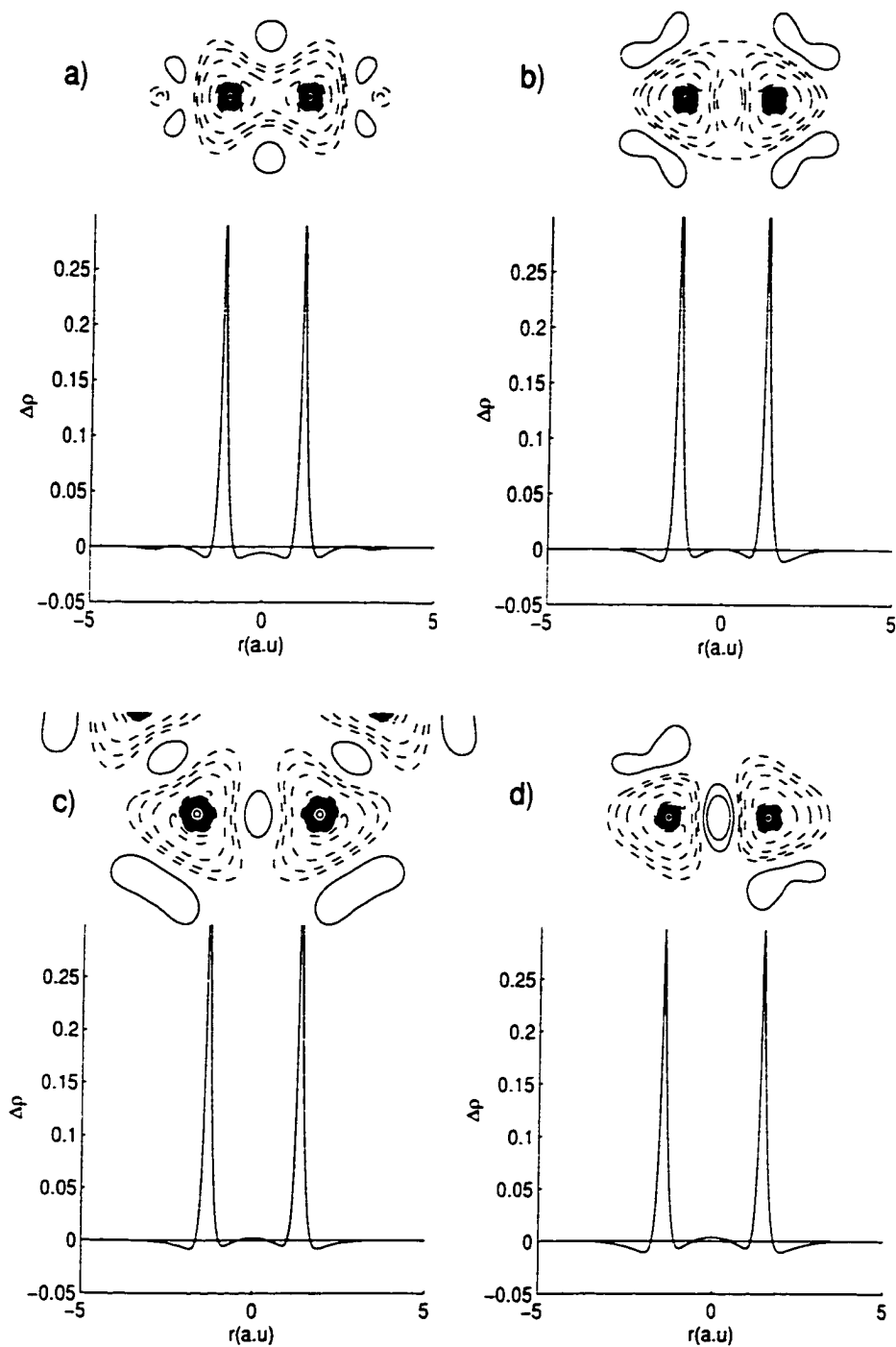


Figure 3.2: QCISD-BP86 density difference plots for C_2H_2 (a), C_2H_4 (b), C_6H_6 (c) and C_2H_6 (d).

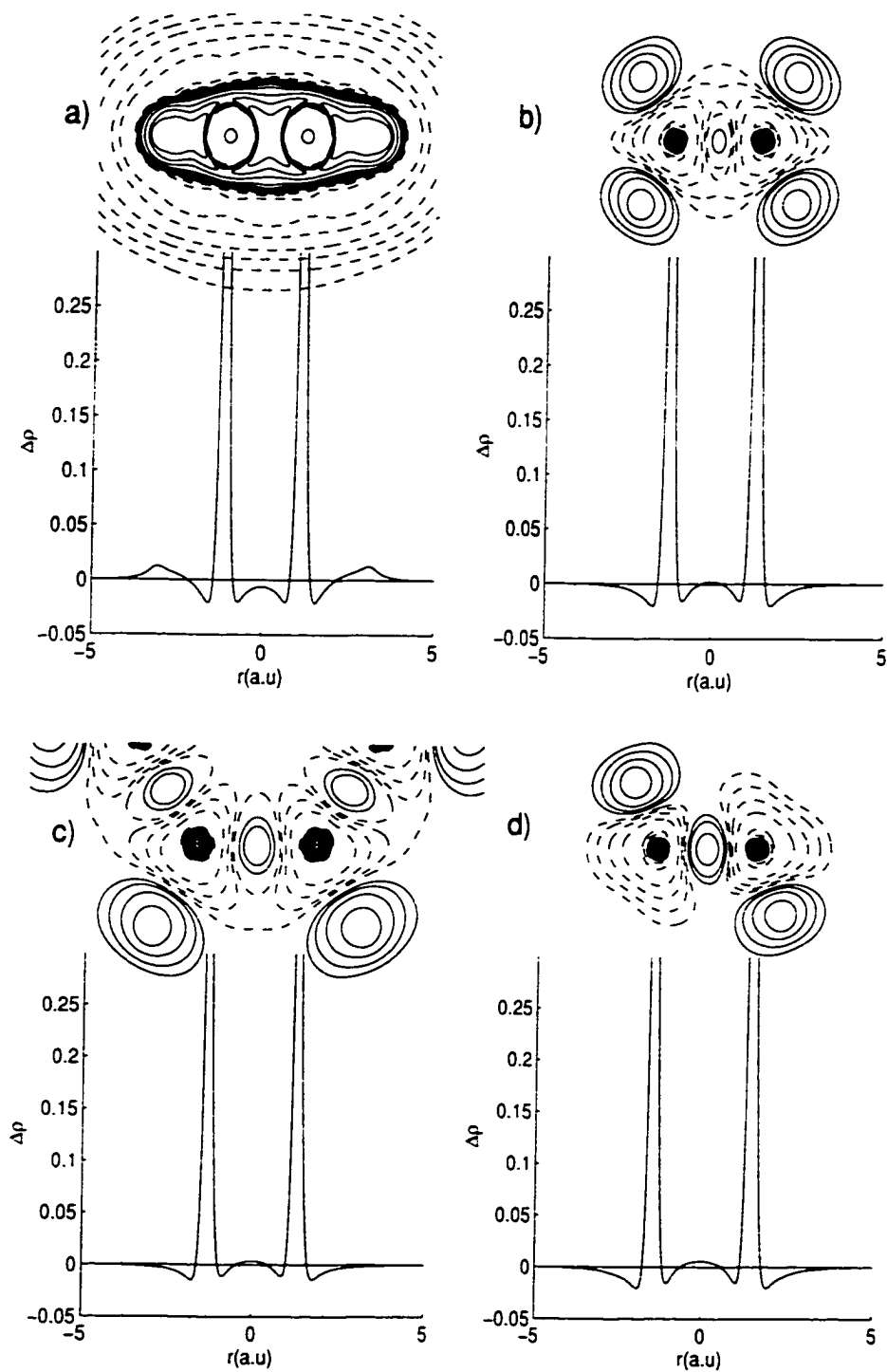


Figure 3.3: QCISD-SVWN density difference plots for C_2H_2 (a), C_2H_4 (b), C_6H_6 (c) and C_2H_6 (d).

though, is functional dependent. The final and most prominent feature of the density difference plots along the carbon-carbon bonds is the very large spikes of positive density differences near the carbon atoms. These large differences in core electron density may not prove to be too problematic since the core density is usually not as chemically significant as the valence electron density. However, the large differences will make it difficult to calculate properties which need a good estimation of the core electron density, such as the hyperfine coupling constant.¹⁹

By examining the planar density difference plots, the behaviour of the functionals within the carbon-hydrogen bonding region and around the carbon and hydrogen atoms can be assessed. Unlike the carbon-carbon bonding region the density difference within the carbon-hydrogen bonding regions are relatively independent of the molecule but are still dependent on the functional used. The BLYP functional underestimates the electron density around the hydrogen atom giving observable positive density differences but moving within the bonding region the density differences become very close to zero. BP86 gives a better description of the hydrogen atoms, with no discernible density difference contours, but tends to slightly underestimate the electron density within the carbon-hydrogen bond. Finally, the SVWN functional has the most interesting behaviour with large negative density differences near the carbon atom which increase throughout the bond to finally give substantial positive values around the hydrogen atom. Two other notable features are also observed in the planar density difference plots. The first feature is exhibited by all functionals in all molecules and is a region of negative density differences surrounding the carbon atoms. The shape of these regions differs between molecules while the size of these regions differs between functionals with SVWN giving the largest areas and BLYP the smallest. The other feature is only exhibited in the BLYP and BP86 plots which yield

small areas of positive density differences adjacent to the carbon-hydrogen bonding region of all molecules and adjacent to the carbon-carbon bonding region of ethyne.

The hybrid functionals used in this study are based upon the Becke three-parameter expression for the inclusion of HF exchange energy²⁰ and use either the Lee, Yang and Parr gradient-corrected correlation functional, B3LYP, or the Perdew 1986 gradient-corrected correlation functional, B3P86. These two functionals lead to an improvement over the results obtained with the non-hybrid functionals and yield electron densities with the best overall qualitative agreement with the QCISD electron density (see figures 3.4 and 3.5). The outlines of the plots along the carbon-carbon bonds are similar to those of the non-hybrid functionals with the minimum values near the carbon atom moving to a maximum at the bond midpoint. However, the range of density differences is much smaller with the hybrid functionals which yield a flatter graph. This leads to bond midpoint values which are very close to zero for ethene, benzene and ethane and only one bond midpoint value with a positive density difference, observed in ethane using the B3P86 functional. This indicates an improvement in the calculation of the electron density in both the σ and π bonds. Finally, the very large positive density differences at the carbon atomic centres are also still present with only slightly smaller maximum values.

The planar density difference plots again show many improvements over the non-hybrid plots with notable changes around the carbon-hydrogen bonding regions. B3LYP continues to overestimate the electron density around the hydrogens but the areas of negative density differences are much smaller than those shown with BLYP. However, negative density differences are now found within the bonding region instead of the region of zero density differences exhibited with BLYP. For B3P86 the density differences around the hydrogen and within the bonding region are approximately

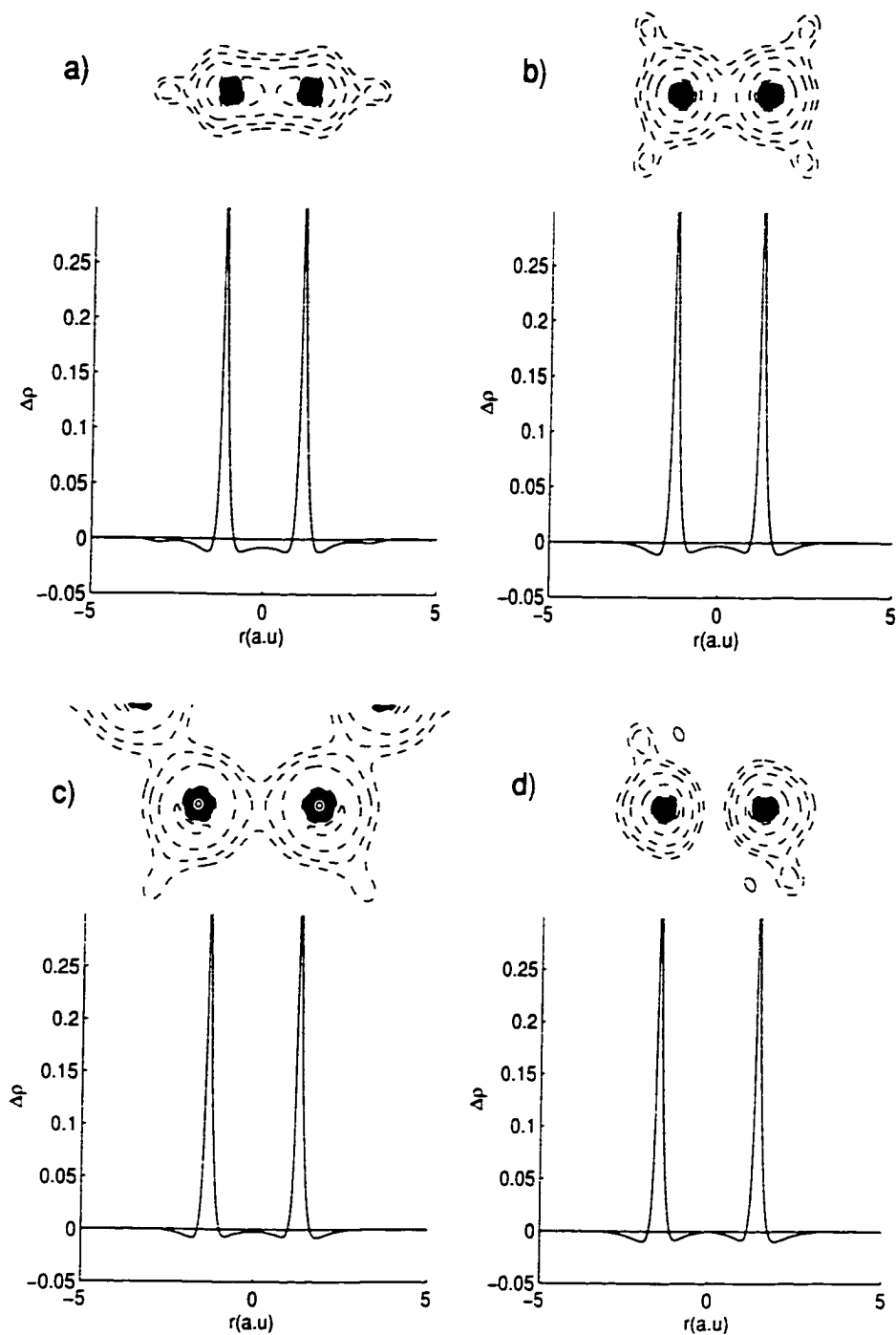


Figure 3.4: QCISD-B3LYP density difference plots for C_2H_2 (a), C_2H_4 (b), C_6H_6 (c) and C_2H_6 (d).

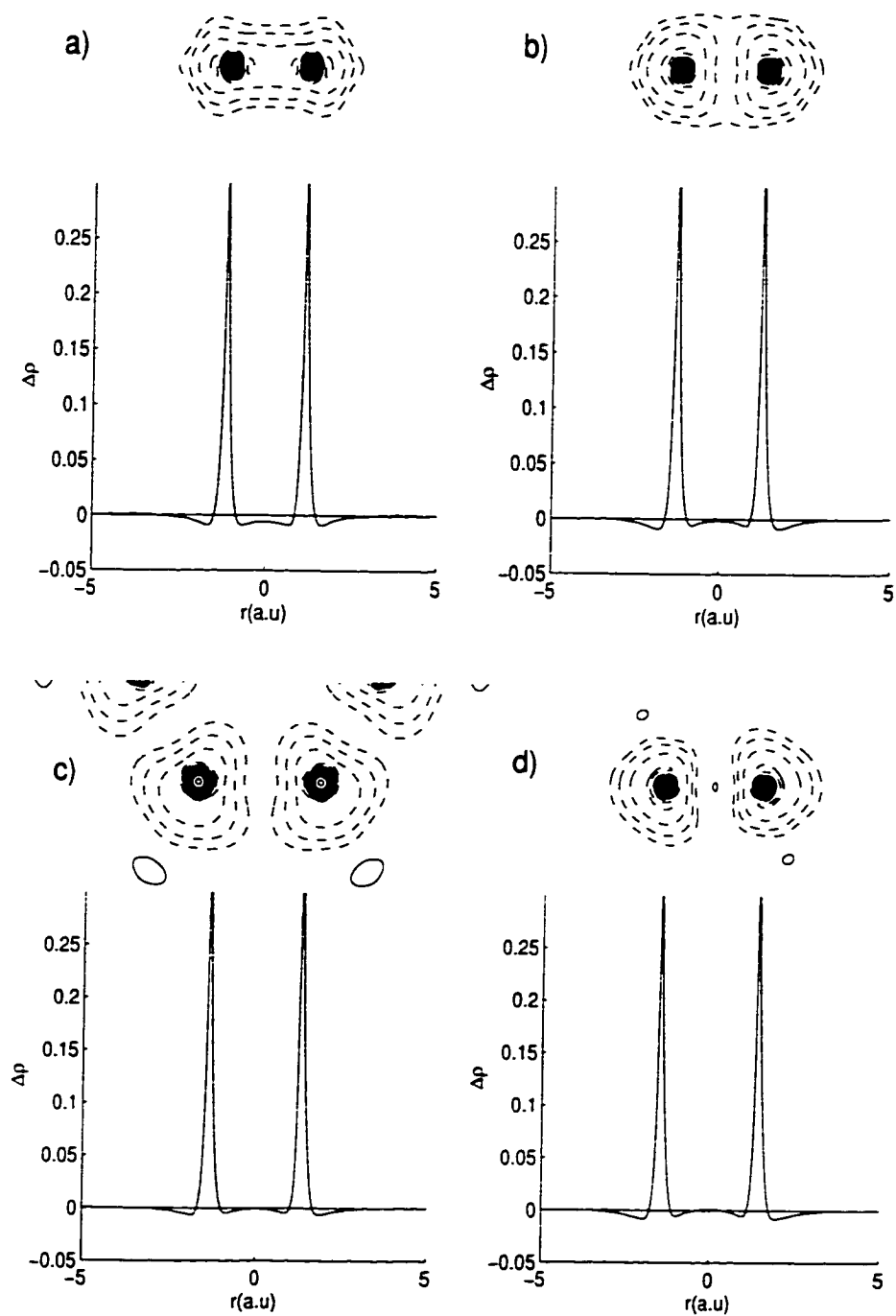


Figure 3.5: QCISD-B3P86 density difference plots for C_2H_2 (a), C_2H_4 (b), C_6H_6 (c) and C_2H_6 (d).

zero for ethyne and ethene but small areas of positive density differences are observed around the hydrogens of benzene and ethane. Missing from the planar density difference plots of the hybrid functionals are the regions of positive density differences around the hydrogen bonds and around the carbon-carbon bond of ethyne. Unfortunately, though, the region around the carbon shows no noticeable improvements with negative density differences that are approximately the same size and shape.

HF and MP2 yield results, as shown in figures 3.6 and 3.7 which are much different than those exhibited by the various DFT functionals. The plots comparing the HF density with the QCISD density along the carbon-carbon bonds are not very dependent on the molecule being studied. These plots exhibit small positive density differences at the carbon centres which decrease moving towards the bond midpoint. The density difference passes through zero at a point about one quarter of the way towards the bond midpoint and continues to decrease to a minimum value at the bond midpoint. The MP2 plots as expected improve upon the HF plots with very small negative density difference values at the carbon centres. Within the bond the density differences are very close to zero with only a couple of molecules showing small positive density differences. The small observed density differences in both plots are probably due to the fact that the QCISD and MP2 electron densities are derived from the HF density. Thus only small perturbations due to electron correlation should be observed within the electron density.

The planar density difference plots exhibit the large differences between the HF and QCISD densities. Large areas of positive density differences are observed around each carbon and hydrogen atom along with large areas of negative density differences within the bonding regions. The size and shapes of these regions vary depending on the molecule. However, the areas of positive density differences around the carbon

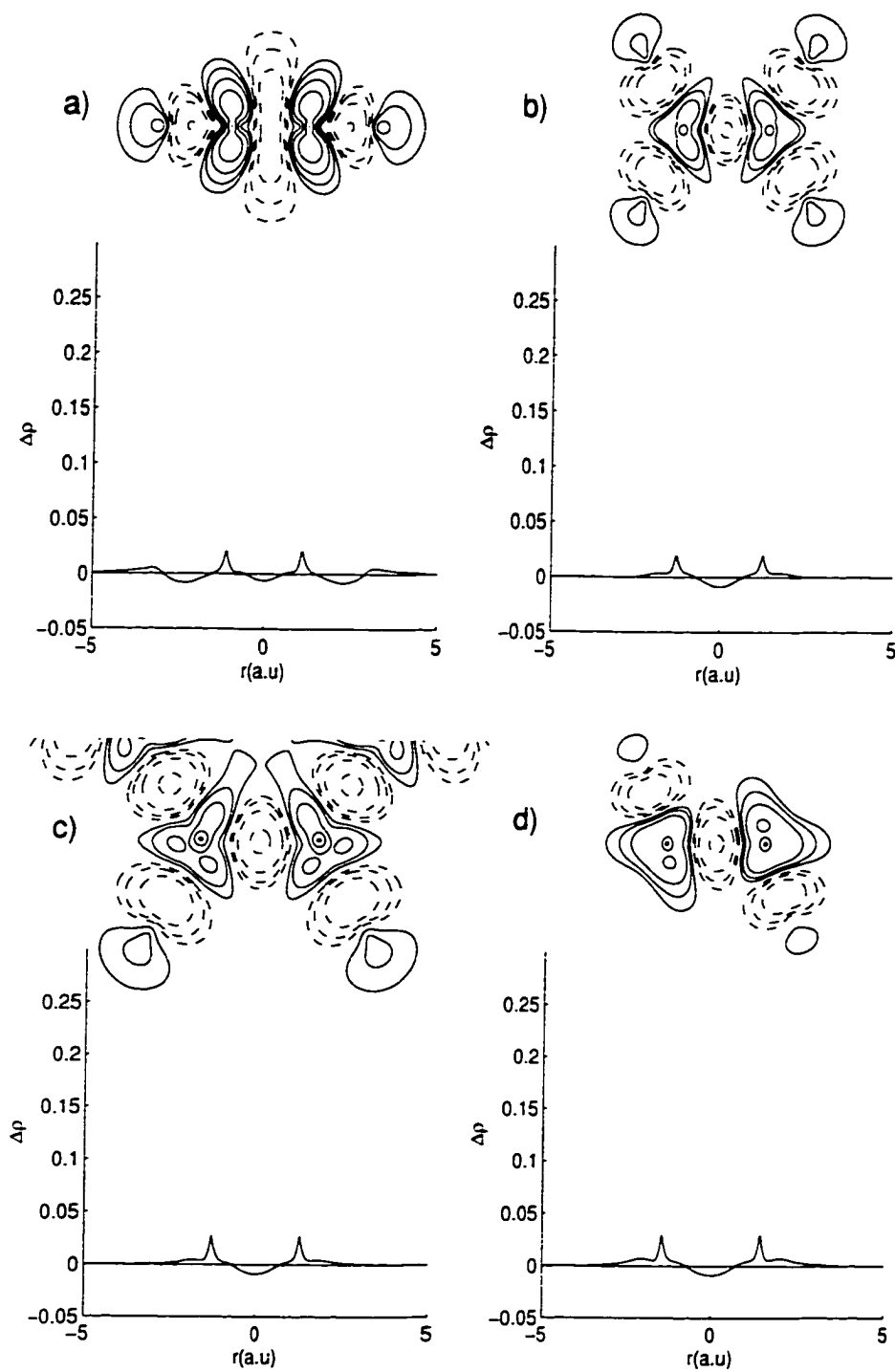


Figure 3.6: QCISD-HF density difference plots for C_2H_2 (a), C_2H_4 (b), C_6H_6 (c) and C_2H_6 (d).

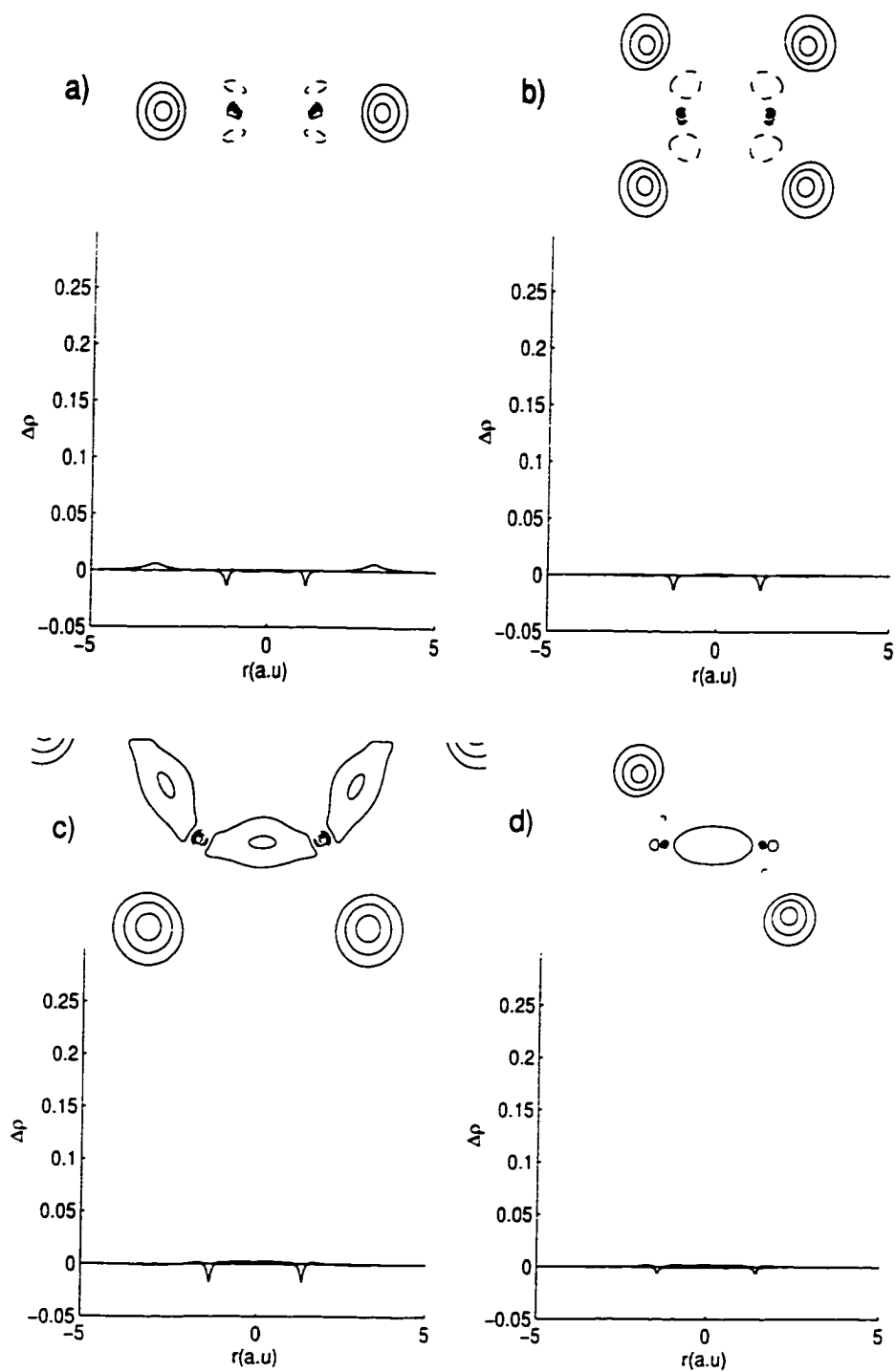


Figure 3.7: QCISD-MP2 density difference plots for C_2H_2 (a), C_2H_4 (b), C_6H_6 (c) and C_2H_6 (d).

atoms tend to occupy the surrounding non-bonding regions while for the hydrogen atoms the positive density differences are found to point away from the bonding regions. While the negative density difference regions tend to occupy large areas in and around the bonds. The MP2 plots are much improved with only very few areas with any discernible density differences. The only feature found in all four molecules are the regions of positive density differences around the hydrogen atoms. Other noteworthy features are the small areas of negative density differences to either side of the carbon atoms in ethyne and ethene and the very small region of positive density differences close to the carbon atoms in ethane.

3.3 Expanding on the Density Difference Plot: Reoptimising the Becke Three-Parameter Expression

The results of density difference plots indicated that through a simple process information about an electronic density could be obtained. However, density difference plots by their very nature are qualitative and cannot be automated and therefore have a narrow focus. A simple method, though, can be extrapolated from these plots to quantitatively assess the difference between two electron densities. This method involves calculating the electron density of a molecule using two different methods at its experimental geometry. Then the densities are evaluated at each point on a large three-dimensional grid and the difference between the two values is calculated. Finally, all of the differences over the grid are summed to give a quantitative measure of the density difference. This method apart from being quantitative is also easily automated and thus can be used as a tool to analyse and improve exchange-correlation energy functionals.

To study the effectiveness of this expression of the density difference a hybrid

functional of the form,

$$E_{xc} = AE_{HF}^x + B(E_x^{LSDA} + \Delta E_x^{B88}) + C(E_c^{LSDA} + \Delta E_c^{P86}) \quad (3.5)$$

was optimised to find the values for A , B , and C which gave the smallest quantitative density differences. To find the optimum values of A , B , and C , densities were calculated using this functional and were compared to the calculated QCISD density using the method above. Using a least-squares fit the difference between the two densities was minimised and the optimum values were found. Since, A , B and C are optimised with respect to the QCISD density, molecular properties calculated with the optimum values should be in good agreement with calculated QCISD properties. The form of this hybrid functional is similar to Becke's three-parameter expression²⁰ but has one important difference being that it does not recover the uniform electron gas limit.

For this investigation electron densities and molecular properties were calculated using the Gaussian 92/DFT²¹ and the Gaussian 94¹² computational packages. All calculations were carried out using Dunning's aug-CC-PVDZ basis set.¹³ For the O₂ system the spin unrestricted cases of QCISD¹¹ and DFT were used. The regular rectangular grid used for these calculations had 150 points in each of the x, y, and z directions. The sampling was carried out in a cube with 4 Å sides. A point-by-point comparison between the QCISD and the DFT densities was then performed and the root-mean-square average was calculated. The minimum for the average density difference was then found using a golden section search.

Geometry optimisations and frequency calculations were then performed using the optimised values of A , B , and C . The results from these calculations were then compared to QCISD, B3P86¹⁸ and experimental values.

3.4 Results and Discussion

Table 3.1 shows the optimised values for A , B , and C obtained for H_2 , N_2 , O_2 , F_2 , CO and HF . As can be seen the values for A and B , which correspond to the exact exchange energy and the density functional exchange energy, are similar for each molecule. However, the value for C , which corresponds to the density functional correlation energy, varies by a large amount, from 0.993 for O_2 to 0.322 for F_2 . This range in the value of C makes it difficult to create a set of universal parameters for this functional. However, since the correlation energy is approximately an order of magnitude smaller than the exchange energy the fluctuation in C is less critical.

Table 3.1: Optimised parameters for H_2 , N_2 , O_2 , F_2 , CO and HF .

	H_2	N_2	O_2	F_2	CO	HF	Ave.
A	0.267	0.252	0.233	0.245	0.245	0.245	0.247
B	0.721	0.721	0.713	0.721	0.717	0.721	0.719
C	0.789	0.515	0.993	0.322	0.488	0.811	0.653

The molecular properties, shown in table 3.2, calculated using the optimised parameters are encouraging with the optimised values generally being in better agreement with QCISD than B3P86. It is important to note that comparisons are to the calculated QCISD results and not to experimental values since the new functionals parameters were optimised with respect to the QCISD density. Under this type of comparison the B3P86 functional may not perform as well as the new functional since it was optimised with respect to experimental data. The O_2 , N_2 , and F_2 bond lengths were between 0.001 to 0.007 Å shorter with the new functional when compared to the QCISD values while B3P86 underestimates the bond lengths by 0.012 to 0.036 Å, for the same molecules. The shortening of the bond lengths yields the expected overestimation in the associated calculated frequencies with the optimised parameters giving

frequencies that are 36 to 102 cm^{-1} too large while the B3P86 frequencies range from being 85 to 141 cm^{-1} too large. Both functionals give good agreement for the H_2

Table 3.2: Comparison of results obtained using optimised values of A , B and C with B3P86, QCISD and experimental results.

		B3P86	Optimised	QCISD	Experiment ^a
H_2	r_e	0.760	0.762	0.761	0.741
	ν	4373	4350	4349	4401
N_2	r_e	1.103	1.112	1.115	1.098
	ν	2459	2410	2374	2360
O_2	r_e	1.202	1.214	1.221	1.207
	ν	1684	1645	1543	1580
F_2	r_e	1.389	1.424	1.425	1.417
	ν	1055	987	924	891
HF	r_e	0.922	0.930	0.922	0.917
	ν	4130	4053	4118	4139
	μ	1.800	1.799	1.801	1.82
CO	r_e	1.132	1.145	1.142	1.128
	ν	2201	2135	2134	2170
	μ	0.095	0.080	0.065	0.112

^a From ref. ²

and CO bond lengths with only small underestimations, B3P86 by 0.001 and 0.010 Å respectively, and the optimised functionals by 0.001 and 0.003 Å, respectively. However, the B3P86 frequencies overestimate those calculated using QCISD by 24 cm^{-1} for H_2 and 67 cm^{-1} for CO while the functionals using the different optimised parameters yield frequencies only 1 cm^{-1} larger than QCISD for both molecules. HF is the only exception with B3P86 molecular properties being in better agreement with QCISD than the optimised functional. However, the results from the optimised functional, a lengthening of the bond by 0.008 Å and a lowering of the frequency by 63 cm^{-1} , are consistent with the magnitudes of the differences shown in the other molecules and it is the only case where the optimised parameters overestimate the bond length by a significant amount.

A closer examination of the electron density differences for the HF case is shown in figures 3.8 and 3.9. Like the previous plots the density differences are calculated in the plane of the molecule and along the hydrogen-fluorine bond. Large positive density differences are observed near the heavy atom, fluorine, with B3P86 exhibiting a maximum of approximately 0.6 a.u. while the optimised parameters give a maximum of just over 0.8 a.u. indicating that B3P86 gives a better description of the core electron density. However, the optimised functional exhibits a much more rapid de-

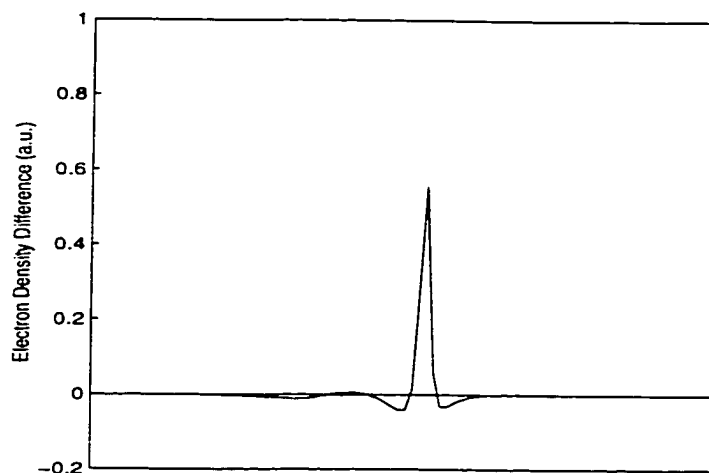
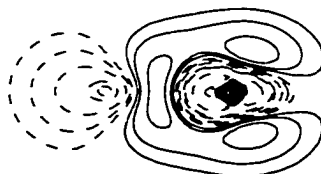


Figure 3.8: QCISD-B3P86 density difference plots for HF.

crease in the density differences around the fluorine atom. This may indicate that the valence electron density may be more heavily weighted than the core electron density during the optimisation step. So in molecules for which the core electron density is

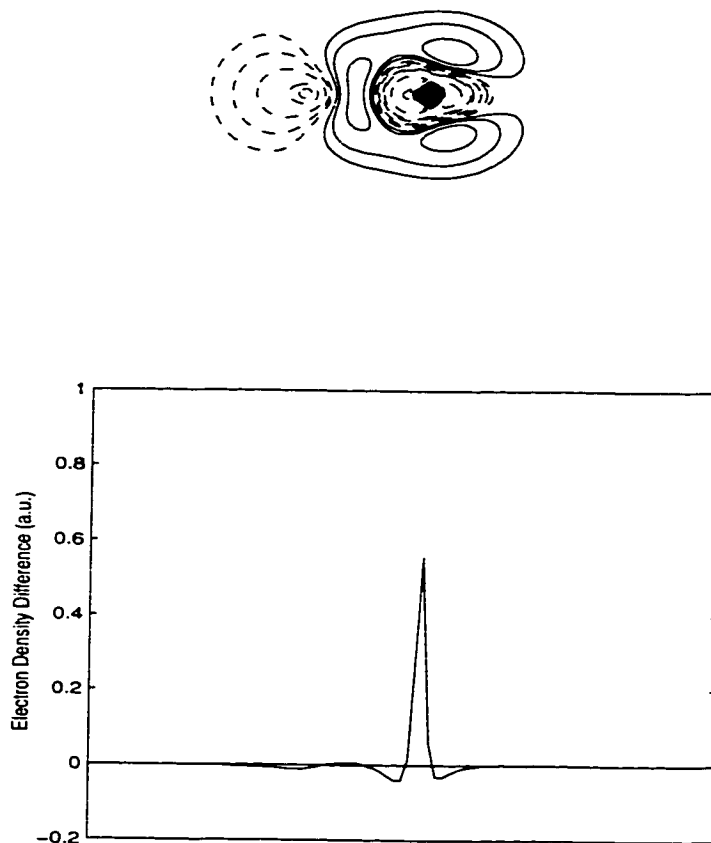


Figure 3.9: QCISD-new hybrid functional density difference plots for HF.

important, such as HF which has a high ionic character, the optimised parameters may not perform as well as other functionals. However, for molecules which don't have as much dependence on the core and depend more on its valence density then the optimised parameters may perform as well if not better than B3P86.

Table 3.3 gives the energetics for the functionals using the optimised parameters and also for B3P86. This table also exhibits the convergence of the optimised parameters towards the QCISD values. Clearly, there is still room for improvement. However, a new method for comparing densities is needed since the proposed method is inadequate. Finally, the B3P86 energies generally are in better agreement with experiment than the other two values.

Table 3.3: Comparison of total energies calculated at the experimental geometries.

	B3P86	Optimised	QCISD	Experiment*
H ₂	-1.21039	-1.18329	-1.16461	-1.1635 ²²
N ₂	-109.78475	-109.06938	-109.28666	-109.5376
O ₂	-150.62711	-149.76003	-149.96215	-150.3224
F ₂	-199.84525	-198.47879	-199.14297	-199.5214
HF	-100.63615	-100.18687	-100.26407	-100.4563 ²³
CO	-113.57002	-112.68346	-113.06883	-113.3199

*energies calculated from

$$\sum E_{atoms}^{expt} - (E^{Rel} + MassCorr. + LambCorr.) + D_0^{expt23-26}$$

3.5 Conclusions

The use of density difference plots has helped to give a good qualitative picture of the performance of current DFT functionals. The present study shows that although current DFT functionals give good approximations of the electron densities problems do arise most significantly near heavy atomic centres and in the regions surrounding them. Also, DFT functionals tend to give good approximations of the densities near bond midpoints but tend to overestimate the density when moving from the midpoint towards an atomic centre. However, the plots are not without limitations yielding only quantitative results and having to be done visually.

Expanding on the density difference plots by calculating a quantitative value yielded a new tool to compare densities. This tool allowed for the optimisation of a new hybrid functional which yielded encouraging results. The optimum parameters exhibited properties which tended to converged to the QCISD density as would be expected. However, all of the calculations used the optimised parameters found for each molecule and a recalculation of optimum parameters for every new molecule is not feasible. Unfortunately the average values found from the molecules studied fared poorly and their results are not shown. A study with more molecules may come up

with more universal values but the large fluctuation in the value of C is disconcerting. This functional may still yield better results but before continuing with the design of new functionals new methods and tools for comparing densities are needed. The following chapters outline a few such techniques and will hopefully yield better results.

References

- [1] C. W. Bauschlicher, Jr., *Chem. Phys. Lett.* **246**, 41 (1995).
- [2] B. G. Johnson, P. M. W. Gill, and J. A. Pople, *J. Chem. Phys.* **98**, 5612 (1993).
- [3] M. Sola, J. Mestres, R. Carbó, and M. Duran, *J. Chem. Phys.* **104**, 636 (1996).
- [4] J. Wang, L. A. Eriksson, B. G. Johnson, and R. J. Boyd, *J. Phys. Chem.* **100**, 5274 (1996).
- [5] J. Wang, B. G. Johnson, R. J. Boyd, and L. A. Eriksson, *J. Phys. Chem.* **100**, 6317 (1996).
- [6] J. Wang, Z. Shi, R. J. Boyd, and C. A. Gonzalez, *J. Phys. Chem.* **98**, 6988 (1994).
- [7] R. G. Parr and W. Yang, *Density-Functional Theory of Atoms and Molecules*, Oxford University Press, 1989.
- [8] R. McWeeny, *Methods of Molecular Quantum Mechanics*, Academic Press, 1989.
- [9] K. B. Wiberg, C. M. Hadad, T. J. LePage, C. M. Breneman, and M. J. Frisch, *J. Phys. Chem.* **96**, 671 (1992).
- [10] E. R. Davidson, *Reduced Density Matrices in Quantum Chemistry*, Academic Press, 1976.

- [11] J. A. Pople, M. Head-Gordon, and K. Raghavachari, *J. Chem. Phys.* **87**, 5968 (1987).
- [12] M. J. Frisch, G. W. Trucks, H. B. Schlegel, P. M. W. Gill, B. G. Johnson, M. A. Robb, J. R. Cheeseman, T. A. Keith, G. A. Petersson, J. A. Montgomery, K. Raghavachari, M. A. Al-Laham, V. G. Zakrzewski, J. V. Ortiz, J. B. Foresman, J. Cioslowski, B. B. Stefanov, A. Nanayakkara, M. Challacombe, C. Peng, P. Y. Ayala, W. Chen, M. W. Wong, J. L. Andres, E. S. Repogle, R. Gomperts, R. L. Martin, D. J. Fox, J. S. Binkley, D. J. DeFrees, J. Baker, J. P. P. Stewart, M. Head-Gordon, C. Gonzalez, and J. A. Pople, *Gaussian 94*, Gaussian, Inc.: Pittsburgh PA, 1995.
- [13] R. A. Kendall and T. H. Dunning, Jr., *J. Chem. Phys.* **96**, 6796 (1992).
- [14] P. A. M. Dirac, *Proc. Cambridge Phil. Soc.* **36**, 376 (1930).
- [15] S. H. Vosko, L. Wilk, and M. Nusair, *Can. J. Phys.* **58**, 1200 (1980).
- [16] A. D. Becke, *Phys. Rev. A* **38**, 3098 (1988).
- [17] C. Lee, W. Yang, and R. G. Parr, *Phys. Rev. B* **37**, 785 (1988).
- [18] J. P. Perdew and W. Yue, *Phys. Rev. B* **33**, 8800 (1986).
- [19] S. D. Wetmore, R. J. Boyd, and L. A. Eriksson, *J. Chem. Phys.* **106**, 7738 (1997).
- [20] A. D. Becke, *J. Chem. Phys.* **98**, 5648 (1993).
- [21] M. J. Frisch, G. W. Trucks, H. B. Schlegel, P. M. W. Gill, B. G. Johnson, M. W. Wong, J. B. Foresman, M. A. Robb, M. Head-Gordon, E. S. Repogle, R. Gomperts, J. L. Andres, K. Raghavachari, J. S. Binkley, C. Gonzalez, R. L.

- Martin, D. J. Fox, D. J. DeFrees, J. Baker, J. P. P. Stewart, and J. A. Pople, Gaussian 92/DFT, 1993.
- [22] J. A. Pople and J. S. Binkley, *Mol. Phys.* **29**, 599 (1975).
- [23] G. A. Petersson, A. Bennett, T. G. Tensfeldt, M. A. Al-Laham, and W. A. Shirley, *J. Chem. Phys.* **89**, 2193 (1988).
- [24] G. Herzberg and K. P. Huber, *Molecular Spectra and Molecular Structure IV Constants of Diatomic Molecules*, Van Nostrand Reinhold Company, New York, 1979.
- [25] A. Veillard and E. Clementi, *J. Chem. Phys.* **49**, 2415 (1968).
- [26] E. Clementi, *IBM J. Res. Dev.* **9**, 2 (1965).

4. An Orbital-Based Density Difference Index

The accuracy of approximate functionals for use in density functional theory (DFT) has usually been based on the comparison of total electronic energies and other molecular properties with experiment or high-level theoretical methods which are known to give accurate results.¹ Although some functionals have exhibited good agreement with these high-level methods with respect to energies and molecular properties,^{2,3} very little is known about the accuracy of DFT electron densities.

Electron densities calculated using DFT are of great importance since all other properties are derived from it. Comparisons of these densities to those calculated using other methods can be very informative but can also be a complex process. In the previous chapter two different methods were studied. The first, a visual comparison performed by examining plots of the difference between two densities, $\Delta\rho$, is onerous and yields only qualitative results.⁴⁻⁶ The second, a comparison of two electron densities over a large three-dimensional grid, can be inconsistent and although some sophisticated multicentre alternatives are available⁷ an analytical method may improve results. Neither of these methods provides a framework for getting a quantitative or even semi-quantitative measure of the differences between two densities. Quantitative results for the difference in electron densities provides better insight into

the approximate DFT densities and also facilitates the use of density differences as a tool for further development of functionals.

The Hohenberg-Kohn⁸ theorem provides the framework for an analysis of the different functionals via a study of the electron density. Through the use of the Kohn-Sham orbitals⁹ and the natural orbitals of wavefunction-based methods a semi-quantitative measure of the differences between two densities will be given. Also, an analysis on how this new measure performs on a variety of small molecules follows.

4.1 Orbital-Based Density Difference Index

The orbital-based density difference index (DDI) was developed to complement the qualitative comparisons of DFT densities and high-level densities which have been previously carried out.^{5,6} This was accomplished by reducing the plots of the density differences into a single quantity. One other approach, the quantum mechanical similarity measure recently proposed by Carbo et al.,¹⁰ has been proposed as a way of obtaining a quantitative difference between two electron densities. However, this approach is dependent on the similarity function used to compare the two densities. The DDI, as developed below, is a method which gives a much more direct comparison of the two densities.

The electron density, by definition, is given as the diagonal element of the first-order density matrix,

$$\rho_1(\mathbf{x}'_1, \mathbf{x}_1) = \sum_{i=1}^M \lambda_i \psi_i(\mathbf{x}'_1) \psi_i^*(\mathbf{x}_1) \quad (4.1)$$

where \mathbf{x}_1 is the combined spatial and spin coordinates of electron 1 and M is the total number of natural orbitals $\{\psi\}$. λ_i is the occupation number of natural orbital ψ_i .

In the Kohn-Sham formalism of density functional theory (DFT), a non-interacting reference system, which has the same electron density as the actual system, is intro-

duced. The density of the reference system is written as,

$$\rho(\mathbf{x}_1) = \rho_1(\mathbf{x}_1, \mathbf{x}_1) = \sum_{i=1}^N n_i \chi_i(\mathbf{x}_1) \chi_i^*(\mathbf{x}_1) \quad (4.2)$$

where N is the number of occupied Kohn-Sham orbitals $\{\chi\}$ and n_i is the occupation number for orbital ϕ_i .

The natural orbitals, $\{\psi\}$, form a complete orthonormal basis set, and hence the Kohn-Sham orbitals can be expressed as linear combinations of $\{\psi\}$; i.e.

$$\chi_i(\mathbf{x}_1) = \sum_{j=1}^M c_{ij} \psi_j(\mathbf{x}_1) \quad (4.3)$$

Substituting Eq.(4.3) into Eq.(4.2) gives,

$$\rho(\mathbf{x}_1) = \sum_{i=1}^N \sum_{j=1}^M \sum_{k=1}^M n_i c_{ij} c_{ik}^* \psi_j(\mathbf{x}_1) \psi_k^*(\mathbf{x}_1) \quad (4.4)$$

This new expression of the Kohn-Sham density allows for a direct comparison of the two densities. Taking the difference between the densities, i.e. Eq.(4.1) minus Eq.(4.4), yields

$$\Delta\rho(\mathbf{x}_1) = \sum_{j=1}^M \left(\lambda_j - \sum_{i=1}^N n_i |c_{ij}|^2 \right) \psi_j(\mathbf{x}_1) \psi_j^*(\mathbf{x}_1) - \sum_{k>j}^M \sum_{i=1}^N 2n_i c_{ij} c_{ik}^* \psi_j(\mathbf{x}_1) \psi_k^*(\mathbf{x}_1). \quad (4.5)$$

Defining a matrix \mathbf{P} , which is analogous to a density matrix, as,

$$\mathbf{P}_{ij} = \sum_{k=1}^N n_k c_{ki} c_{kj}^* \quad (4.6)$$

allows Eq.(4.5) to be simplified to,

$$\Delta\rho(\mathbf{x}_1) = \sum_{i,j=1}^M (\lambda_i\delta_{ij} - \mathbf{P}_{ij}) \psi_i(\mathbf{x}_1)\psi_j^*(\mathbf{x}_1) \quad (4.7)$$

From Eq. (4.7), the root-mean-square density difference index (DDI) can be defined as,

$$D_{RMS} = \sqrt{\int [\Delta\rho(\mathbf{x}_1)]^2 d\mathbf{x}_1}, \quad (4.8)$$

Eq. (4.8) gives a semi-quantitative measure of the difference between the two densities.

From Eq.(4.8), it is obvious that $D=0$ only if the two density distributions are identical. Moreover, if the reference density, given by Eq.(4.1), gives a very accurate description of the molecular properties then it can be treated as the exact density. This makes D a quantitative measure of the differences between the exact and the DFT densities. Thus, one can judge the accuracy of an electron density on the basis of its D value. The QCISD (quadratic configuration interaction method including single and double substitutions)¹¹ density yields molecular properties which are close to experimental values. Analysis using the QCISD density to approximate the exact electron density will be used to test the value of the DDI. MP2 (second-order Møller-Plesset perturbation theory)¹²⁻¹⁵ values are also included for comparison.

Although the density ranges over several orders of magnitude throughout the molecule the value of D is calculated directly without any weighting. As with the case of the three-dimensional grid an accurate and unbiased weighting scheme would be very difficult to find. This is due to the fact that at low densities (large distances) the total energy is dominated by the kinetic energy term and at high densities (small distances) the total energy is dominated by the potential energy term. Thus, for the DDI the choice of equal weighting of the orbitals is reasonable.

The DDI was developed to compare DFT densities to post-Hartree-Fock densities; the DDI can also be used to compare two different post-Hartree-Fock densities. The natural orbital expression for the density, equation (4.1), is analogous to the Kohn-Sham density, equation (4.2), and thus a second natural orbital density can be used for comparison. Other uses for the DDI, such as being part of the development of new functionals, increases the importance of this new index.

4.2 Computational Details

The wavefunctions and the Kohn-Sham orbitals for a series of four homonuclear diatomics were calculated using the Gaussian 94 program.¹⁶ The density differences were calculated using these results.

Three different basis sets, 6-31+G(d)(or 6-31++G(d,p)¹⁷ in the case of H₂), aug-CC-PVDZ and aug-CC-PVTZ,¹⁸ were used to test the basis set dependence of the DDI. Two different types of functionals, pure and hybrid, were used in this study. The four pure functionals are SVWN, BLYP, BP86 and BPW91. SVWN uses the local spin density exchange energy and the Vosko, Wilk and Nusair parameterisation of the local spin density correlation energy.¹⁹ The BLYP, BP86 and BPW91 functionals, however, all use the Becke 88 gradient-corrected exchange functional²⁰ and combine it with the Lee, Yang, and Parr correlation functional,²¹ the Perdew 86 correlation functional²² and the Perdew and Wang 91 correlation functional,²³ respectively.

The three hybrid functionals, B3LYP, B3P86 and B3PW91, use Becke's three parameter expression,²⁴ which allows for the inclusion of part of the exact exchange energy, and mix it with either the Lee, Yang and Parr correlation functional, B3LYP, the Perdew 86 correlation functional, B3P86, or the Perdew and Wang 91 correlation functional, B3PW91.

To allow for direct comparison of densities, experimental values²⁵⁻²⁷ for the equilibrium bond lengths (r_e), and bond angles 0.714 Å for H₂, 1.098 Å for N₂, 1.207 Å for O₂, 1.412 Å for F₂, 1.2324 Å for HB, 0.917 Å for HF, 1.065 Å for the HC and 1.153 Å for the CN bond lengths in HCN, 0.959 Å for the HO bond length and 103.9° for the HOH bond angle in H₂O and 1.208 Å for the CO and 1.116 Å for the HC bond lengths and 116.5° for the HCH bond angle in H₂CO were used.

4.3 Results and Discussion

Table 4.1 lists the calculated DDIs between the QCISD and DFT densities for four molecules with seven methods and three basis sets. These values show that the fluctuations in the indices are much larger from one functional to another than they are from one basis set to another. Figure 4.1 illustrates the functional and basis set dependence of the QCISD-DFT DDI for H₂, while figure 4.2 illustrates the functional dependence of the QCISD-DFT DDIs for N₂, O₂, and F₂ using the aug-CC-PVDZ basis set. The values in the graphs and in the tables demonstrate that the DDI does give at least a semi-quantitative, if not quantitative, measure of the accuracy of the approximate DFT densities.

The profile in figure 4.1 reveals three distinct functional groupings for the H₂ molecule. The first group consists of the functionals with the largest DDIs and contains BLYP and SVWN. It is not surprising that these functionals give the largest DDIs since SVWN and BLYP, compared to other functionals, give mediocre results for a variety of properties.^{3,28-30} The next set of functionals, BP86, BPW91, and B3LYP, yield substantially smaller DDIs, by 0.02 to 0.03. The inclusion of two "pure" functionals, BP86 and BPW91, with hybrid functional, B3LYP, within this group is noteworthy. The smallest DDIs are obtained with B3P86 and B3PW91. These groupings

Table 4.1: QCISD-DFT values for the density difference index.

Molecule	Functional	Basis Set		
		6-31+G(d,p)	aug-CC-PVDZ	aug-CC-PVTZ
H ₂	SVWN	0.0899	0.0877	0.0981
	BLYP	0.0838	0.0895	0.0956
	BP86	0.0620	0.0664	0.0711
	BPW91	0.0589	0.0668	0.0681
	B3LYP	0.0640	0.0679	0.0679
	B3P86	0.0457	0.0496	0.0529
	B3PW91	0.0480	0.0533	0.0555
	(MP2)*	0.0203	0.0219	0.0206
N ₂	SVWN	0.2126	0.2194	0.2215
	BLYP	0.2197	0.2274	0.2275
	BP86	0.1963	0.2028	0.2011
	BPW91	0.1999	0.2071	0.2022
	B3LYP	0.1826	0.1877	0.1872
	B3P86	0.1719	0.1765	0.1732
	B3PW91	0.1735	0.1785	0.1732
	(MP2)*	0.0613	0.0644	0.0699
O ₂	SVWN	0.1747	0.1757	0.1822
	BLYP	0.1912	0.1908	0.1930
	BP86	0.1632	0.1622	0.1638
	BPW91	0.1658	0.1654	0.1637
	B3LYP	0.1485	0.1478	0.1492
	B3P86	0.1346	0.1344	0.1320
	B3PW91	0.1363	0.1362	0.1332
	(MP2)*	0.0560	0.0568	0.0602
F ₂	SVWN	0.2360	0.2367	0.2446
	BLYP	0.2517	0.2507	0.2530
	BP86	0.2178	0.2168	0.2207
	BPW91	0.2178	0.2172	0.2176
	B3LYP	0.1999	0.1967	0.1963
	B3P86	0.1813	0.1784	0.1761
	B3PW91	0.1833	0.1806	0.1775
	(MP2)*	0.0651	0.0675	0.0742

*QCISD-MP2 DDI's

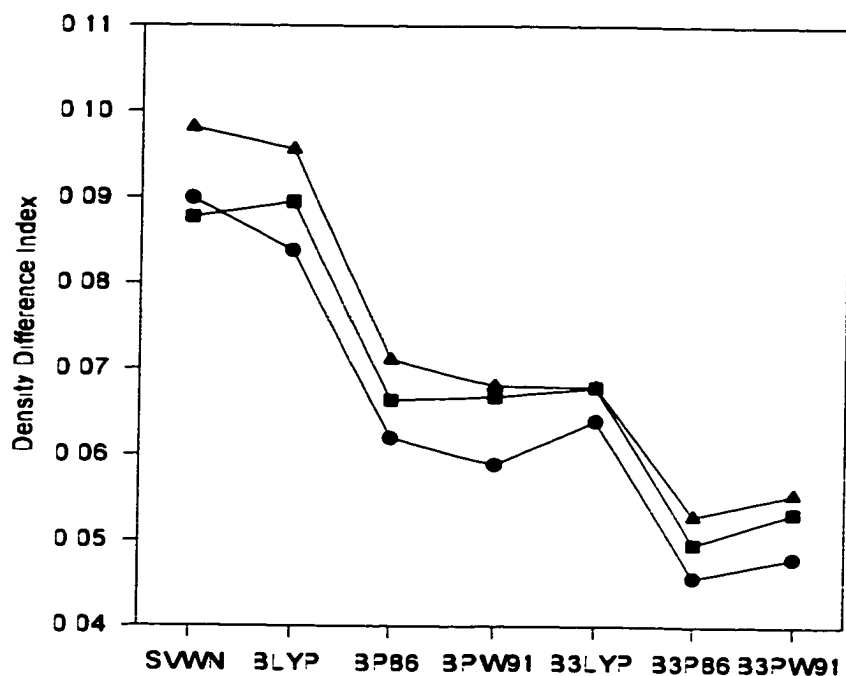


Figure 4.1: Functional and basis set dependence of QCISD-DFT DDIs for H_2 :
● 6-31++G**, ■ aug-CC-PVDZ, and ▲ aug-CC-PVTZ.

were also found for the case of H_2 in previous work which compared the H_2 approximate DFT density and the QCISD density visually.⁵ However, the second grouping is unexpected since molecular properties calculated with B3LYP usually differ significantly from the corresponding values calculated with BP86 and BPW91. It is generally accepted that the hybrid functionals give molecular properties which are similar in value to other high-level treatments.^{2,31,32} Thus the fact that the B3P86 and B3PW91 DDIs indicate that they give densities which are the closest to the other high-level treatments is not unexpected. H_2 , though, is a special case and before any general conclusions can be drawn other molecules must be considered.

The results shown in figure 4.2 for N_2 , O_2 and F_2 indicate that BLYP and SVWN give the largest DDIs, as observed for H_2 . There is then a steady decrease in the DDIs

with BP86 and BPW91 giving the next lowest DDIs and then B3LYP giving an even further lowering in the index. As in the case of H_2 , the smallest DDIs are obtained with B3P86 and B3PW91. This grouping of the functionals is more in accordance with what has been found in the past, with the hybrid methods giving values which indicate densities that are the closest to the high-level densities.

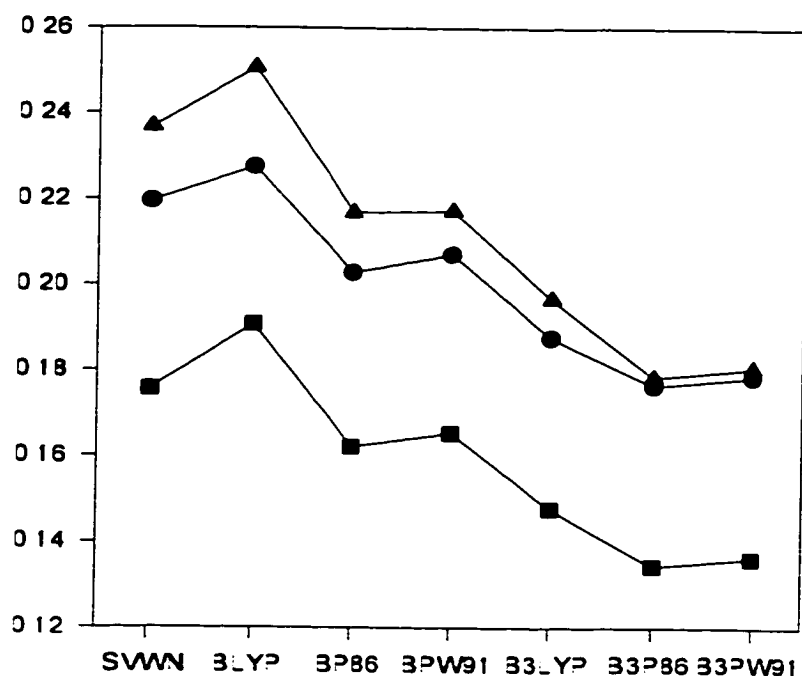


Figure 4.2: Functional dependence of the QCISD-DFT DDIs obtained with the aug-CC-PVDZ basis set: ● N_2 , ▲ O_2 , and ■ F_2 .

In table 4.2 and in figures 4.3 and 4.4 the MP2 density is used to approximate the exact density. The same conclusions about the approximate DFT densities can be made from the MP2-DFT DDIs as were drawn from the QCISD-DFT DDIs above. However, even though the profiles in the two series of graphs are similar the QCISD-DFT indices are 0.01-0.02 larger than the MP2-DFT values. Also, the MP2 DDI values span a smaller range than the QCISD DDI values. This indicates that the DFT

densities approximate the MP2 density better than they approximate the QCISD density. Of note, though, are the QCISD-MP2 values in table 4.1 which range from 0.02 to 0.07. This indicates that even though the DFT densities approximate the MP2 density better than the QCISD density there is a qualitative difference between the QCISD and MP2 densities and the DFT densities.

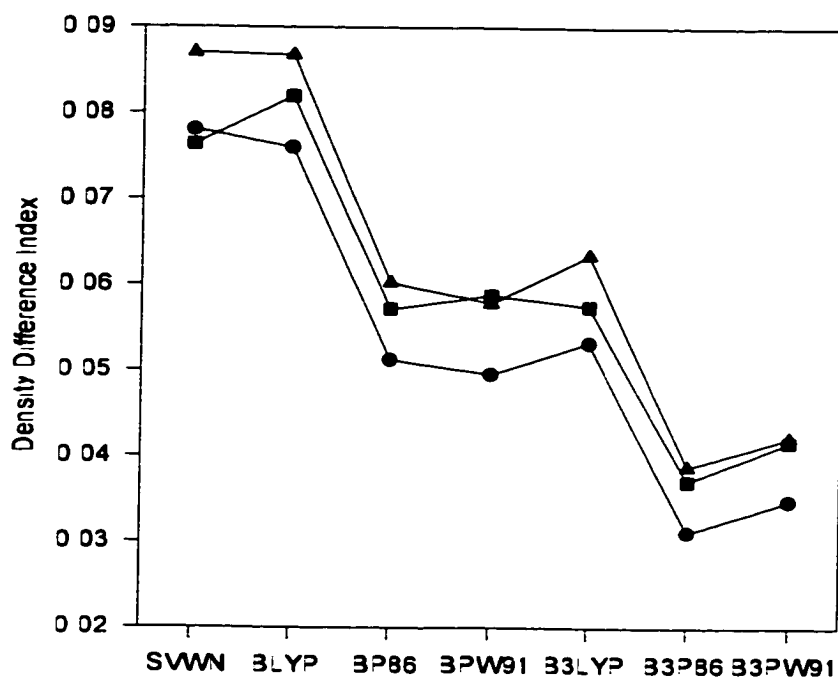


Figure 4.3: Functional and basis set dependence of MP2-DFT DDIs for H_2 :
● 6-31++G**, ■ aug-CC-PVDZ, and ▲ aug-CC-PVTZ.

Many studies based on using hybrid functionals,^{2,31,32} the B3LYP functional in particular, have yielded molecular properties which are in close agreement to those calculated with MP2. The MP2-DFT DDIs for hybrid functionals give values which are much smaller than the non-hybrid methods. This indicates that these functionals give densities which have strongest similarities to the MP2 density as indicated by the previous studies.

Table 4.2: MP2-DFT values for the density difference index.

Molecule	Functional	Basis Set		
		6-31++G(d,p)	aug-CC-PVDZ	aug-CC-PVTZ
H ₂	SVWN	0.0781	0.0764	0.0870
	BLYP	0.0760	0.0820	0.0868
	BP86	0.0513	0.0572	0.0603
	BPW91	0.0496	0.0588	0.0579
	B3LYP	0.0533	0.0575	0.0635
	B3P86	0.0311	0.0371	0.0388
	B3PW91	0.0348	0.0417	0.0422
N ₂	SVWN	0.1844	0.1889	0.1924
	BLYP	0.1920	0.1965	0.1980
	BP86	0.1720	0.1760	0.1762
	BPW91	0.1760	0.1814	0.1780
	B3LYP	0.1696	0.1719	0.1746
	B3P86	0.1645	0.1676	0.1668
	B3PW91	0.1652	0.1689	0.1671
O ₂	SVWN	0.1551	0.1553	0.1576
	BLYP	0.1693	0.1674	0.1649
	BP86	0.1393	0.1374	0.1353
	BPW91	0.1426	0.1415	0.1363
	B3LYP	0.1350	0.1334	0.1315
	B3P86	0.1217	0.1217	0.1176
	B3PW91	0.1238	0.1239	0.1191
F ₂	SVWN	0.1943	0.1943	0.1951
	BLYP	0.2077	0.2055	0.2000
	BP86	0.1761	0.1741	0.1712
	BPW91	0.1783	0.1766	0.1711
	B3LYP	0.1697	0.1671	0.1609
	B3P86	0.1592	0.1574	0.1513
	B3PW91	0.1609	0.1590	0.1526

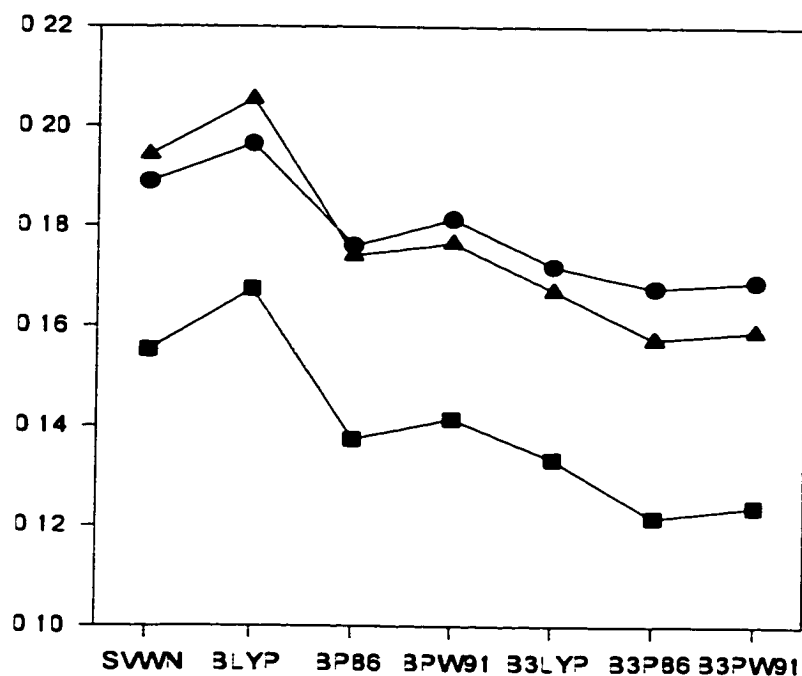


Figure 4.4: Functional dependence of the MP2-DFT DDIs obtained with the aug-CC-PVDZ basis set: ● N₂, ■ O₂, and ▲ F₂.

Although the three basis sets used differ substantially in the number of basis functions, the basis set dependence is much more subtle than the functional dependence. For H₂, the DDIs between the MP2 or QCISD densities and the DFT densities increase as the basis set size is increased. There is one exception to this generalisation, the SVWN has a minimal value with the aug-CC-PVDZ basis set. Examining the two tables shows that for the nitrogen molecule the same trend is repeated for the SVWN, BLYP and B3LYP functionals when comparing MP2 densities to DFT densities and for the SVWN, and BLYP functionals when comparing QCISD densities to DFT densities. For all other calculated N₂ DDIs the values start off at a minimum with the 6-31+G(d) basis set and then increase to a maximum with aug-CC-PVDZ and then decrease again slightly with aug-CC-PVTZ.

With the exception of the SVWN functional, the basis set dependence of the DDIs between MP2 and DFT densities for O_2 and F_2 is the same for all functionals. These DDIs start out at a maximal value with the 6-31+G(d) basis set and decrease with increasing basis set size. Thus the aug-CC-PVTZ basis set gives the minimal DDI for these functionals while the aug-CC-PVDZ value is in between the other two. For SVWN the exact opposite trend is shown with the minimal value given with the 6-31+G(d) basis set and the maximal value given with the aug-CC-PVTZ basis set.

Examining the basis set dependence of the DDIs for O_2 and F_2 between QCISD densities and DFT densities gives a more complicated picture. The SVWN functional, as in all other cases, has a minimal value using 6-31+G(d) and a maximal value using aug-CC-PVTZ. The BLYP and B3LYP functionals give minimal values with the aug-CC-PVDZ basis set and maximal values with the aug-CC-PVTZ basis set. All other functionals give maximal values with the 6-31+G(d) basis set and minimal values with the aug-CC-PVTZ basis set.

After this in-depth examination of H_2 , N_2 , O_2 and F_2 the DDI was tested on a variety of other molecules, as seen in tables 4.3 and 4.4. In view of the fairly weak basis set dependence noted above the DDIs for the additional molecules were only calculated using the aug-CC-PVDZ basis set. As in the case of the diatomics the DDIs were calculated using the same two reference densities, QCISD and MP2.

The results from these molecules do not differ significantly from those found with the homonuclear diatomics. The SVWN and BLYP approximate functionals give the largest DDIs, with SVWN being the largest for HB and H_2CO , BLYP being the largest for HCN, HF and H_2O , and with both values being approximately the same for CO. The BP86 and BPW91 approximate functionals again show a marked improvement, of about 0.02 for most cases, over the BLYP and SVWN. Finally, the

Table 4.3: Values for the density difference index for a variety of molecules using the aug-CC-PVDZ basis set.

Molecule	Reference	SVWN	BLYP	BP86	BPW91	B3P86	B3PW91	B3LYP
	Density							
HB	QCISD	0.2367	0.2282	0.2124	0.2097	0.1912	0.1917	0.2024
	MP2	0.1764	0.1643	0.1472	0.1479	0.1154	0.1157	0.1244
HF	QCISD	0.1495	0.1767	0.1344	0.1336	0.0904	0.0946	0.1202
	MP2	0.1238	0.1508	0.1128	0.1141	0.0852	0.0878	0.1022
CO	QCISD	0.2343	0.2347	0.2146	0.2172	0.1732	0.1754	0.1834
	MP2	0.1818	0.1829	0.1632	0.1692	0.1508	0.1522	0.1539
HCN	QCISD	0.2375	0.2423	0.2199	0.2231	0.1872	0.1884	0.1989
	MP2	0.2016	0.2059	0.1860	0.1907	0.1687	0.1695	0.1749
H ₂ O	QCISD	0.1610	0.1829	0.1423	0.1397	0.1043	0.1066	0.1299
	MP2	0.1287	0.1544	0.1199	0.1218	0.1030	0.1044	0.1128
H ₂ CO	QCISD	0.2722	0.2677	0.2439	0.2449	0.1907	0.1926	0.2040
	MP2	0.2235	0.2170	0.1948	0.1987	0.1604	0.1616	0.1663

hybrid methods decrease the DDI as expected, and give the lowest DDIs for these molecules. Also, comparison of the relative magnitudes of the DDIs using the QCISD density as a reference and the DDIs using the MP2 density as a reference shows that the MP2-DFT DDIs are smaller by about 0.03 in most cases.

Table 4.4 compares the DDI values of C₂H₂, C₂H₄, C₂H₆, and C₆H₆ with the density difference plots of the previous chapter. Again it is apparent that the DFT densities give much better agreement with MP2 values than with QCISD values. Examining specific functionals shows that SVWN has an increase in its DDIs from ethyne to ethene to ethane while BLYP and BP86 only exhibit an increase between ethyne and ethene and then show a slight decrease in the DDIs from ethene to ethane. The hybrid functionals, B3LYP and B3P86, yield the same trends as BLYP and

Table 4.4: Values for the density difference index for C_2H_n , $n = 2, 4, 6$ using the aug-CC-PVDZ basis set and C_6H_6 using the CC-PVDZ basis set.

Molecule	Reference	SVWN	BLYP	BP86	B3P86	B3LYP
	Density					
C ₂ H ₂	QCISD	0.2467	0.2495	0.2213	0.1905	0.2061
	MP2	0.2065	0.2092	0.1829	0.1611	0.1710
C ₂ H ₄	QCISD	0.2802	0.2581	0.2348	0.1972	0.2089
	MP2	0.2357	0.2167	0.1941	0.1622	0.1683
C ₂ H ₆	QCISD	0.3017	0.2517	0.2278	0.1856	0.1979
	MP2	0.2547	0.2171	0.1888	0.1531	0.1650
C ₆ H ₆	QCISD	0.4272	0.3947	0.3710	0.3104	0.3208
	MP2	0.3728	0.3531	0.3213	0.2739	0.2889

BP86 but yield a substantially larger decrease in the DDI when moving from ethene to ethane. Comparing with the density difference plots of the previous chapter the DDIs for SVWN echo what is observed in the plots. While for the other functionals the changes between ethyne and ethene are difficult to discern but there is a definite improvement in the density difference plots between ethyne or ethene and ethane which is also exhibited in the DDIs. Benzene has three times the number of carbon and hydrogen atoms as does ethyne and could then be expected to yield a DDI approximately three times that of ethyne but benzene only gives values approximately 1.5 to 2 times as large.

4.4 Conclusions

The DDI introduces a new tool for comparing the differences between two electron densities by reducing it to a single quantitative value. Calculations using the DDI

have supplied results which are consistent with the density difference plots given in chapter 3. Specifically, the DDI values show that the SVWN and BLYP functionals yield electron densities the least similar to the QCISD electron density while the hybrid functionals, B3LYP, B3P86, and B3PW91, yield electron densities which are the most similar to the QCISD electron density.

Comparison of DDIs, though, can be problematic and a normalisation of the densities may simplify future work. This normalisation is equivalent to dividing the DDI by the number of electrons in the molecule yielding the DDI/electron and would not reduce the efficiency or accuracy of the DDI calculations. Using these DDI/electron values to compare benzene and ethyne it is much easier to see that the B3P86 functional yields better densities for benzene than ethyne since the QCISD-B3P86 DDI/electron of benzene is 0.0074 while the QCISD-B3P86 DDI/electron of ethyne is 0.0136.

Although this tool was designed as a quantitative tool for use in functional development it has also shown that there are qualitative differences between the QCISD or MP2 densities and the approximate DFT densities. Unfortunately, the DDI does not actually express what this difference is and thus more information is needed about electron densities calculated with approximate DFT functionals.

References

- [1] B. G. Johnson, P. M. W. Gill, and J. A. Pople, *J. Chem. Phys.* **98**, 5612 (1993).
- [2] C. W. Bauschlicher, Jr., *Chem. Phys. Lett.* **246**, 41 (1995).
- [3] J. M. Seminario and P. Politzer, editors, *Modern Density Functional Theory: A Tool for Chemistry*, Elsevier, 1995.

-
- [4] J. Wang, Z. Shi, R. J. Boyd, and C. A. Gonzalez, *J. Phys. Chem.* **98**, 6988 (1994).
- [5] J. Wang, L. A. Eriksson, B. G. Johnson, and R. J. Boyd, *J. Phys. Chem.* **100**, 5274 (1996).
- [6] J. Wang, B. G. Johnson, R. J. Boyd, and L. A. Eriksson, *J. Phys. Chem.* **100**, 6317 (1996).
- [7] A. D. Becke, *Phys. Rev. A* **38**, 3098 (1988).
- [8] P. Hohenberg and W. Kohn, *Phys. Rev.* **136**, 864 (1964).
- [9] W. Kohn and L. J. Sham, *Phys. Rev.* **140**, A1133 (1965).
- [10] M. Sola, J. Mestres, R. Carbó, and M. Duran, *J. Chem. Phys.* **104**, 636 (1996).
- [11] J. A. Pople, M. Head-Gordon, and K. Raghavachari, *J. Chem. Phys.* **87**, 5968 (1987).
- [12] C. Møller and M. S. Plesset, *Phys. Rev.* **46**, 618 (1934).
- [13] J. A. Pople, R. Seeger, and R. Krishnan, *Int. J. Quant. Chem. Symp.* **11**, 149 (1977).
- [14] R. Krishnan and J. A. Pople, *Int. J. Quant. Chem.* **14**, 91 (1978).
- [15] R. Krishnan and J. A. Pople, *J. Chem. Phys.* **72**, 4244 (1980).
- [16] M. J. Frisch, G. W. Trucks, H. B. Schlegel, P. M. W. Gill, B. G. Johnson, M. A. Robb, J. R. Cheeseman, T. A. Keith, G. A. Petersson, J. A. Montgomery, K. Raghavachari, M. A. Al-Laham, V. G. Zakrzewski, J. V. Ortiz, J. B. Foresman, J. Cioslowski, B. B. Stefanov, A. Nanayakkara, M. Challacombe, C. Peng,

- P. Y. Ayala, W. Chen, M. W. Wong, J. L. Andres, E. S. Repogle, R. Gomperts, R. L. Martin, D. J. Fox, J. S. Binkley, D. J. DeFrees, J. Baker, J. P. P. Stewart, M. Head-Gordon, C. Gonzalez, and J. A. Pople, *Gaussian 94*, Gaussian, Inc.: Pittsburgh PA, 1995.
- [17] P. C. Hariharan and J. A. Pople, *Chem. Phys. Lett.* **66**, 217 (1972).
- [18] R. A. Kendall and T. H. Dunning, Jr., *J. Chem. Phys.* **96**, 6796 (1992).
- [19] S. H. Vosko, L. Wilk, and M. Nusair, *Can. J. Phys.* **58**, 1200 (1980).
- [20] A. D. Becke, *J. Chem. Phys.* **96**, 2155 (1992).
- [21] C. Lee, W. Yang, and R. G. Parr, *Phys. Rev. B* **37**, 785 (1988).
- [22] J. P. Perdew and W. Yue, *Phys. Rev. B* **33**, 8800 (1986).
- [23] J. P. Perdew, J. A. Chevary, S. H. Vosko, K. A. Jackson, M. R. Pederson, D. J. Singh, and C. Fiolhais, *Phys. Rev. B* **46**, 6671 (1992).
- [24] A. D. Becke, *J. Chem. Phys.* **98**, 5648 (1993).
- [25] S. Bourcier, *Selected Constants: Spectroscopic Data Relative to Diatomic Molecules*, Pergamon Press, 1970.
- [26] G. Herzberg and K. P. Huber, *Molecular Spectra and Molecular Structure IV Constants of Diatomic Molecules*, Van Nostrand Reinhold Company, New York, 1979.
- [27] K.-H. Hellwege, editor, *Numerical Data and Functional Relationships in Science and Technology*, volume 7 of *Group 2*, Landolt-Börnstein, Springer-Verlag Berlin, 1976, New Series.

-
- [28] C. S. C. Lee, *J. Chem. Phys.* **98**, 8004 (1993).
- [29] P. M. W. Gill, B. G. Johnson, and J. A. Pople, *Chem. Phys. Lett.* **197**, 499 (1992).
- [30] R. J. Hall, N. A. Burton, I. H. Hillier, and P. E. Young, *Chem. Phys. Lett.* **220**, 129 (1994).
- [31] R. Sustmann, W. Sicking, and R. Huisgen, *J. Am. Chem. Soc.* **117**, 9679 (1995).
- [32] P. J. Stephens, F. J. Devlin, C. F. Chablowski, and M. J. Frisch, *J. Phys. Chem.* **98**, 11623 (1994).

5. A Spin-Polarisation Index

For closed-shell systems accurate total electron densities calculated using approximate density functional theory (DFT) methods should lead to accurate molecular properties since the α and β electron densities are equal.¹ Open-shell systems, though, do not have equal numbers of α and β electrons and the differences in their distribution, referred to as the spin polarisation, is an important factor for some molecular properties such as the hyperfine coupling constant.² Thus, DFT not only has to calculate an accurate total electron density but also give an accurate description of the spin polarisation in order to yield accurate molecular properties for open-shell molecules.

Comparisons of the total electron density calculated using approximate DFT methods to those calculated using high-level *ab initio* methods given in previous chapters have revealed that the DFT densities are reasonably accurate but there are still some qualitative differences.³⁻⁷ These studies, though, do not supply any information on the spin polarisation for open-shell molecules. Also, Pople *et al.*⁸ have recently developed a theory to measure the quality of an energy functional. Their preliminary results for the local spin density (LSD) energy functional, suggests that the α , β spin density partition of the first-row atoms and a selected set of closed-shell molecules overestimates both the $\alpha\alpha + \beta\beta$ and the $\alpha\beta$ correlation energies. These

two factors underline the necessity for quantitative studies of the differences between the α and β electron densities.

Unfortunately, theoretical rationalisation of the spin polarisation has been quite difficult and thus theoretical values of the spin related properties are highly dependent on the choice of the method and the basis set. This chapter will examine a new method which gives a quantitative measure of the difference between the α and β densities of a molecule and will report the results of some calculations for a few representative molecules, with a special emphasis on O_2 . It is anticipated that the spin-density polarisation index (SPI) may also prove to be useful in the creation of functionals that take into account the explicit difference between α and β densities.

5.1 Spin-Density Polarisation Index

The total electron density ρ can be partitioned as a sum of the α and β spin densities, ρ^α and ρ^β , respectively. Since open-shell systems have a different number of α - and β -spin electrons, there is a polarisation of the spin-densities. One way to gauge the spin-polarisation at a point \mathbf{r} can be given as,

$$\rho^{\alpha-\beta}(\mathbf{r}) = \rho^\alpha(\mathbf{r}) - \rho^\beta(\mathbf{r}) \quad (5.1)$$

However, it is important to also have a simple reliable quantitative measure of the total spin-density polarisation that can serve to measure the inadequacies of the various methods and/or basis sets.

The Euclidean distance between the α and β densities, $d_{\alpha\beta}$, can be used as a

polarisation index. Thus, the spin-density polarisation index (SPI) can be defined as,

$$d_{\alpha\beta} = \sqrt{\int d\mathbf{r}[\rho^\alpha(\mathbf{r}) - \rho^\beta(\mathbf{r})]^2} \quad (5.2)$$

This equation is modelled after the quantum molecular similarity measure (QMSM) introduced by Carbo et al.^{3,9} However, for the SPI different densities for the α and β spins of a single molecule are compared while for the QMSM method the densities from two different methods and/or molecules are compared.

Equation 5.2 can be rewritten as

$$d_{\alpha\beta} = \sqrt{Z_{\alpha\alpha} + Z_{\beta\beta} - 2Z_{\alpha\beta}} \quad (5.3)$$

which resembles a distance-like dissimilarity index introduced by previous authors.¹⁰

Here,

$$Z_{\alpha\alpha} = \int d\mathbf{r}\rho^\alpha(\mathbf{r})\rho^\alpha(\mathbf{r}) \quad (5.4)$$

and

$$Z_{\alpha\beta} = \int d\mathbf{r}\rho^\alpha(\mathbf{r})\rho^\beta(\mathbf{r}) \quad (5.5)$$

An analogous integral to equation 5.4 holds for β spin. For a restricted closed-shell calculation $d_{\alpha\beta} = 0$ since $\rho^\alpha = \rho^\beta$, by definition.

The evaluation of the integrals in equations 5.4 and 5.5, has been discussed by Carbo et al.^{3,9} Recently, however, another approach¹¹ has shown that for any single-determinant wave function Ψ built from N^α α -spin and N^β β -spin orbitals, the electron-electron coalescence density $I(\mathbf{0})$ of such a wavefunction is,

$$I(\mathbf{0}) = \int d\mathbf{r}\rho^\alpha(\mathbf{r})\rho^\beta(\mathbf{r}) \quad (5.6)$$

Here the α and β density functions are given by $\rho^\alpha(\mathbf{r}) = \sum_{i=1}^{N^\alpha} |\psi_i^\alpha(\mathbf{r})|^2$ and $\rho^\beta(\mathbf{r}) = \sum_{i=1}^{N^\beta} |\psi_i^\beta(\mathbf{r})|^2$, respectively. Therefore, one can avoid calculating the integral of the right-hand-side of equation 5.6 simply by calculating the value of the function $I(\mathbf{r})$ at $\mathbf{r} = \mathbf{0}$, which for single determinant Hartree-Fock-like wavefunctions has been previously cast into a convenient closed analytical form.¹² For the higher level methods beyond Hartree-Fock one can express the wavefunction in terms of its natural orbitals. The wavefunction, so expressed, is a working tool which allows us to define the α and β densities unambiguously but is not equivalent to the post Hartree-Fock wavefunction since it cannot be reduced to a single determinant using the natural orbitals. Hence, the $I(\mathbf{0})$ in these cases is the value of the required integral but cannot be associated with the post Hartree-Fock electron-electron coalescence density. Indeed it has been shown that it represents a very tight upper bound of the true coalescence density.¹¹ Taking advantage of this fact the previously derived formulae for $I(\mathbf{r})$ have been used to efficiently calculate $I(\mathbf{0})$ and consequently the required values for $Z_{\alpha\alpha}$, $Z_{\beta\beta}$ and $Z_{\alpha\beta}$.

5.2 Computational Details

The molecules were optimised using Gaussian 94¹³ at each level of theory, allowing for nuclear as well as electronic relaxation. The SPIs were calculated as described above from the computed electron densities.

The electron densities were obtained using two different types of methods, wavefunction based methods and density functional methods. The wavefunction based methods used were Hartree-Fock, second-order [MP2]¹⁴⁻¹⁷ and fourth-order, including single, double and quadruple excitations [MP4(SDQ)] Møller-Plesset perturbation theory, and quadratic configuration interaction including single and double excitations [QCISD].¹⁸ The density functional methods included two approximate “pure” func-

tionals and two hybrid functionals. The pure functionals were SVWN, which uses the local spin density exchange energy¹⁹ with the Vosko, Wilk, and Nusair parameterisation of the local spin density correlation energy,²⁰ and BPW91, which combines the Becke 88 gradient-corrected exchange energy²¹ with the Perdew and Wang 91 gradient-corrected correlation energy.²² The hybrid methods both use Becke's three-parameter expression²³ for the inclusion of Hartree-Fock exchange energy and the Becke 88 gradient correction to the exchange energy. The B3LYP functional uses the Lee, Yang and Parr gradient correction to the correlation energy²⁴ while the B3PW91 functional uses the Perdew and Wang 91 gradient correction to the correlation energy.

Since all of the molecules in this study have open shells the unrestricted formalism was used with most of the above methods. With the Hartree-Fock method, however, the restricted-open-shell (ROHF) and the unrestricted (UHF) formalisms were used. The aug-CC-PVDZ, aug-CC-PVTZ,²⁵ aug-CC-PCVDZ,^{26,27} IGLO-III,²⁸ and 6-311+G(d)^{29,30} basis sets were used for the O₂ calculations. For all other molecules, the aug-CC-PVDZ basis set was used, with the exception of NO₂ for which the CC-PVDZ basis set was used.

5.3 Results and Discussion

The O₂ molecule is expected to give a large SPI due to its triplet ground state and was used to evaluate the effect of basis sets and methods on the index. The calculated SPIs, shown in table 5.1, give very interesting results. It is apparent that the only significant difference in the SPI values due to basis sets is seen between Pople's 6-311+G(d) basis set and the other basis sets used. Despite the fact that there is a difference in the values the trends are the same from one method to another. The IGLO-III basis set gives values which are consistent with those given by the

aug-CC-PVDZ basis set. The similarity between the results obtained with the aug-CC-PCVDZ and the aug-CC-PVDZ basis sets indicates that the effects of the core electrons on the SPI are negligible, and hence the spin polarisation effects ought to be due primarily to the valence electrons.

In contrast with the relatively small basis set effects, the theoretical method has a large effect on the SPI values. As with the DDI all SPIs will be compared to the QCISD SPI, which using the aug-CC-PVTZ basis set is 0.3872 and is assumed to be closest to the “correct” value. The Hartree-Fock values are surprising with the unrestricted formalism overestimating the SPI value, giving a value of 0.5319 for the aug-CC-PVTZ basis set, while the SPI for the restricted open-shell formalism almost vanishes. The trend of very small SPIs is continued with the “pure” DFT functionals, SVWN and BPW91, with results that are approximately 0.23 smaller than the QCISD SPI. However, the addition of Hartree-Fock exchange, through the use of the Becke hybrid exchange functional, does increase the SPI values as expected. These values are less than but comparable in magnitude to the MP2 SPIs. MP4(SDQ) gives almost the same result as obtained by QCISD with an SPI of 0.3735 for the aug-CC-PVTZ basis set. In summary, the HF method overestimates the spin-density polarisation, and inclusion of electron correlation effects through the Møller-Plesset perturbation theory reduces it appreciably below the exact value. Increasing the order of the perturbation expansion converges to the exact value (compare the SPIs for QCISD and MP4(SDQ) in Table 5.1). The approximate DFT methods investigated in this study clearly underestimate the spin-density polarisation index with the local spin density(LSD) energy functional, SVWN, yielding only half of the exact SPI value. Inclusion of non-local gradient corrections to both the exchange and correlation functionals, through the BPW91 approximate functional, slightly increases the SPI

Table 5.1: Spin-density polarisation index values for ${}^3\Sigma^- \text{O}_2$

Basis Set	Method									
	UHF	ROHF	SVWN	BPW91	B3PW91	B3LYP	MP2	MP4(SDQ)	QCISD	
6-311+G(d)	0.4739	0.0000	0.1379	0.1574	0.2174	0.2229	0.2565	0.3333	0.3463	
aug-CC-PVDZ	0.5349	0.0003	0.1490	0.1777	0.2433	0.2459	0.2892	0.3746	0.3898	
aug-CC-PCVDZ	0.5339	0.0002	0.1493	0.1781	0.2434	0.2458	0.2897	0.4428*	0.3903	
aug-CC-PVTZ	0.5319	0.0003	0.1532	0.1881	0.2513	0.2525	0.2887	0.3735	0.3872	
IGLO-III	0.5376	0.0002	0.1515	0.1809	0.2468	0.2492	0.2936	0.3784	0.3932	
*from MP4(SDQ)/aug-CC-PCVDZ//QCISD/aug-CC-PCVDZ, single point calculation.										

values. Finally, the hybrid functionals, B3PW91 and B3LYP, increase further the spin-density polarisation, with the latter giving values comparable to the MP2 ones, but still far from the exact QCISD results.

In order to shed light on the origins of the spin-density polarisations mentioned above, plots of the radial distribution of the spherically-averaged spin density were made to visualise differences between methods and/or basis sets. Notice that the SPI is a quantity averaged over the whole molecule, while the spherically-averaged spin-density is a quantity which varies according to the radial distance from the chosen origin. For all figures, the origin is chosen to be the centre of symmetry. Figures 5.1 and 5.2 show the difference between the α and β spherically-averaged density near the origin, i.e. near the bond midpoint. Figure 5.1 shows that all wavefunction-based methods, but one, give β electron densities which are greater than the α electron densities. This implies that near the centre of the bond there is a build up of β electrons. For the one method for which this doesn't happen, ROHF, the β and α electron densities are exactly equal at the origin.

In Figure 5.2 the density functional method is examined near the origin in the binding region with the QCISD density difference given as a reference. With all of the functionals used in the present study the α electron density is larger than the β electron density. This excess α density is decreased by the addition of the HF exchange. However, even the hybrid methods give more α than β density which is the opposite of what the wavefunction based methods predict. This supports the recent conclusions of Pople *et al.*⁸ who have found that the relative contributions of $\alpha\alpha + \beta\beta$ and $\alpha\beta$ correlations to chemical bond energies are poorly given by the use of the LSD functional.

The O₂ atomisation energies in Table 5.2 show that the "pure" DFT methods

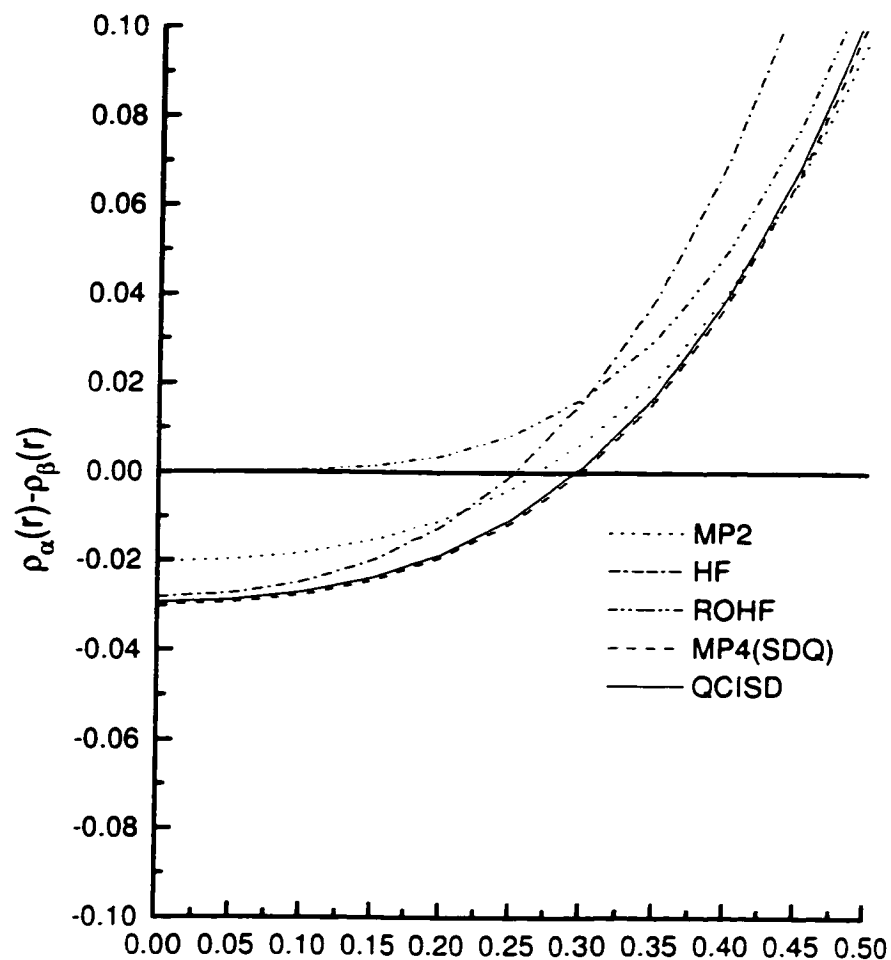


Figure 5.1: Plot of the radial distribution of the spherically averaged spin-density difference for wave function based methods using the aug-CC-PVDZ basis set for O_2 .

overestimate the experimental atomisation energy by as much as 57 kcal/mol. The hybrid DFT methods, while giving much better atomisation energies, still overestimate the experimental value by about 2 kcal/mol. The MP2 atomisation energy is the closest to experiment with only a 0.1 kcal/mol difference between the calculated and experimental values due to fortuitous cancellation of errors. The other two high-level wavefunction methods both underestimate the experimental value by about 18 kcal/mol. Finally the UHF and ROHF methods as expected give approximately 1/3 of the experimental atomisation energy. This trend, the overestimation by the

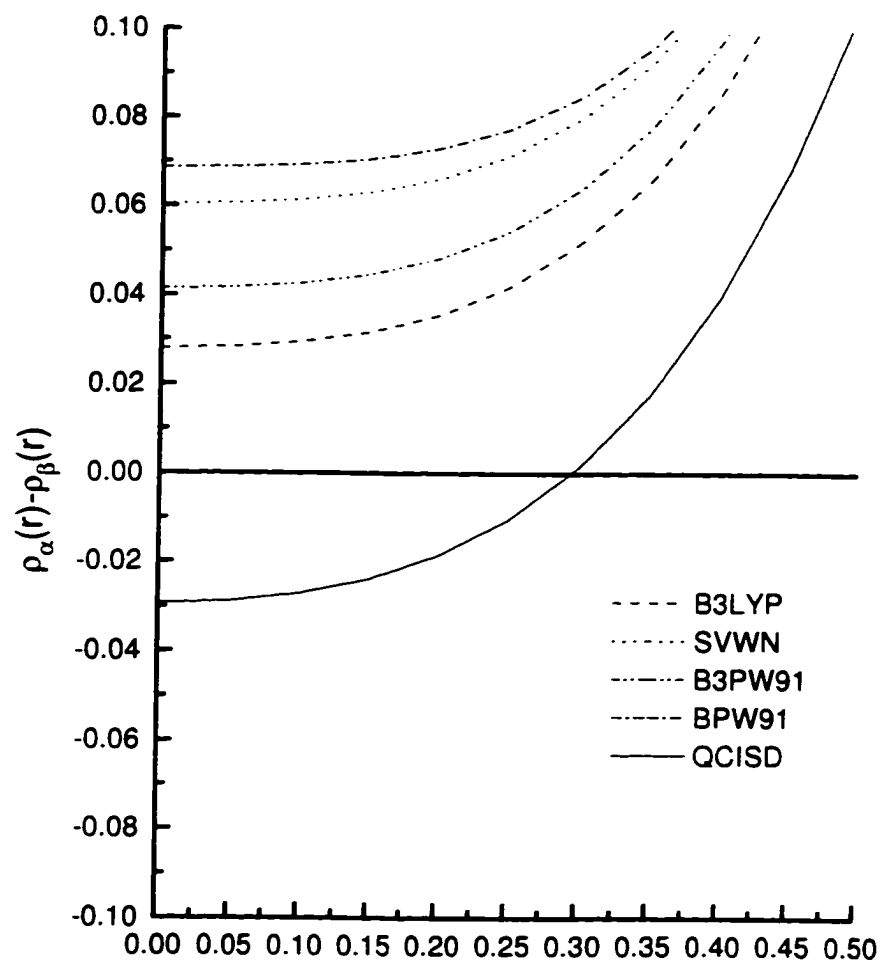


Figure 5.2: Plot of the radial distribution of the spherically averaged spin-density difference for DFT based methods using the aug-CC-PVDZ basis set for O_2 .

DFT methods and the underestimation by the wavefunction methods, is interesting in view of the α and β densities at the bond midpoint. The DFT methods, as mentioned above, have a larger α density at the midpoint. However, for pure functionals the amount of excess α density is greater than that of the hybrid functionals, while for the wavefunction-based methods there is actually a larger β electron density at the midpoint. Thus the build up of β electrons near the midpoint of the bond may be associated with a lowering of the calculated atomisation energy of O_2 .

Comparison of the radial distribution of the spherically-averaged α density to

Table 5.2: Atomisation energies (in a.u.) for O₂ using the aug-CC-PVDZ basis set

Method	O ₂ Energy	ZPE Correction	Atomisation Energy
HF	-149.64747	0.004498	0.04856
ROHF	-149.62624	0.004588	0.03869
SVWN	-149.60730	0.003718	0.2788
BPW91	-150.35069	0.003532	0.2149
B3PW91	-150.29315	0.003828	0.1932
B3LYP	-150.35255	0.003736	0.1914
MP2	-150.01120	0.003229	0.1883
MP4(SDQ)	-150.01569	0.003617	0.1601
QCISD	-150.01614	0.003682	0.1587
Experiment			0.1880

the radial distribution of the spherically averaged β density, as shown in Figure 5.3, indicates that the β density goes through a minimum near the atomic centres. A corresponding minimum, though, is not found in the α electron density distribution with all methods and basis sets yielding α electron distributions similar in form to that given for QCISD in Figure 5.3. Figures 5.4 and 5.5 show that this minimum is not an artifact of just the QCISD density but is apparent for all methods. Also, comparison of the HF densities calculated using different basis sets, as plotted in Figure 5.6, shows that this minimum is not due to the choice of basis set. The minima of the higher level wavefunction methods (MP2, MP4(SDQ), and QCISD), as shown in Figure 5.4, are shallow in comparison to the UHF and the ROHF wells, while the DFT-based methods exhibit wells which are similar in form to the reference QCISD minimum, Figure 5.5. The α distributions for the rest of the methods and basis sets, although not shown are similar in form to the one shown for QCISD in Figure 5.3 and do not exhibit minima. This implies a distinct difference in the qualitative behaviour of the α - and β -spin densities in the binding region with the α -spin density monotonically

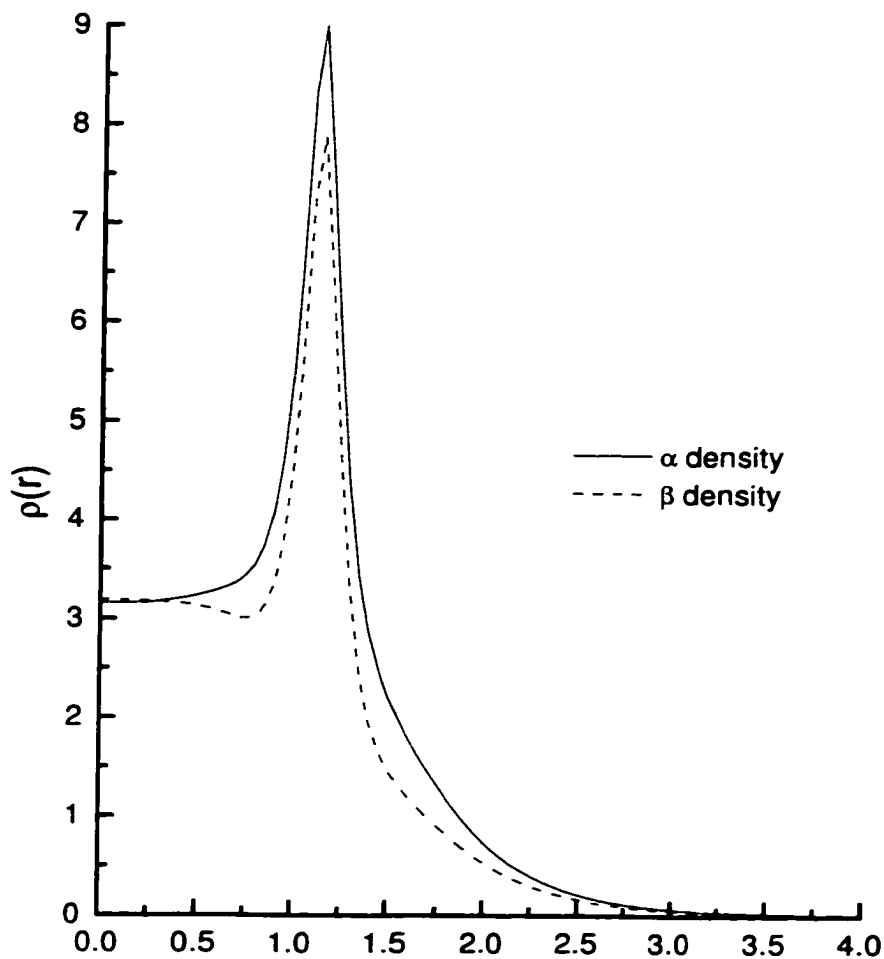


Figure 5.3: Graph of the spherically averaged QCISD densities using the aug-CC-PVDZ basis set for O_2 .

decreasing as a function of r from the nucleus to the bond midpoint, while the β -spin density exhibits a build-up of density at the bond midpoint along with a minimum toward the nucleus.

The SPIs for a variety of molecules, table 5.3, provide further insight into the spin-polarisation given by each of the methods. The results for many of these molecules, CH, NH, OH, CN and CH_3 are not as method dependent as was observed for the O_2 molecule. Thus, accurate values for the properties which depend on the molecular spin-polarisation should be easier to obtain for these molecules. However, for FO,

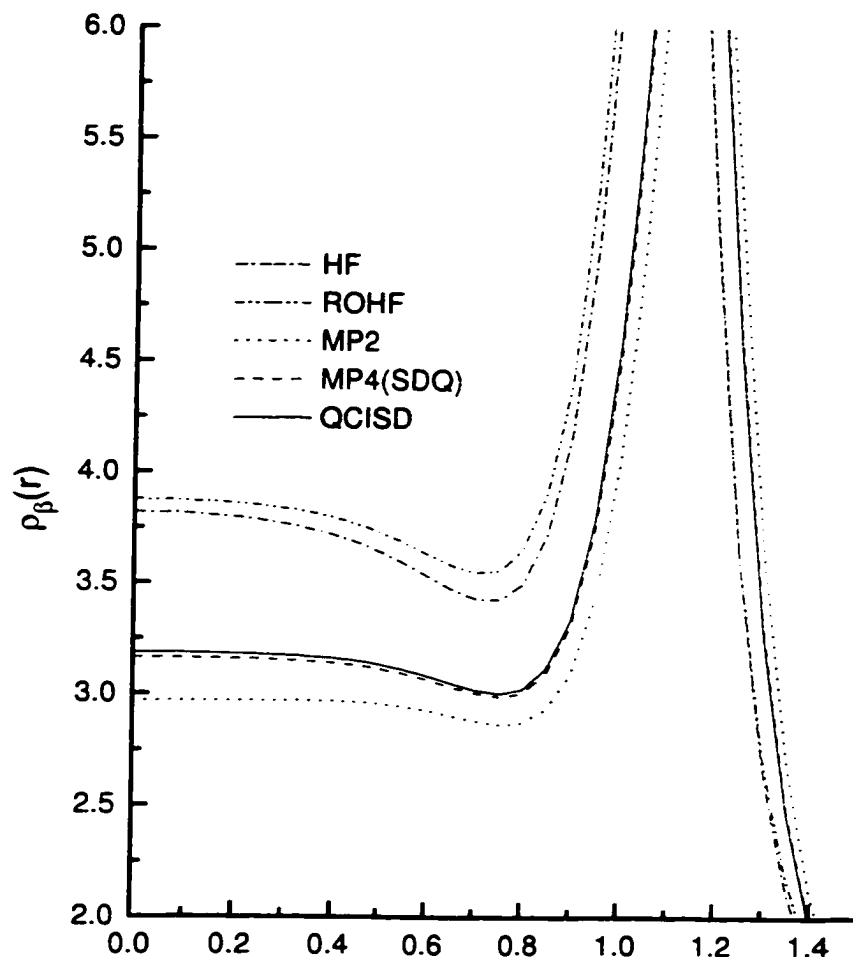


Figure 5.4: Plot of the spherically averaged β densities for the wave function based methods using the aug-CC-PVDZ basis set for O_2 .

NO and NO_2 , the SPIs again show large fluctuations depending on the method used, and parallel the results found for O_2 . This implies that spin partitioning can be quite difficult for certain molecules, especially ones containing oxygen. The CH molecule was also calculated using the aug-CC-PCVDZ basis set to account for polarisation of the core electrons. The results are similar to those obtained with the CC-PVDZ basis set and indicates that the core electrons do not have a large impact on the spin polarisation. Also the change in basis set size does not significantly change the SPI values.

Table 5.3: Spin density polarisation index values for selected molecules calculated by use of the aug-CC-PVDZ basis set

Molecule	Method										
	UHF	ROHF	SVWN	BPW91	B3PW91	B3LYP	MP2	MP4(SDQ)	QCISD		
CH(² Π)	0.4202	0.3987	0.4113	0.4137	0.4158	0.4186	0.4107	0.4073	0.4071		
(aug-CC-PCVDZ)	0.4203	0.3988	0.4112	0.4135	0.4156	0.4185	0.4108	0.4075	0.4073		
NH(³ Σ)	0.8964	0.8736	0.8945	0.8893	0.8924	0.8972	0.8811	0.8785	0.8785		
OH(² Π)	0.7146	0.6805	0.7027	0.7060	0.7085	0.7086	0.7006	0.7001	0.6996		
CN(² Π)	0.2580	0.2300	0.2713	0.2555	0.2625	0.2758	0.3436	0.2630	0.2539		
FO(² Π)	0.4272	0.3147	0.1317	0.1844	0.2391	0.2424	0.3604	0.3562	0.3330		
NO(² Π)	0.2365	0.0336	0.0688	0.0931	0.1189	0.1200	0.2365	0.2084	0.1820		
CH ₃ (² A ₂ '')	0.3959	0.3688	0.3853	0.3937	0.3951	0.3938	0.3833	0.3832	0.3845		
*NO ₂ (² A ₂)	0.5881	0.0000	0.1194	0.1728	0.2571	0.2553	0.3293	0.3618	0.3351		

*For the NO₂ molecule the CC-PVDZ basis set is used as explained in the text.

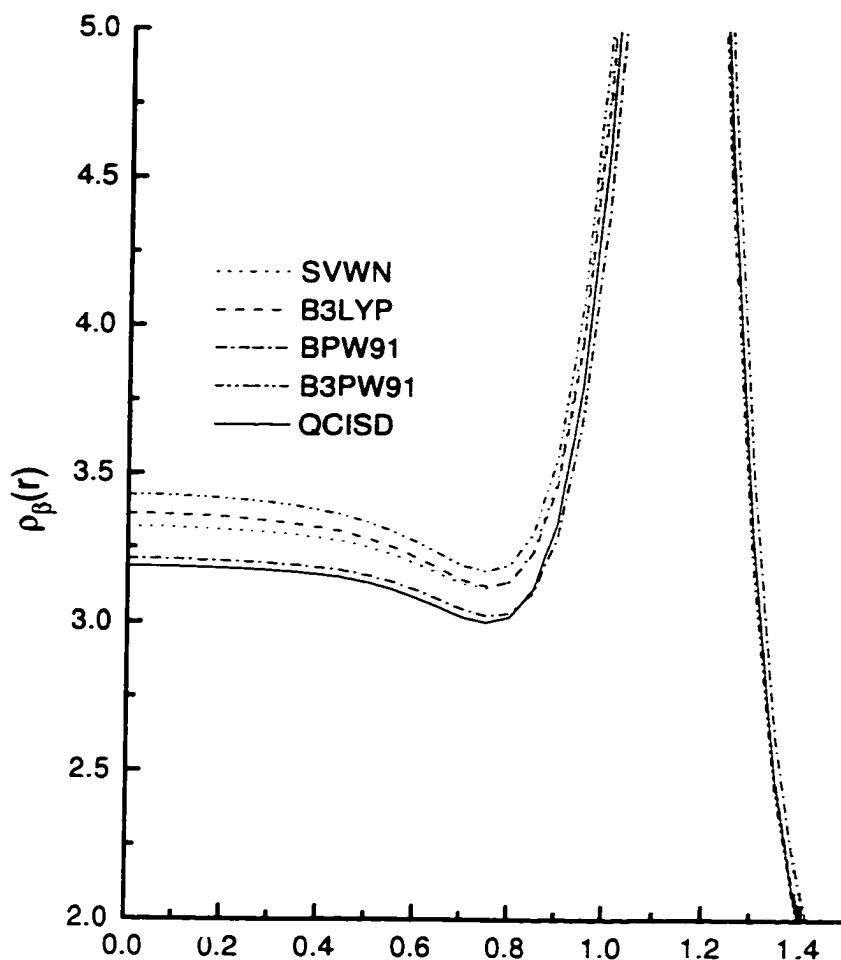


Figure 5.5: Plot of the spherically averaged β densities for the DFT based methods using the aug-CC-PVDZ basis set for O_2 .

NO_2 has been reported³¹ to have a very high spin contamination for the 2A_2 electronic state when calculated with the UHF method and a basis set similar to CC-PVDZ. Thus to compare the SPIs for a molecule which gives a very high spin contamination the NO_2 geometries and SPIs were calculated for the 2A_2 electronic state using the CC-PVDZ basis set. The UHF wavefunction gave a value of 1.1262 for $\langle S^2 \rangle$, which is much larger than the pure spin state value of 0.75. This confirmed that the wavefunction is highly spin contaminated and this leads to a very large SPI. The ROHF method which by definition does not have any spin contamination yields

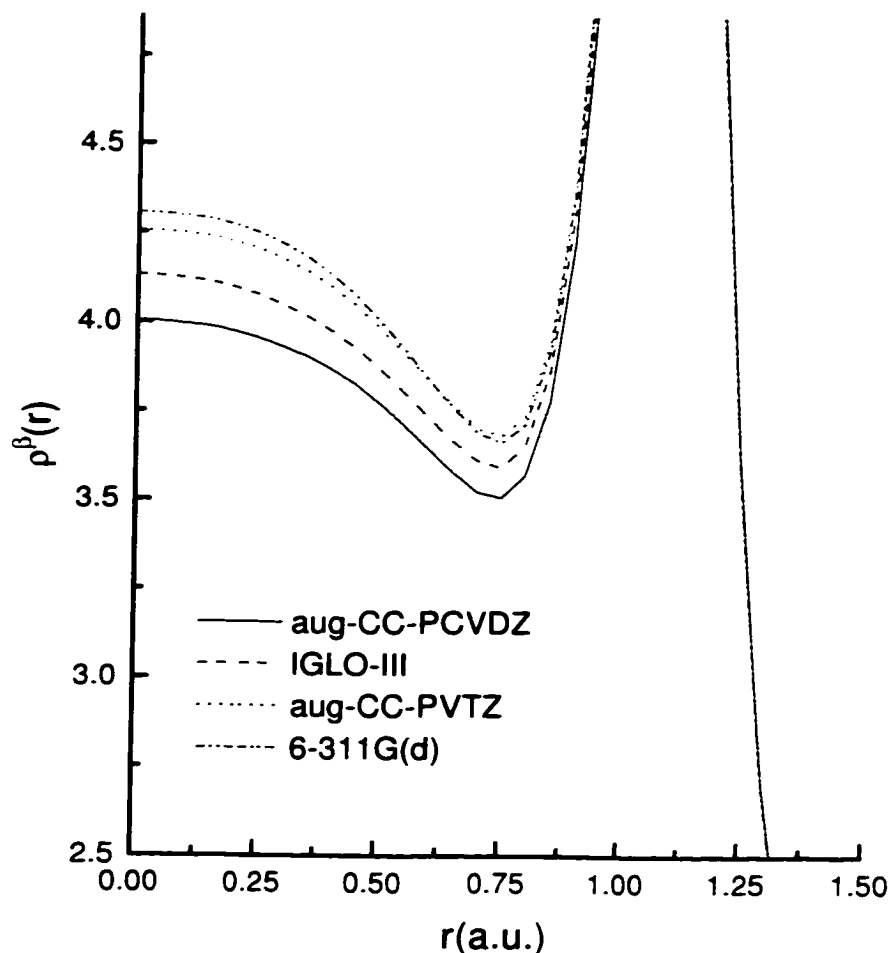


Figure 5.6: Plot of the spherically averaged β density calculated with the Hartree-Fock method using a variety of basis sets for O_2 .

a SPI of approximately zero. The approximate DFT functionals also give very low SPIs, with the hybrid values again giving larger values than the other two. The corresponding values for $\langle S^2 \rangle$, 0.7595 for SVWN, 0.7747 for BPW91, 0.8084 for B3LYP and 0.8101 for B3PW91, are quite small compared to the UHF reference and do not exhibit much spin contamination. The higher-level methods give much lower SPIs, with the QCISD value being 0.3351. Previously the spin contamination in CCSD calculations for this molecule was quite small even if the UHF reference wavefunction was highly spin contaminated.³¹ Therefore, since the QCISD wavefunction is very

similar to the CCSD wavefunction it is assumed that it also has a small spin contamination. The QCISD SPI value for this molecule reflects this low spin contamination with a value of 0.3351. All other high-level methods gave similar results. Thus, it can be seen that methods which have only a small degree of spin contamination yield smaller SPIs.

The size of these SPIs raises some interesting points. NO has a very low SPI which indicates that within molecular frameworks the $Z_{\alpha\alpha}$ and $Z_{\beta\beta}$ values should be quite similar which could indicate a delocalisation of the extra α electron. This also seems to be true for the CN species. The CH, CH₃ and FO values indicate that the extra α electron is more localised but there still may be some degree of delocalisation. Finally, the large value given by OH indicates that the extra α electron is mainly localised on the oxygen atom. The NH species cannot be directly compared to the others, it is a triplet state while the others are doublets. Comparing it to the previous O₂ values, however, indicates that, much like OH, NH localises the extra α electron density on the nitrogen atom.

Table 5.4, expands the SPI into the three corresponding integrals, $Z_{\alpha\alpha}$, $Z_{\beta\beta}$ and $Z_{\alpha\beta}$, for O₂, FO and NO. $Z_{\alpha\alpha}$ is significantly larger than the $Z_{\beta\beta}$ for the UHF method, while for the ROHF method the values are closer. For both methods the $Z_{\alpha\beta}$ results are approximately the same. For the density functional methods all of the integrals are smaller than the corresponding values found for QCISD. The difference between the $Z_{\alpha\alpha}$ and the $Z_{\beta\beta}$ quantities is also much smaller than that found with QCISD. This shows that the density functional methods spread out the densities much more than the other methods. Finally, the MP methods seem to slightly overestimate the three integrals but are still comparable to the QCISD values.

Table 5.4: Z values for selected molecules calculated by use of the aug-CC-PVDZ basis set

Molecule	Method										
	UHF	ROHF	SVWN	BPW91	B3PW91	B3LYP	MP2	MP4(SDQ)	QCISD		
FO	$Z_{\alpha\alpha}$	391.74	385.96	389.59	389.94	390.03	392.66	392.71	392.58		
	$Z_{\beta\beta}$	389.02	384.80	388.17	388.06	388.05	389.26	389.49	389.91		
	$Z_{\alpha\beta}$	390.56	385.67	388.86	388.97	389.01	390.89	391.03	391.18		
NO	$d_{\alpha\beta}$	0.4272	0.1317	0.1844	0.2391	0.2424	0.3604	0.3562	0.3330		
	$Z_{\alpha\alpha}$	268.83	261.55	264.06	264.35	267.37	266.40	266.03	265.18		
	$Z_{\beta\beta}$	264.29	261.06	263.49	263.58	263.54	263.44	264.33	264.02		
	$Z_{\alpha\beta}$	265.03	261.31	263.77	263.95	267.95	265.39	265.16	264.58		
	$d_{\alpha\beta}$	0.2365	0.0688	0.0931	0.1189	0.1200	0.2365	0.2084	0.1820		
	$Z_{\alpha\alpha}$	325.72	319.27	322.11	322.71	322.75	324.19	324.72	324.82		
O ₂	$Z_{\beta\beta}$	320.55	317.89	320.49	320.43	320.36	321.49	321.16	321.09		
	$Z_{\alpha\beta}$	322.99	318.57	321.28	321.54	321.53	322.79	322.87	322.88		
	$d_{\alpha\beta}$	0.5349	0.1490	0.1777	0.2433	0.2459	0.2892	0.3746	0.3898		

5.4 Conclusions

An overlap-like similarity measure has been created for the purpose of quantifying the spin polarisation within a molecule. A thorough investigation of the spin density polarisation index (SPI) for O_2 was completed to investigate method and basis set dependencies. The choice of the basis set used only had a small effect upon the calculated SPIs. However, there was some extreme method dependencies observed for O_2 with DFT results being substantially lower than QCISD results and ROHF giving a zero SPI.

The investigation of O_2 also included plots of the spherically averaged α and β electronic densities which have two prominent features. The first feature occurs near the bond midpoint and shows that the wavefunction based methods predict larger β electron densities in this region while the density functional methods predict larger α electron densities. The second feature observed is a minimum in the β density near the nuclei which is not mirrored in the α density. This feature, unlike the first, is not method dependent.

The O_2 results led to the calculation of the SPI for eight other small molecules. For five of these molecules all of the calculated SPIs were in reasonably good agreement. However, for the other three molecules method dependencies similar to O_2 were observed with DFT SPIs being relatively low. It is of interest to note that these molecules, FO, NO, NO_2 and O_2 , all have their unpaired electrons in either anti-bonding or non-bonding orbitals which gives further indications that DFT has trouble with these types of orbitals. To investigate the method dependencies of the SPI it was broken down into its components for FO, NO and O_2 . The results show that for DFT the $Z_{\alpha\alpha}$ and $Z_{\beta\beta}$ values are smaller and closer together than the corresponding QCISD values.

The results obtained with the SPI show that the handling of the spin polarisation is not straightforward for any method. Moreover, the current approximate DFT functionals have problems calculating the spin polarisations for some molecules. This problem was not observed with the density difference index of the previous chapter and indicates how the SPI can give additional information about DFT densities. However, the spherically averaged results shown for O₂ give another example of the differences between the DFT and wavefunction based densities. These differences are quite interesting and have led to further investigations into spherically averaged properties.

References

- [1] R. G. Parr and W. Yang, *Density-Functional Theory of Atoms and Molecules*, Oxford University Press, 1989.
- [2] D. W. Davies, *The Theory of the Electric and Magnetic Properties of Molecules*, John Wiley & Sons, London, 1967.
- [3] M. Sola, J. Mestres, R. Carbó, and M. Duran, *J. Chem. Phys.* **104**, 636 (1996).
- [4] J. Wang, L. A. Eriksson, B. G. Johnson, and R. J. Boyd, *J. Phys. Chem.* **100**, 5274 (1996).
- [5] J. Wang, B. G. Johnson, R. J. Boyd, and L. A. Eriksson, *J. Phys. Chem.* **100**, 6317 (1996).
- [6] J. Wang, Z. Shi, R. J. Boyd, and C. A. Gonzalez, *J. Phys. Chem.* **98**, 6988 (1994).
- [7] S. K. Worsnop, J. Wang, and R. J. Boyd, *J. Chem. Phys.* **107**, 17 (1997).

- [8] J. A. Pople, R. D. Adamson, and P. M. W. Gill, *J. Phys. Chem.* **100**, 6348 (1996).
- [9] R. Carbó, M. Arnau, and L. Leyda, *Adv. Quantum Chem.* **25**, 757 (1994).
- [10] D. L. Cooper and N. L. Allan, *J. Am. Chem. Soc.* **114**, 4773 (1992), and references therein.
- [11] J. M. Ugalde and C. Sarasola, *Phys. Rev. A.* **49**, 3081 (1994).
- [12] J. M. Ugalde, C. Sarasola, L. Dominguez, and R. J. Boyd, *J. Math. Chem.* **6**, 51 (1991).
- [13] M. J. Frisch, G. W. Trucks, H. B. Schlegel, P. M. W. Gill, B. G. Johnson, M. A. Robb, J. R. Cheeseman, T. A. Keith, G. A. Petersson, J. A. Montgomery, K. Raghavachari, M. A. Al-Laham, V. G. Zakrzewski, J. V. Ortiz, J. B. Foresman, J. Cioslowski, B. B. Stefanov, A. Nanayakkara, M. Challacombe, C. Peng, P. Y. Ayala, W. Chen, M. W. Wong, J. L. Andres, E. S. Repogle, R. Gomperts, R. L. Martin, D. J. Fox, J. S. Binkley, D. J. DeFrees, J. Baker, J. P. P. Stewart, M. Head-Gordon, C. Gonzalez, and J. A. Pople, *Gaussian 94*, Gaussian, Inc.: Pittsburgh PA, 1995.
- [14] C. Møller and M. S. Plesset, *Phys. Rev.* **46**, 618 (1934).
- [15] J. A. Pople, R. Seeger, and R. Krishnan, *Int. J. Quant. Chem. Symp.* **11**, 149 (1977).
- [16] R. Krishnan and J. A. Pople, *Int. J. Quant. Chem.* **14**, 91 (1978).
- [17] R. Krishnan and J. A. Pople, *J. Chem. Phys.* **72**, 4244 (1980).

- [18] J. A. Pople, M. Head-Gordon, and K. Raghavachari, *J. Chem. Phys.* **87**, 5968 (1987).
- [19] P. A. M. Dirac, *Proc. Cambridge Phil. Soc.* **36**, 376 (1930).
- [20] S. H. Vosko, L. Wilk, and M. Nusair, *Can. J. Phys.* **58**, 1200 (1980).
- [21] A. D. Becke, *J. Chem. Phys.* **96**, 2155 (1992).
- [22] J. P. Perdew, J. A. Chevary, S. H. Vosko, K. A. Jackson, M. R. Pederson, D. J. Singh, and C. Fiolhais, *Phys. Rev. B* **46**, 6671 (1992).
- [23] A. D. Becke, *J. Chem. Phys.* **98**, 5648 (1993).
- [24] C. Lee, W. Yang, and R. G. Parr, *Phys. Rev. B* **37**, 785 (1988).
- [25] R. A. Kendall and T. H. Dunning, Jr., *J. Chem. Phys.* **96**, 6796 (1992).
- [26] T. H. Dunning, Jr., *J. Chem. Phys.* **90**, 1007 (1989).
- [27] Basis sets were obtained from the Extensible Computational Chemistry Environment Basis Set Database. Version 1.0, as developed and distributed by the Molecular Science Computing Facility, Environmental and Molecular Sciences Laboratory which is part of the Pacific Northwest Laboratory, P.O. Box 999, Richland, Washington 99352, USA, and funded by the U.S. Department of Energy. The Pacific Northwest Laboratory is a multi-program laboratory operated by Battelle Memorial Institute for the U.S. Department of Energy under contract DE-AC06-76RLO 1830. Contact David Feller, Karen Schuchardt, or Don Jones for further information.

-
- [28] W. Kutzelnigg, U. Fleischer, and M. Schindler, *NMR-Basic Principles and Progress*, volume 23, Springer, Heidelberg, 1990, The IGLO-III basis set consists of an $(11s7p2d/6s2p)$ primitive set contracted to $[7s6p2d/4s2p]$.
- [29] A. D. McLean and G. S. Chandler, *J. Chem. Phys.* **72**, 5639 (1980).
- [30] R. Krishnan, J. S. Binkley, R. Seeger, and J. A. Pople, *J. Chem. Phys.* **72**, 650 (1980).
- [31] J. F. Stanton, *J. Chem. Phys.* **101**, 371 (1994).

6. Radial Moments of the Electron Density

The previous chapters have presented tools for assessing the spin polarisation of a molecule and the difference between two electron densities. Although both of these tools provide insight into different aspects of the electron densities they cannot be directly related to observable properties. Without a direct comparison to experimental values these tools must depend on other high-level methods for comparison. A calculable value which gives results that are directly comparable to experimental values while also giving insight into the accuracy of electron densities would complete a set of tools with which electron densities can be studied.

The radial moments of the electron density, $\langle r^n \rangle = \int \rho(r)r^n d\tau$, can be related to many measurable electronic properties such as the diamagnetic susceptibility and the nuclear shielding factor.¹⁻⁵ Also, the various powers of the radial distance sample the short- and long-range electron densities differently giving some insight into the behaviour of the density in various regions in space. These molecular properties satisfy both of the above criteria and hence fit in perfectly with the two previous methods. However, even though the radial moments are accessible from Compton scattering and small-angle electron scattering data^{6,7} experimental measurement of these values can be problematic which means that reliable experimental results are

available only for a small number of molecules.

Until recently the moments of the electron density, $\langle r^n \rangle$, have been calculated using numerical techniques.^{8,9} This provided accurate results but also limited the calculations for larger molecules. New analytical methods to generate these moments have recently been published.^{10,11} These methods are much more flexible than numerical techniques and are capable of including the effects of solvation, which have not been investigated previously. This chapter provides a complete overview of the algorithm of Sarasola *et al.*¹¹ for the analytical calculation of radial moments. Using this algorithm the $\langle r^n \rangle$, $n = -1, 1, 2, 3$ values are generated for a selected set of molecules. Comparison of these values with experimental results shows that this analytical method is accurate for a series of molecules. Also, two different solvation models are employed to determine the effect of a solvent upon calculated radial moments which provides indirect evidence on the effect of a solvent on the molecular electron densities.

The studies presented in the previous chapters have all focussed on the accuracy of electron densities obtained with density functional theory (DFT). This chapter is no exception as it discusses the accuracy of the moments given by five different approximate exchange-correlation functionals. The values from other methods are also given for comparison and also to connect to previous results where only theoretical results were available. As with the other tools, the radial moments of the electron density will hopefully provide enough insight into the electron density to be used as a tool to refine exchange-correlation functionals.

6.1 Analytical Calculation of the Radial Moments of the Electron Density

The following is the analytical method to calculate the radial moments given by Sarasola *et al.*¹¹ which was used for this investigation and all calculations were carried out at the centre of mass for each molecule. The radial moments of the electron density are spherically averaged properties given by,

$$\langle r^n \rangle = \int \rho(r) r^n dr \quad (6.1)$$

where n is an integer and $\rho(r)$ is given by the expression,

$$\rho(r) = \int \rho(\mathbf{r}) r^2 \sin \theta d\phi d\theta \quad (6.2)$$

and $\rho(\mathbf{r})$ is the just the single particle density $\rho(\mathbf{x}_1; \mathbf{x}_1)$ as given in chapter 3. By use of the natural or Kohn-Sham orbitals, $\psi_\mu(\mathbf{r})$, this density can be easily expressed in terms of the elements of the density matrix, \mathbf{P} , as follows,

$$\rho(\mathbf{r}) = \sum_{\mu, \nu} P_{\mu\nu} \psi_\mu(\mathbf{r}) \psi_\nu(\mathbf{r}) \quad (6.3)$$

Using the customary expansion of the molecular orbitals as a linear combination of primitive Gaussians, i.e.

$$\psi_\nu(\mathbf{r}) = \sum_A c_A G_A(\mathbf{r}) \quad (6.4)$$

$$G_A(\mathbf{r}) \equiv G_A(\mathbf{r}; \alpha, \mathbf{R}_A, k, l, m) = (x - X_A)^k (y - Y_A)^l (z - Z_A)^m e^{-\alpha|\mathbf{r} - \mathbf{R}_A|^2} \quad (6.5)$$

the radial moments of the density can be cast in the form,

$$\langle r^n \rangle = \sum_{\mu, \nu} P_{\mu\nu} \sum_{A, B} c_{ACB} \int r^n G_A(\mathbf{r}) G_B(\mathbf{r}) r^2 \sin \theta d\phi d\theta dr \quad (6.6)$$

The Gaussian product theorem¹² allows the product of the two primitive Gaussians, G_A and G_B , to be contracted into a single Gaussian, G_P ,

$$G_P(\mathbf{r}) = K \sum_{k=0}^{k_A+k_B} \sum_{l=0}^{l_A+l_B} \sum_{m=0}^{m_A+m_B} f_k f_l f_m (x - X_P)^k (y - Y_P)^l (z - Z_P)^m e^{(-\gamma|\mathbf{r}-\mathbf{R}_P|^2)} \quad (6.7)$$

where

$$K = \exp\left(\frac{-\alpha_A \alpha_B |\mathbf{R}_A - \mathbf{R}_B|^2}{\alpha_A + \alpha_B}\right) \quad (6.8)$$

$$\gamma = \alpha_A + \alpha_B \quad (6.9)$$

$$\mathbf{R}_P = \frac{\alpha_A \mathbf{R}_A + \alpha_B \mathbf{R}_B}{\gamma} \quad (6.10)$$

The expression for the coefficients, f_k , f_l and f_m , can be found in standard references.¹²

Linear molecules can easily be rotated so that $X_P = Y_P = 0$ and $Z_P = \mathbf{R}_P$ while for nonlinear molecules a coordinate transformation for each pair of nuclei within a molecule can be defined to make both atoms lie on the z axis, such that $X_P = Y_P = 0$.¹³ This allows the integral in equation 6.6 to be expressed in terms of,

$$I(n) = \int r^n x^k y^l (z - R_P)^m e^{(-\gamma|\mathbf{r}-\mathbf{R}_P|^2)} r^2 \sin \theta d\phi d\theta dr \quad (6.11)$$

To establish a common coordinate system the Cartesians in the above expression are

converted into spherical polar coordinates,

$$I(n) = \int r^{(n+2)} (r \sin \theta \cos \phi)^k (r \sin \theta \sin \phi)^l (r \cos \theta - R_P)^m e^{-\gamma(r^2 + R_P^2 - 2rR_P \cos \theta)} \sin \theta d\phi d\theta dr \quad (6.12)$$

This expression can then be expanded and after collecting terms has the form,

$$I(n) = \sum_{s=0}^m \binom{m}{s} (-R_P)^{m-s} \int_0^\infty \left[\int_0^\pi e^{2\gamma r R_P \cos \theta} (\sin \theta)^{k+l+1} (\cos \theta)^s d\theta \right] r^{n+k+l+s+2} e^{-\gamma(r^2 + R_P^2)} dr \int_0^{2\pi} (\cos \phi)^k (\sin \phi)^l d\phi \quad (6.13)$$

The integration over ϕ is solved with the use of the Beta function, $B(x,y)$,

$$\int_0^{2\pi} (\cos \phi)^k (\sin \phi)^l d\phi = \begin{cases} 2B\left(\frac{k+1}{2}, \frac{l+1}{2}\right) & \text{if } k \text{ and } l \text{ even} \\ 0 & \text{otherwise} \end{cases} \quad (6.14)$$

A transformation of the θ integral must be used before being able to solve it analytically, the final integral has the form,

$$\int_0^{2\pi} e^{2\gamma r R_P \cos \theta} (\sin \theta)^{k+l+1} (\cos \theta)^s d\theta = \sum_{t=0}^{\frac{k+l}{2}} \binom{\frac{k+l}{2}}{t} (-1)^{\frac{k+l}{2}-t} \int_0^\pi e^{2\gamma r R_P \cos \theta} (\cos \theta)^{k+l+s-2t} \sin \theta d\theta \quad (6.15)$$

This can then be simplified to give,

$$\int_0^\pi e^{2\gamma r R_P \cos \theta} (\cos \theta)^{k+l+s-2t} \sin \theta d\theta = \int_{-1}^1 e^{a\mu} \mu^q d\mu \quad (6.16)$$

with $a = 2\gamma r R_P$, $q = k + l + s - 2t$ and $\mu = \cos \theta$. This new expression for the integral can now be expressed analytically as,

$$\int_{-1}^1 e^{a\mu} \mu^q d\mu = e^a \left(\frac{1}{a} + \sum_{u=1}^q \frac{(-1)^u q!}{(q-u)! a^{u+1}} \right) - (-1)^q e^{-a} \left(\frac{1}{a} + \sum_{u=1}^q \frac{q!}{(q-u)! a^{u+1}} \right) \quad (6.17)$$

The integrals over r can be solved using the $S(u)$ and $R(u)$ integral functions, namely

$$S(u) = \int_0^\infty e^{-\gamma(r-R_P)^2} r^u dr \quad (6.18)$$

and

$$R(u) = \int_0^\infty e^{-\gamma(r+R_P)^2} r^u dr \quad (6.19)$$

Analytical solutions to these integrals are achieved recursively using the relations,

$$S(u+2) = \frac{a+1}{2\gamma} S(u) + r_P S(u+1) \quad (6.20)$$

and

$$R(u+2) = \frac{a+1}{2\gamma} R(u) - R_P R(u+1) \quad (6.21)$$

Using the error function the initial cases of $u = 0$ and $u = 1$ have been solved so that,

$$S(0) = \frac{1}{2} \sqrt{\frac{\pi}{\gamma}} [1 + \operatorname{erf}(\sqrt{\gamma} R_P)] \quad (6.22)$$

$$S(1) = \frac{e^{-\gamma R_P^2}}{2\gamma} + \frac{R_P}{2} \sqrt{\frac{\pi}{\gamma}} [1 + \operatorname{erf}(\sqrt{\gamma} R_P)] \quad (6.23)$$

$$R(0) = \frac{1}{2} \sqrt{\frac{\pi}{\gamma}} [1 - \operatorname{erf}(\sqrt{\gamma} R_P)] \quad (6.24)$$

$$R(1) = \frac{e^{-\gamma R_P^2}}{2\gamma} - \frac{R_P}{2} \sqrt{\frac{\pi}{\gamma}} [1 + \operatorname{erf}(\sqrt{\gamma} R_P)] \quad (6.25)$$

Gathering the various solutions for the integrations over r , θ and ϕ allows the integral from equation 6.13 to be cast into the following analytical form,

$$\begin{aligned}
 I(n) = & 2B\left(\frac{k+1}{2}, \frac{l+1}{2}\right) \sum_{s=0}^m \binom{m}{s} (-R_P)^{(m-s)} \sum_{t=0}^{\frac{k+l}{2}} \binom{\frac{k+l}{2}}{t} (-1)^{\frac{k+l}{2}-t} \\
 & \left[\frac{S(v)}{2\gamma R_P} + \sum_{u=1}^q \frac{S(v-u)(-1)^u q!}{(q-u)!(2\gamma R_P)^{u+1}} \right. \\
 & \left. + (-1)^{q+1} \left(\frac{R(v)}{2\gamma R_P} + \sum_{u=1}^q \frac{R(v-u)q!}{(q-u)!(2\gamma R_P)^{u+1}} \right) \right] \quad (6.26)
 \end{aligned}$$

with the variables q and v defined as, $q = k + l + s - 2t$ and $v = n + k + l + m + 1$. This closed form completes the equations needed to calculate $\langle r^n \rangle$ analytically.

6.2 Computational Details

All molecular geometries were optimised at the same level of theory used to calculate the electron density and the associated radial moments. All computations were carried out with Gaussian 94.¹⁴

The electron densities were obtained using both methods based on the Hartree-Fock (HF) ground state wavefunction and density functional methods. Second-order Moller-Plesset perturbation theory [MP2],¹⁵⁻¹⁸ configuration interaction including single and double excitations [CISD] and quadratic configuration interaction including single and double excitations [QCISD]¹⁹ are methods which are known to give accurate molecular properties and are used in this study for comparison. The approximate exchange-correlation functionals used in the DFT calculations include three “pure” functionals and two hybrid functionals which include some HF exchange energy. The pure functionals used were SVWN, which uses the local spin density exchange functional²⁰ with the Vosko, Wilk, and Nusair parameterisation of the local spin density

correlation functional,²¹ BPW91, which combines the Becke 88 gradient-corrected exchange functional²² with the Perdew and Wang 91 gradient-corrected correlation functional,²³ and BLYP which also uses the Becke 88 exchange functional but combines it with the Lee, Yang and Parr gradient-corrected correlation functional.²⁴ The hybrid methods both use Becke's three-parameter expression²⁵ for the inclusion of Hartree-Fock exchange energy and the Becke 88 gradient correction to the exchange functional. The B3LYP functional uses the Lee, Yang and Parr gradient correction to the correlation functional while the B3PW91 functional uses the Perdew and Wang 91 gradient correction to the correlation functional.

A previous study using this analytical method suggested that H₂ exhibited an oscillatory behaviour in the radial moments as the number of polarisation functions was increased.¹¹ In order to investigate whether or not a similar trend is observed in larger systems two larger molecules, N₂ and H₂O, are studied using the QCISD and MP2 methods along with a variety of basis sets. Polarisation functions, d and f functions for N and O and p and d functions for H, were added to the 6-311G and 6-311+G basis sets to analyse their effects on the moments.^{26,27} Subsequent calculations using the CC-PVDZ and CC-PVTZ basis sets as well as their augmented counterparts were also done for comparison.²⁸

After the basis set analysis was completed, calculations on ten small molecules using all of the methods described above and the 6-311G(2df,p) basis set were carried out. Finally, two solvation model calculations were performed using HF and all the DFT functionals to investigate their effect on the radial moments. The two models used were the basic Onsager model and a modified Tomasi polarised continuum model known as the self-consistent isodensity polarised continuum model [SCI-PCM]. Due to the limitations inherent in the Onsager model, results for N₂ and CH₄ molecules

could not be obtained using this model since neither of them has a dipole moment.

6.3 Results and Discussion

Table 1 shows the results for N_2 and H_2O obtained using the various basis sets. The N_2 results shown in figure 1 do not reveal an oscillatory behaviour as was previously found for the H_2 case. The QCISD and MP2 methods give comparable results with QCISD

Table 6.1: Radial moments of the electron density for N_2 and H_2O calculated using the MP2 and QCISD methods with a variety of basis sets.

Molecule	Method	Basis Set	Moment				
			$\langle r^{-1} \rangle$	$\langle r \rangle$	$\langle r^2 \rangle$	$\langle r^3 \rangle$	
N_2	MP2	6-311G	11.0841	21.8476	41.1917	92.2934	
		6-311G(d)	11.4442	21.3350	39.6081	88.0673	
		6-311G(2d)	11.5024	21.2600	39.3540	87.2798	
		6-311G(2df)	11.5338	21.2292	39.2719	87.0867	
		6-311+G	11.0677	21.9404	41.8034	95.6926	
		6-311+G(d)	11.4354	21.4052	40.0889	90.7574	
		6-311+G(2d)	11.4969	21.3208	39.7909	89.8133	
		6-311+G(2df)	11.5271	21.2873	39.6824	89.4526	
		CC-PVDZ	11.3677	21.4053	39.6860	87.6647	
		CC-PVTZ	11.5290	21.2597	39.4697	88.1713	
		aug-CC-PVDZ	11.3355	21.5455	40.5318	92.1039	
		aug-CC-PVTZ	11.5218	21.2926	39.6874	89.4894	
		QCISD	6-311G	11.2550	21.6195	40.5092	90.4606
			6-311G(d)	11.5655	21.1734	39.1146	86.7018
	6-311G(2d)		11.6265	21.0929	38.8294	85.7659	
	6-311G(2df)		11.6585	21.0616	38.7430	85.5460	
	6-311+G		11.2429	21.7046	41.0903	93.7418	
	6-311+G(d)		11.5586	21.2349	39.5419	89.1078	
	6-311+G(2d)		11.6207	21.1505	39.2384	88.1230	
	6-311+G(2df)		11.6526	21.1146	39.1159	87.6912	
	CC-PVDZ		11.4854	21.2481	39.2153	86.4056	
	CC-PVTZ		11.6535	21.0910	38.9306	86.5706	
	aug-CC-PVDZ		11.4589	21.3685	39.9537	90.3284	
	aug-CC-PVTZ		11.6505	21.1133	39.0931	87.6164	

Molecule	Method	Basis Set	Moment			
			$\langle r^{-1} \rangle$	$\langle r \rangle$	$\langle r^2 \rangle$	$\langle r^3 \rangle$
H ₂ O						
	MP2					
		6-311G	19.6483	11.5305	19.5232	40.8610
		6-311G(d,p)	19.3018	11.4345	19.1166	39.5756
		6-311G(2d,p)	19.3398	11.4440	19.1609	39.7521
		6-311G(2d,2p)	19.3669	11.4377	19.1438	39.7076
		6-311G(2df,p)	19.3686	11.4272	19.1015	39.5679
		6-311G(2df,2pd)	19.3518	11.4297	19.1135	39.6311
		6-311+G	19.6699	11.6996	20.4722	45.2727
		6-311+G(d,p)	19.3193	11.5952	20.0188	43.7805
		6-311+G(2d,p)	19.3709	11.5966	20.0195	43.7578
		6-311+G(2d,2p)	19.3773	11.5840	19.9641	43.5402
		6-311+G(2df,p)	19.3960	11.5772	19.9431	43.4886
		6-311+G(2df,2pd)	19.3640	11.5735	19.9227	43.4309
		CC-PVDZ	19.2009	11.4252	18.9946	38.9692
		CC-PVTZ	19.3505	11.4846	19.3890	40.7678
		aug-CC-PVDZ	19.2593	11.6518	20.2473	44.7800
		aug-CC-PVTZ	19.3566	11.5899	20.0231	44.0146
	QCISD					
		6-311G	19.6169	11.5357	19.5274	40.8313
		6-311G(d,p)	19.3146	11.4281	19.0769	39.3959
		6-311G(2d,p)	19.3545	11.4356	19.1114	39.5310
		6-311G(2d,2p)	19.3754	11.4286	19.0906	39.4744
		6-311G(2df,p)	19.3847	11.4164	19.0422	39.3137
		6-311G(2df,2pd)	19.3688	11.4170	19.0453	39.3448
		6-311+G	19.6380	11.6951	20.4291	45.0534
		6-311+G(d,p)	19.3336	11.5733	19.8963	43.2296
		6-311+G(2d,p)	19.3861	11.5717	19.8810	43.1351
		6-311+G(2d,2p)	19.4041	11.5562	19.8160	42.8911
		6-311+G(2df,p)	19.4125	11.5483	19.7856	42.7871
		6-311+G(2df,2pd)	19.3940	11.5408	19.7508	42.6807
		CC-PVDZ	19.2128	11.4235	18.9787	38.8803
		CC-PVTZ	19.3791	11.4629	19.2824	40.3423
		aug-CC-PVDZ	19.2835	11.6276	20.1172	44.1913
		aug-CC-PVTZ	19.3900	11.5533	19.8299	43.1637

having slightly higher values for $\langle r^{-1} \rangle$ and lower values for the positive powers of r . Addition of the first set of d polarisation functions to the 6-311G and 6-311+G basis set leads to a sharp increase for $\langle r^{-1} \rangle$ and a sharp decrease for all other moments. The second set of d polarisation functions has a similar influence on the moments, increasing $\langle r^{-1} \rangle$ and decreasing the rest, but the change is much smaller. Finally, the addition of f polarisation functions to the 2d polarisation functions produces only small variations in the moments and suggests that the moments are converging to a limiting value.

The addition of polarisation functions to the 6-311G and 6-311+G basis sets provides a much different result for H₂O than noted above for N₂ (See figure 2). The most notable change in the moments comes with the addition of the (d,p) polarisation functions with all moments decreasing significantly. The addition of more polarisation functions yields very small oscillations around the (d,p) value for $\langle r \rangle$, $\langle r^2 \rangle$ and $\langle r^3 \rangle$. This may correspond to the previous H₂ results which also exhibited oscillations in their values with the addition of polarisation functions. The r^{-1} moment is the exception: after the initial sharp decrease its value starts to increase again with the addition of polarisation functions until the (2df,p) set of polarisation functions is reached after which there is a small decrease in value with the (2df,2pd) set of polarisation functions.

The data in Table 1 also show that the addition of diffuse functions to a given basis set leads to an increase in the moments for $n > 0$ and a very small decrease in $\langle r^{-1} \rangle$. This observation holds for N₂ and H₂O with both the MP2 and QCISD methods. Moreover, the effect on $\langle r^2 \rangle$ and $\langle r^3 \rangle$ of introducing diffuse basis functions is greater than that of adding polarisation functions to a basis set. This is readily understood because the higher powers of n sample the long-range behaviour

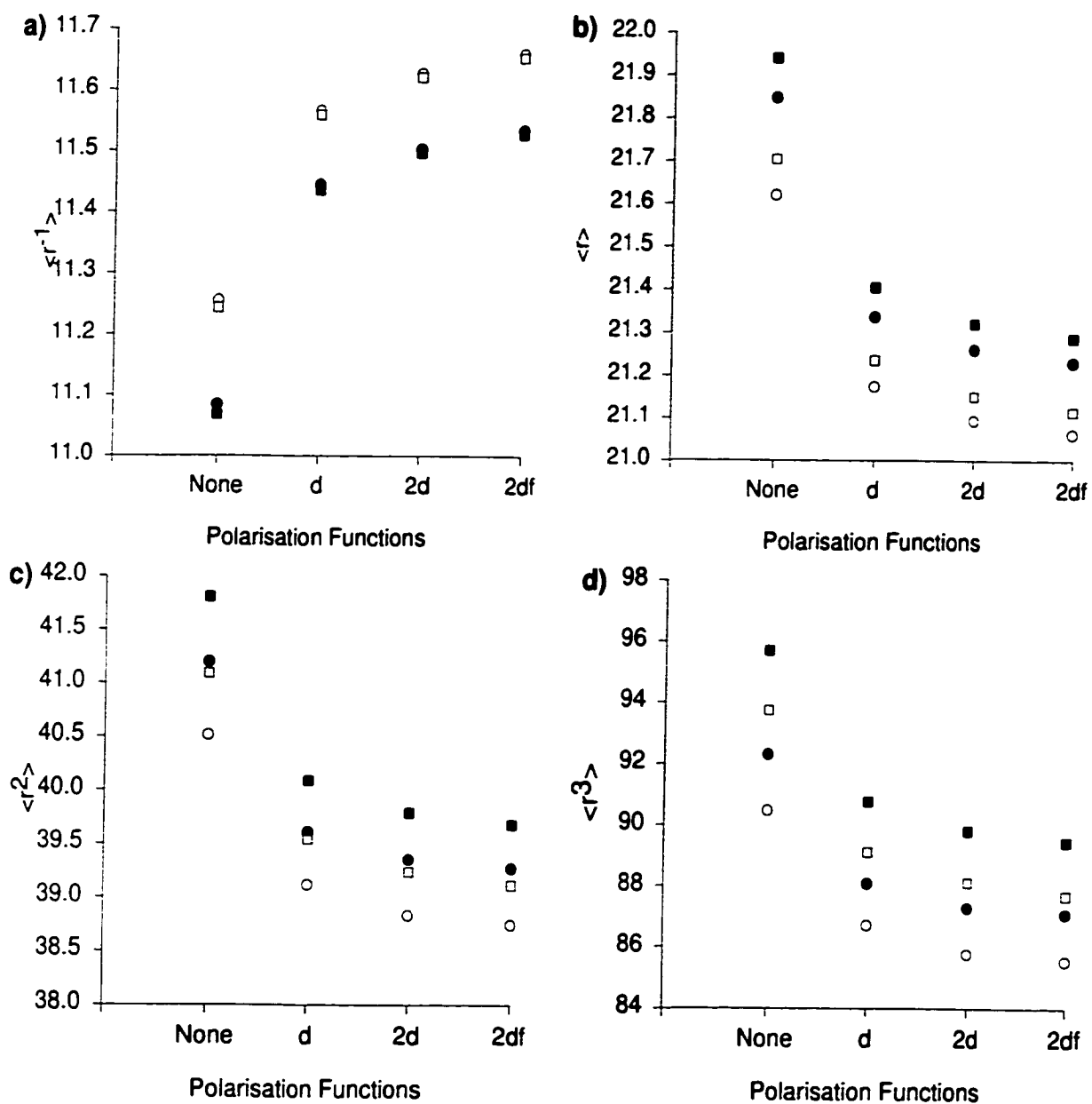


Figure 6.1: The effect of additional polarisation functions for N_2 using both the QCISD and MP2 methods. (● MP2 with the 6-311G basis set, ■ MP2 with the 6-311+G basis set, ○ QCISD with the 6-311G basis set and □ QCISD with the 6-311+G basis set)

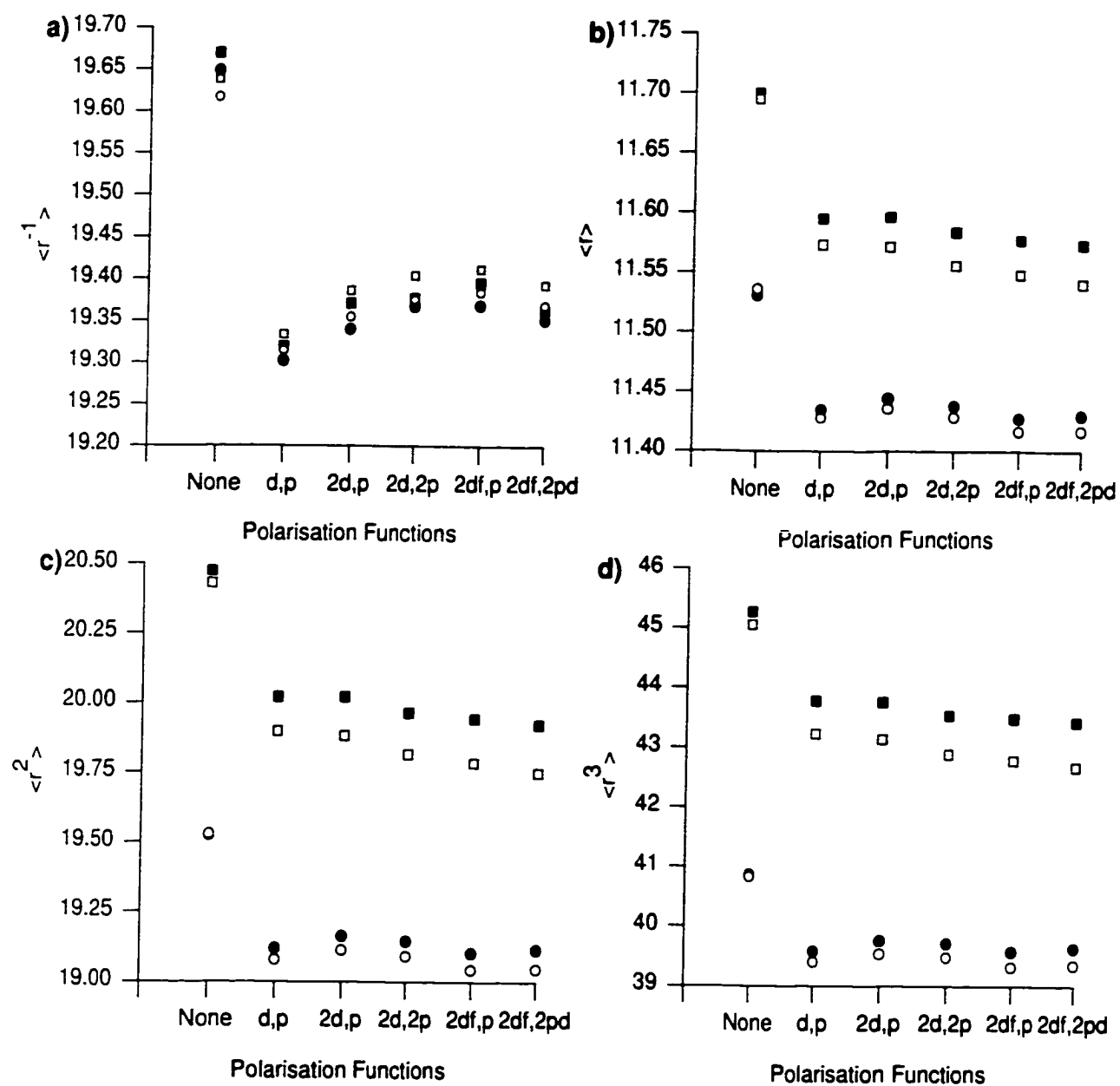


Figure 6.2: The effect of additional polarisation functions for H₂O using both the QCISD and MP2 methods. (● MP2 with the 6-311G basis set, ■ MP2 with the 6-311+G basis set, ○ QCISD with the 6-311G basis set and □ QCISD with the 6-311+G basis set)

of the electron density which is the region in which the diffuse functions are most important.

Experimental values for the r^2 moment have been determined for both N_2 and H_2O . The three experimental values for N_2 were obtained using high energy-electron scattering and yield 35.7 ± 0.7 ,²⁹ 37.2 ± 0.2 ³⁰ and 38.7 ± 0.2 .³¹ The most recent value, 38.7 ± 0.2 , compares well with the moments obtained using the 6-311G(2df) and the 6-311+G(2df) basis sets, with the MP2 method yielding 39.27 and 39.68 and the QCISD method giving 38.74 and 39.12, respectively. For H_2O the experimental value of 18.40 ± 2.40 ³² has a large uncertainty but compares reasonably well with the 6-311G(2df,p) basis set values of 19.10 and 19.04 with the MP2 and QCISD methods, respectively. The use of diffuse functions, as noted before, increases $\langle r \rangle$, $\langle r^2 \rangle$, and $\langle r^3 \rangle$ significantly but the $\langle r^2 \rangle$ values fall within the uncertainty range shown for the experimental value. Comparing the present N_2 and H_2O moments with the previously calculated moments of Wang and Smith¹⁰ and also those by Feller, Boyle and Davidson⁹ indicates that although the new values are slightly lower they are reasonably close to the previous values. The non-augmented double and triple zeta Dunning basis sets values for N_2 and H_2O are close to the 6-311G(2df,p) values while the augmented versions of these basis sets compare well with the 6-311+G(2df,p) basis set. The increased values for $\langle r \rangle$, $\langle r^2 \rangle$ and $\langle r^3 \rangle$ from both the augmented Dunning basis sets and the 6-311+G basis set may represent an artificial increase in the size of the electron cloud due to the addition of diffuse functions. To avoid any problems diffuse functions were not used and the 6-311G(2df,p) basis set was used for the remainder of the calculations.

Table 2 shows the moments calculated for the ten molecules by using the 6-311G(2df,p) basis set and a variety of methods. The first two molecules, N_2 and CO ,

Table 6.2: Radial moments of the density calculated at the centre of mass using the 6-311G(2df,p) basis set and a variety of methods.

Molecule	Method	Moment			
		$\langle r^{-1} \rangle$	$\langle r \rangle$	$\langle r^2 \rangle$	$\langle r^3 \rangle$
N ₂	B3LYP	11.7131	20.9892	38.5392	85.0736
	B3PW91	11.7127	20.9696	38.4180	84.5133
	BLYP	11.6162	21.1197	38.9597	86.3460
	BPW91	11.6204	21.0869	38.7804	85.5560
	SVWN	11.6765	21.0418	38.7257	85.6925
	HF	11.9027	20.7694	37.8716	83.1043
	MP2	11.5338	21.2292	39.2719	87.0867
	CISD	11.7304	20.9662	38.4423	84.6658
	QCISD	11.6585	21.0616	38.7430	85.5460
CO	B3LYP	11.8189	21.0937	39.5650	90.7936
	B3PW91	11.8182	21.0727	39.4263	90.0918
	BLYP	11.7260	21.2266	40.0207	92.2890
	BPW91	11.7288	21.1934	39.8200	91.3083
	SVWN	11.7940	21.1357	39.7302	91.3926
	HF	11.9860	20.8796	38.8600	88.5116
	MP2	11.7198	21.2383	40.0349	92.1632
	CISD	11.8471	21.0477	39.3677	89.9570
	QCISD	11.7784	21.1415	39.6727	90.8905
CH ₄	B3LYP	16.7341	15.9715	35.8067	95.1651
	B3PW91	16.7337	15.9362	35.5628	93.8570
	BLYP	16.7302	16.0407	36.2014	97.0088
	BPW91	16.7317	15.9887	35.8514	95.1570
	SVWN	16.6603	16.0202	36.0845	96.4022
	HF	16.7092	15.9413	35.4612	93.0902
	MP2	16.7319	15.9653	35.7114	94.5088
	CISD	16.7269	15.9563	35.6135	93.9059
	QCISD	16.7222	15.9834	35.7578	94.5322

Molecule	Method	Moment			
		$\langle r^{-1} \rangle$	$\langle r \rangle$	$\langle r^2 \rangle$	$\langle r^3 \rangle$
NH ₃	B3LYP	16.8345	13.5643	26.4047	62.5539
	B3PW91	16.8283	13.5340	26.2124	61.6128
	BLYP	16.6490	13.6507	26.8171	64.3023
	BPW91	16.6535	13.6034	26.5294	62.9117
	SVWN	16.7658	13.6176	26.6488	63.4770
	HF	17.0697	13.4649	25.8386	59.9504
	MP2	16.8069	13.5628	26.3397	62.0937
	CISD	16.8369	13.5348	26.1759	61.3327
	QCISD	16.7830	13.5628	26.3034	61.8396
H ₂ O	B3LYP	19.3970	11.4291	19.1553	39.8987
	B3PW91	19.4025	11.4067	19.0316	39.3593
	BLYP	19.2868	11.4912	19.4314	40.9640
	BPW91	19.3047	11.4577	19.2508	40.1771
	SVWN	19.3191	11.4748	19.3310	40.4685
	HF	19.5935	11.3233	18.6457	37.8882
	MP2	19.3686	11.4272	19.1015	39.5679
	CISD	19.4281	11.3948	18.9530	38.9948
	QCISD	19.3847	11.4164	19.0422	39.3137
HF	B3LYP	23.7625	9.5211	13.4938	24.0924
	B3PW91	23.7709	9.5098	13.4394	23.8893
	BLYP	23.7060	9.5564	13.6348	24.5651
	BPW91	23.7209	9.5400	13.5567	24.2722
	SVWN	23.6702	9.5592	13.6176	24.4358
	HF	23.8730	9.4503	13.1921	23.0749
	MP2	23.7682	9.5205	13.4636	23.9305
	CISD	23.7950	9.4998	13.3841	23.6776
	QCISD	23.7757	9.5113	13.4263	23.8088
PH ₃	B3LYP	39.4068	23.5552	55.7905	169.6639
	B3PW91	39.3252	23.4984	55.3406	166.9329
	BLYP	39.1721	23.6484	56.3585	172.7083
	BPW91	39.0843	23.5640	55.7123	168.8457
	SVWN	38.9294	23.5891	55.9659	170.7538
	HF	40.0278	23.5327	55.5616	167.7199
	MP2	39.5619	23.5266	55.5335	167.8507
	CISD	39.6131	23.5189	55.4478	167.1792
	QCISD	39.5164	23.5415	55.5737	167.8084

Molecule	Method	Moment			
		$\langle r^{-1} \rangle$	$\langle r \rangle$	$\langle r^2 \rangle$	$\langle r^3 \rangle$
H₂S					
	B3LYP	44.9893	20.8725	44.4550	124.5433
	B3PW91	44.9704	20.8113	44.0164	122.0563
	BLYP	44.8274	20.9437	44.8899	126.8131
	BPW91	44.8340	20.8569	44.2823	123.4031
	SVWN	44.7416	20.8933	44.5577	125.0720
	HF	45.3179	20.8412	44.1324	122.3220
	MP2	45.0380	20.8570	44.2616	123.1455
	CISD	45.0800	20.8400	44.1326	122.3556
	QCISD	45.0184	20.8585	44.2350	122.8446
CH₃OH					
	B3LYP	11.1310	35.6786	84.3461	232.9274
	B3PW91	11.1763	35.5510	83.7364	230.2145
	BLYP	11.0277	35.9713	85.7269	238.8266
	BPW91	11.0818	35.8030	84.8808	234.9218
	SVWN	11.2329	35.5137	83.9640	232.7309
	HF	11.2736	35.3107	82.5866	225.1541
	MP2	11.1452	35.6303	84.0652	231.4260
	CISD	11.2100	35.4542	83.3346	228.8354
	QCISD	11.1566	35.6104	83.9686	230.9188
CH₃SH					
	B3LYP	16.1814	54.7565	146.4143	470.0249
	B3PW91	16.2715	54.4615	144.7929	461.8121
	BLYP	16.0375	55.1907	148.6980	481.1179
	BPW91	16.1618	54.7792	146.4314	469.6152
	SVWN	16.4252	53.9796	142.5771	453.4708
	HF	16.2793	54.4821	144.8629	461.5786
	MP2	16.2597	54.5230	145.2274	464.4152
	CISD	16.2821	54.4467	144.7146	461.2604
	QCISD	16.2201	54.6282	145.6718	465.9191

are isoelectronic and yield similar results but with the CO moments being slightly larger than the N₂ moments. The increased $\langle r^{-1} \rangle$ value could be due to the shifting of the centre of mass towards the oxygen atom and thus there should be a slightly larger electron density near the origin. This shift of the centre of mass along with the fact that the C-O bond is slightly longer than the N-N bond will yield larger moments for $n > 0$. As was previously stated the QCISD method gives moments that compare very well with experimental values and therefore the QCISD method will be the standard used for comparisons with all of the molecules. Comparison of the DFT functionals with the QCISD values yields very interesting results with the B3LYP and BPW91 functionals giving the best agreement while the BLYP and B3PW91 functionals give only fair agreement with the QCISD values. Furthermore, the BLYP and B3PW91 functionals are on opposite sides of the QCISD values with the BLYP functional underestimating $\langle r^{-1} \rangle$ and overestimating the others and B3PW91 overestimating $\langle r^{-1} \rangle$ and underestimating the others. The local spin density functional, SVWN, gives unexpectedly good agreement with the QCISD values. Hartree-Fock results are poor as is expected since they lack electron correlation with the $\langle r^{-1} \rangle$ values being too large and the rest being too small. This shows that HF underestimates the size of the electron cloud and puts more density within the bonding region than other methods. This observation is consistent with the results of previous studies of the effect of electron correlation on the one-electron distributions of small atoms.^{33,34} The MP2 results, surprisingly, are relatively poor also, with $\langle r^{-1} \rangle$ being too small and $\langle r \rangle$, $\langle r^2 \rangle$, and $\langle r^3 \rangle$ too large which could indicate that the MP2 electron density is too diffuse. The CISD moments are also quite poor but differ in the opposite direction than the MP2 moments. A more detailed discussion of the electron density in CO as calculated by various conventional *ab initio* and

density functional methods has already been done giving more information.³⁵

The high symmetries of the molecules within the neutral ten-electron series, CH₄, NH₃, H₂O and HF, should lead to electron clouds which are close to spherical in nature. Thus, as the atomic number of the heavy atom, A, in the binary hydrides, AH_n, increases $\langle r \rangle$, $\langle r^2 \rangle$ and $\langle r^3 \rangle$ decrease and $\langle r^{-1} \rangle$ increases. These observations are consistent with a contraction of the electron cloud and a concomitant shortening of the A-H bond length. In this series the r^2 moment for CH₄ has been determined, yielding a value of $33.69 \pm 0.72^{8,36}$ which corresponds reasonably well to both the QCISD and CISD values, 35.61 and 35.76, respectively. The CH₃OH and CH₄SH molecules, which have non-spherical electron clouds, have small $\langle r^{-1} \rangle$ values when compared to the other moments which indicates that there is only a small amount of electron density near the centre of mass. The $\langle r \rangle$, $\langle r^2 \rangle$ and $\langle r^3 \rangle$ values indicate a large electron cloud as expected with significant differences between the $\langle r \rangle$ and $\langle r^2 \rangle$ values and between the $\langle r^2 \rangle$ and $\langle r^3 \rangle$ values. This indicates that the electron density continues to have a substantial magnitude at distances quite far from the centre of mass. This behaviour is also exhibited in the H₂S and PH₃ molecules which is expected since there is an increased number of electrons as well as a much larger electron cloud due to the inclusion of third-row elements.

Comparison of the current values to previously calculated moments reveals an interesting trend. The calculated $\langle r \rangle$, $\langle r^2 \rangle$ and $\langle r^3 \rangle$ values from Wang and Smith¹⁰ and the calculated $\langle r^2 \rangle$ values from Feller, Boyle and Davidson⁹ for H₂O, CO, N₂, NH₃, and HF are all slightly larger than the current values. Thus, this method seems to predict an electron cloud which is slightly smaller than what previous calculations predict. The $\langle r^2 \rangle$ value of Feller, Boyle and Davidson⁹ for H₂S seems

to contradict this trend since it is smaller than the current calculation. However, the reported $\langle r^2 \rangle$ value for PH_3 of 26.6669 by Davidson *et al.*⁹ is clearly wrong and suggests that an error may have been made in the calculations for molecules with second-row elements.

The accuracy of different methods, when compared to the QCISD method, is quite varied. The hybrid DFT functionals give generally good agreement with the QCISD results, with B3PW91 usually being better than B3LYP. For non-polar or slightly polar molecules these hybrid functionals tend to overestimate $\langle r^{-1} \rangle$ and underestimate the $n > 0$ moments. As the polarity increases, though, the $\langle r^{-1} \rangle$ values decrease while the $\langle r \rangle$, $\langle r^2 \rangle$ and $\langle r^3 \rangle$ values increase with respect to the QCISD values. This helps to increase the accuracy of these methods as the polarity increases. However, when the molecules become too polar the $\langle r^{-1} \rangle$ values become too small and $\langle r \rangle$, $\langle r^2 \rangle$ and $\langle r^3 \rangle$ become too large. The r^{-1} moment is underestimated for HF, PH_3 and H_2S with both methods and also for CH_3OH and CH_3SH with B3LYP while the other moments are overestimated for HF only with B3PW91 and in all but N_2 , CO and CH_4 with B3LYP. The inclusion of second-row elements decreases the accuracy of both of these methods. For the larger non-spherical molecule CH_3OH the accuracy of these methods is quite good but when coupled with a second-row element, in CH_3SH , the accuracy of these methods falls off once again. The 'pure' DFT functionals, SVWN, BLYP and BPW91, give inferior results when compared to the hybrid functionals. For all molecules both the BLYP and BPW91 methods underestimate $\langle r^{-1} \rangle$ and overestimate the other moments with the one exception being that both methods overestimate the r^{-1} moment of CH_4 . As the polarity of the molecules increases these two methods show a decrease in the $\langle r^{-1} \rangle$ values and increased values for the other moments which actually

decreases the accuracy of both methods. The addition of second-row elements also decreases the accuracy of BLYP but does not have a significant effect with the BPW91 functional while the CH₃OH and CH₃SH molecules, though, are a problem for both of these methods. The behaviour of SVWN is quite similar to BLYP and BPW91 with only a few exceptions. Again as the polarity of the molecules increases SVWN's agreement with the QCISD values worsens while the addition of second-row elements does affect SVWN but not to the extent seen with BLYP.

Hartree-Fock is known to give poor molecular properties since it does not include electron correlation and this is again reflected in the poor values of the radial moments. For all molecules except CH₄, the r^{-1} moment is overestimated while $\langle r \rangle$, $\langle r^2 \rangle$ and $\langle r^3 \rangle$ are all underestimated which indicates that Hartree-Fock gives a much too compact electron cloud. For CH₄ the $\langle r^{-1} \rangle$ value along with the $\langle r \rangle$, $\langle r^2 \rangle$ and $\langle r^3 \rangle$ values are all too small. Increased molecular polarity only decreases the accuracy of the Hartree-Fock moments, however, the addition of second-row elements does not affect the accuracy of the moments to the extent seen with the 'pure' DFT functionals. It is interesting to note that these qualitative observations for the Hartree-Fock method are not easily discerned from the published correlation difference density plots.³⁷ MP2 does not give any clear trends but the results are in much better agreement with the QCISD moments than Hartree-Fock, as expected. It is well known that MP2 often overcorrects the problems of the Hartree-Fock wavefunction but this is not done in any systematic way and could account for the lack of any clear trends. The best overall agreement with the QCISD values comes from the CISD values. For all molecules, CISD overestimates $\langle r^{-1} \rangle$ and underestimates $\langle r \rangle$, $\langle r^2 \rangle$ and $\langle r^3 \rangle$. However, unlike the above observations with the Hartree-Fock method the agreement between CISD and QCISD values increases as

the molecular polarity increases. The addition of second-row elements has little effect on the accuracy of the CISD values, as was observed with the Hartree-Fock method.

6.4 The Effects of Solvation on the Radial Moments of the Density

Tables 6.4, 6.4, 6.4 and 6.4 list the differences between the solvated and the gas-phase radial moments as calculated for the ten molecules by use of the Onsager and SCI-PCM solvation models, respectively. It is readily apparent that both models generally give the same trends in the calculated changes in the moments first as the molecules are dissolved in benzene and then as the dielectric constant is increased through the use of two other solvents, chlorobenzene and water. In particular, most of the polar molecules exhibit an overall decrease in the size of their electron clouds upon dissolution in benzene, as seen in the decreased $\langle r^3 \rangle$ values. This shrinking of the electron cloud continues as the dielectric constant is increased. The CO molecule is the only polar molecule which exhibits higher moments in benzene than in the gas-phase. Furthermore, the CO moments increase as the dielectric constant increases. Although this result is opposite to that observed for the other polar molecules the increased moments are evidence that the electron distribution is shifting so as to make the molecule more polar. In fact, upon close examination of the moments of the polar molecules there is evidence that their polarity increases in solution. Moreover, the higher the dielectric constant the greater the increase in the polarity of the molecule. Since the radial moments are spherically averaged, it is not possible to determine exactly how the electron distributions are rearranged but the above argument does agree with previous observations.³⁸⁻⁴⁰ The effects of dissolving the two non-polar molecules, N₂ and CH₄, are different. The N₂ molecule, like CO, gives larger moments in benzene which also increase as the solvent's dielectric constant increases. CH₄,

Table 6.3: The difference between the solvated and gas phase r^{-1} and r moments as calculated at the centre of mass using the 6-311G(2df,p) basis set and the Onsager solvation model.

Molecule	Method	Benzene ($\epsilon = 2.274$)		Chlorobenzene ($\epsilon = 5.62$)		Water ($\epsilon = 78.54$)	
		$\langle r^{-1} \rangle$	$\langle r \rangle$	$\langle r^{-1} \rangle$	$\langle r \rangle$	$\langle r^{-1} \rangle$	$\langle r \rangle$
CO							
	B3LYP	0.0004	0.0000	0.0007	-0.0001	0.0009	0.0000
	B3PW91	0.0004	0.0001	0.0005	-0.0001	0.0009	0.0002
	BLYP	0.0004	-0.0001	0.0007	-0.0002	0.0010	-0.0001
	BPW91	0.0006	0.0001	0.0010	0.0001	0.0014	0.0001
	SVWN	0.0006	-0.0001	0.0010	0.0000	0.0013	0.0000
	HF	-0.0004	0.0001	-0.0005	0.0005	-0.0008	0.0004
NH ₃							
	B3LYP	-0.0707	0.0022	-0.1110	0.0021	-0.1424	0.0023
	B3PW91	-0.0644	0.0016	-0.1053	0.0018	-0.1376	0.0018
	BLYP	-0.0683	0.0002	-0.1093	-0.0001	-0.1384	-0.0008
	BPW91	-0.0634	-0.0002	-0.1003	-0.0007	-0.1278	-0.0009
	SVWN	-0.0770	0.0022	-0.1267	0.0029	-0.1603	0.0041
	HF	-0.0641	0.0019	-0.1066	0.0029	-0.1396	0.0035
H ₂ O							
	B3LYP	-0.0260	-0.0039	-0.0458	-0.0061	-0.0601	-0.0075
	B3PW91	-0.0258	-0.0035	-0.0437	-0.0053	-0.0580	-0.0069
	BLYP	-0.0225	-0.0045	-0.0389	-0.0074	-0.0522	-0.0095
	BPW91	-0.0249	-0.0035	-0.0421	-0.0061	-0.0557	-0.0078
	SVWN	-0.0268	-0.0041	-0.0518	-0.0061	-0.0715	-0.0073
	HF	-0.0286	-0.0021	-0.0480	-0.0030	-0.0622	-0.0035
HF							
	B3LYP	-0.0036	-0.0026	-0.0062	-0.0042	-0.0084	-0.0055
	B3PW91	-0.0036	-0.0023	-0.0062	-0.0037	-0.0085	-0.0049
	BLYP	-0.0031	-0.0030	-0.0052	-0.0049	-0.0071	-0.0063
	BPW91	-0.0033	-0.0028	-0.0057	-0.0044	-0.0077	-0.0057
	SVWN	-0.0039	-0.0026	-0.0068	-0.0042	-0.0093	-0.0054
	HF	-0.0052	-0.0017	-0.0083	-0.0028	-0.0109	-0.0035

Molecule	Method	Benzene ($\epsilon = 2.274$)		Chlorobenzene ($\epsilon = 5.62$)		Water ($\epsilon = 78.54$)	
		$\langle r^{-1} \rangle$	$\langle r \rangle$	$\langle r^{-1} \rangle$	$\langle r \rangle$	$\langle r^{-1} \rangle$	$\langle r \rangle$
PH ₃							
	B3LYP	0.0187	-0.0019	0.0290	-0.0045	0.0378	-0.0069
	B3PW91	0.0197	-0.0017	0.0301	-0.0043	0.0386	-0.0065
	BLYP	0.0195	-0.0064	0.0292	-0.0096	0.0374	-0.0118
	BPW91	0.0211	-0.0058	0.0312	-0.0090	0.0396	-0.0117
	SVWN	0.0158	-0.0066	0.0254	-0.0099	0.0339	-0.0123
	HF	0.0237	-0.0019	0.0360	-0.0048	0.0464	-0.0070
H ₂ S							
	B3LYP	0.0061	-0.0019	0.0077	-0.0037	0.0089	-0.0052
	B3PW91	0.0065	-0.0022	0.0079	-0.0038	0.0085	-0.0049
	BLYP	0.0021	-0.0022	0.0039	-0.0043	0.0050	-0.0059
	BPW91	-0.0104	-0.0017	-0.0093	-0.0035	-0.0084	-0.0051
	SVWN	0.0005	-0.0026	0.0000	-0.0025	-0.0002	-0.0059
	HF	0.0029	-0.0024	0.0053	-0.0043	0.0068	-0.0055
CH ₃ OH							
	B3LYP	0.0000	-0.0029	-0.0035	0.0014	-0.0064	0.0045
	B3PW91	-0.0076	0.0103	-0.0113	0.0147	-0.0140	0.0173
	BLYP	-0.0074	0.0099	-0.0117	0.0149	-0.0151	0.0194
	BPW91	-0.0007	-0.0024	-0.0046	0.0020	-0.0077	0.0061
	SVWN	-0.0059	0.0067	-0.0093	0.0101	-0.0121	0.0124
	HF	-0.0071	0.0086	-0.0111	0.0140	-0.0145	0.0180
CH ₃ SH							
	B3LYP	0.0011	-0.0056	0.0024	-0.0103	-0.0016	-0.0045
	B3PW91	-0.0047	0.0073	-0.0071	0.0103	-0.0092	0.0141
	BLYP	-0.0040	0.0070	-0.0068	0.0111	-0.0094	0.0157
	BPW91	0.0019	-0.0095	0.0007	-0.0093	0.0045	-0.0224
	SVWN	-0.0414	0.2780	-0.0426	0.2781	-0.0438	0.2788
	HF	-0.0044	0.0071	-0.0074	0.0126	-0.0101	0.0183

Table 6.4: The difference between the solvated and gas phase r^2 and r^3 moments as calculated at the centre of mass using the 6-311G(2df,p) basis set and the Onsager solvation model.

Molecule	Method	Benzene ($\epsilon = 2.274$)		Chlorobenzene ($\epsilon = 5.62$)		Water ($\epsilon = 78.54$)	
		$\langle r^2 \rangle$	$\langle r^3 \rangle$	$\langle r^2 \rangle$	$\langle r^3 \rangle$	$\langle r^2 \rangle$	$\langle r^3 \rangle$
CO							
	B3LYP	0.0016	0.0122	0.0026	0.0208	0.0039	0.0293
	B3PW91	0.0020	0.0143	0.0029	0.0228	0.0046	0.0324
	BLYP	0.0028	0.0220	0.0047	0.0366	0.0066	0.0496
	BPW91	0.0029	0.0211	0.0049	0.0362	0.0066	0.0485
	SVWN	0.0031	0.0242	0.0057	0.0423	0.0075	0.0561
	HF	-0.0007	-0.0076	-0.0007	-0.0123	-0.0018	-0.0189
NH ₃							
	B3LYP	-0.0037	-0.0349	-0.0114	-0.0771	-0.0170	-0.1091
	B3PW91	-0.0041	-0.0334	-0.0112	-0.0730	-0.0171	-0.1048
	BLYP	-0.0127	-0.0724	-0.0234	-0.1301	-0.0327	-0.1784
	BPW91	-0.0137	-0.0738	-0.0238	-0.1267	-0.0309	-0.1653
	SVWN	-0.0048	-0.0402	-0.0102	-0.0744	-0.0120	-0.0937
	HF	-0.0024	-0.0247	-0.0049	-0.0431	-0.0074	-0.0596
H ₂ O							
	B3LYP	-0.0231	-0.1017	-0.0367	-0.1628	-0.0466	-0.2080
	B3PW91	-0.0209	-0.0915	-0.0329	-0.1457	-0.0426	-0.1883
	BLYP	-0.0264	-0.1181	-0.0435	-0.1950	-0.0562	-0.2525
	BPW91	-0.0223	-0.1004	-0.0374	-0.1673	-0.0483	-0.2166
	SVWN	-0.0247	-0.1092	-0.0379	-0.1705	-0.0477	-0.2165
	HF	-0.0134	-0.0587	-0.0212	-0.0945	-0.0261	-0.1180
HF							
	B3LYP	-0.0120	-0.0471	-0.0197	-0.0772	-0.0255	-0.0998
	B3PW91	-0.0109	-0.0425	-0.0176	-0.0691	-0.0229	-0.0897
	BLYP	-0.0140	-0.0555	-0.0229	-0.0910	-0.0297	-0.1179
	BPW91	-0.0128	-0.0497	-0.0205	-0.0804	-0.0265	-0.1040
	SVWN	-0.0123	-0.0486	-0.0199	-0.0789	-0.0256	-0.1018
	HF	-0.0077	-0.0296	-0.0127	-0.0485	-0.0162	-0.0625

Molecule	Method	Benzene ($\epsilon = 2.274$)		Chlorobenzene ($\epsilon = 5.62$)		Water ($\epsilon = 78.54$)	
		$\langle r^2 \rangle$	$\langle r^3 \rangle$	$\langle r^2 \rangle$	$\langle r^3 \rangle$	$\langle r^2 \rangle$	$\langle r^3 \rangle$
PH ₃							
	B3LYP	-0.0091	-0.0461	-0.0235	-0.1166	-0.0364	-0.1794
	B3PW91	-0.0082	-0.0438	-0.0221	-0.1104	-0.0343	-0.1704
	BLYP	-0.0352	-0.1716	-0.0519	-0.2519	-0.0644	-0.3134
	BPW91	-0.0321	-0.1576	-0.0492	-0.2418	-0.0636	-0.3109
	SVWN	-0.0360	-0.1753	-0.0538	-0.2623	-0.0678	-0.3321
	HF	-0.0084	-0.0413	-0.0236	-0.1137	-0.0350	-0.1676
H ₂ S							
	B3LYP	-0.0114	-0.0573	-0.0214	-0.1055	-0.0297	-0.1446
	B3PW91	-0.0126	-0.0620	-0.0217	-0.1056	-0.0281	-0.1373
	BLYP	-0.0136	-0.0677	-0.0253	-0.1249	-0.0345	-0.1684
	BPW91	-0.0118	-0.0597	-0.0223	-0.1117	-0.0314	-0.1547
	SVWN	-0.0158	-0.0785	-0.0150	-0.0765	-0.0353	-0.1741
	HF	-0.0141	-0.0669	-0.0238	-0.1114	-0.0306	-0.1424
CH ₃ OH							
	B3LYP	-0.0208	-0.1251	-0.0189	-0.1842	-0.0181	-0.2336
	B3PW91	0.0186	-0.0338	0.0206	-0.0932	0.0195	-0.1491
	BLYP	0.0142	-0.0658	0.0178	-0.1278	0.0218	-0.1753
	BPW91	-0.0237	-0.1530	-0.0215	-0.2155	-0.0181	-0.2588
	SVWN	0.0045	-0.0845	0.0029	-0.1581	0.0002	-0.2208
	HF	0.0124	-0.0498	0.0184	-0.0917	0.0226	-0.1254
CH ₃ SH							
	B3LYP	-0.0476	-0.3207	-0.0919	-0.6287	-0.0861	-0.7104
	B3PW91	0.0006	-0.1729	-0.0040	-0.2921	-0.0026	-0.3688
	BLYP	0.0041	-0.1393	0.0022	-0.2628	0.0056	-0.3440
	BPW91	-0.0719	-0.4529	-0.0910	-0.6428	-0.1723	-1.0918
	SVWN	1.6481	7.9328	1.6287	7.7457	1.6155	7.6049
	HF	0.0060	-0.1169	0.0131	-0.1837	0.0244	-0.2156

however, exhibits almost no change in the r^{-1} moment for all solvents. The rest of the moments decrease in benzene and continue to decrease as the dielectric constant increases. This behaviour indicates that the electron cloud contracts but does not put more electron density near the centre of mass.

The Onsager model is the simplest of the two models and as expected gives the smallest variations from the unsolvated case while the SCI-PCM model enhances the effects given by the Onsager method. Although the trends observed from both models agree with each other reasonably well, there are some interesting differences. The Onsager model only produces little if any changes in the $\langle r \rangle$ values for CO yet the SCI-PCM model shows a substantial increase in $\langle r \rangle$. The calculated moments of PH_3 using the Onsager model give the same trend for all methods: $\langle r^{-1} \rangle$ increases with increasing solvent polarity while $\langle r \rangle$, $\langle r^2 \rangle$ and $\langle r^3 \rangle$ give the opposite trends. The SCI-PCM method, like the Onsager method, shows a decrease in the $\langle r \rangle$, $\langle r^2 \rangle$ and $\langle r^3 \rangle$ values when dissolved in benzene, for all cases except the B3PW91 calculation for HF. However, changing the solvent to chlorobenzene from benzene increases the $n>0$ moments; for some methods the moments in solution are even larger than the gas-phase moments. Changing the solvent to water then produces the expected decrease in the $n>0$ moments.

All of the DFT functionals seem to give the same overall trends for the solvation methods with only a few exceptions. The magnitudes of the changes observed in the moments given by the DFT functionals, though, indicate that the changes observed with the hybrid functionals are smaller than those given by the 'pure' functionals. The BLYP functional generally yields the largest change in the electron distribution with either solvation model, while the B3PW91 functional has generally the smallest changes. Comparing the functionals to the HF results indicates that for all molecules

Table 6.5: The difference between the solvated and gas phase r^{-1} and r moments as calculated at the centre of mass using the 6-311G(2df,p) basis set and the SCI-PCM solvation model.

Molecule	Method	Benzene ($\epsilon = 2.274$)		Chlorobenzene ($\epsilon = 5.62$)		Water ($\epsilon = 78.54$)	
		$\langle r^{-1} \rangle$	$\langle r \rangle$	$\langle r^{-1} \rangle$	$\langle r \rangle$	$\langle r^{-1} \rangle$	$\langle r \rangle$
N ₂	B3LYP	0.0005	0.0006	0.0009	0.0011	0.0012	0.0015
	B3PW91	0.0002	0.0000	0.0007	0.0005	0.0011	0.0008
	BLYP	0.0005	0.0007	0.0008	0.0008	0.0012	0.0012
	BPW91	0.0006	0.0008	0.0011	0.0012	0.0014	0.0016
	SVWN	0.0002	0.0004	0.0007	0.0010	0.0010	0.0014
	HF	0.0007	0.0007	0.0011	0.0008	0.0011	0.0009
CO	B3LYP	0.0000	0.0015	0.0003	0.0022	0.0000	0.0035
	B3PW91	0.0001	0.0017	0.0002	0.0028	0.0002	0.0036
	BLYP	0.0004	0.0012	0.0006	0.0021	0.0011	0.0025
	BPW91	0.0006	0.0014	0.0009	0.0023	0.0012	0.0029
	SVWN	0.0005	0.0012	0.0013	0.0004	0.0011	0.0029
	HF	-0.0017	0.0029	-0.0030	0.0048	-0.0041	0.0064
CH ₄	B3LYP	0.0003	-0.0019	0.0003	-0.0029	0.0008	-0.0055
	B3PW91	0.0005	-0.0022	0.0006	-0.0039	0.0005	-0.0038
	BLYP	0.0002	-0.0015	0.0006	-0.0028	0.0007	-0.0038
	BPW91	0.0004	-0.0022	0.0003	-0.0032	0.0005	-0.0040
	SVWN	0.0003	-0.0020	0.0008	-0.0037	0.0009	-0.0048
	HF	0.0002	-0.0012	0.0004	-0.0020	0.0005	-0.0032
NH ₃	B3LYP	-0.0593	-0.0068	-0.0945	-0.0128	-0.1240	-0.0174
	B3PW91	-0.0523	-0.0071	-0.0875	-0.0130	-0.1176	-0.0175
	BLYP	-0.0512	-0.0097	-0.0854	-0.0167	-0.1124	-0.0221
	BPW91	-0.0484	-0.0097	-0.0811	-0.0164	-0.1082	-0.0216
	SVWN	-0.0641	-0.0076	-0.1072	-0.0131	-0.1299	-0.0175
	HF	-0.0564	-0.0060	-0.0954	-0.0103	-0.1268	-0.0136
H ₂ O	B3LYP	-0.0406	0.0046	-0.0167	-0.0264	-0.0242	-0.0348
	B3PW91	-0.0090	-0.0151	-0.0172	-0.0250	-0.0253	-0.0331
	BLYP	-0.0036	-0.0178	-0.0086	-0.0297	-0.0142	-0.0389
	BPW91	-0.0048	-0.0165	-0.0106	-0.0275	-0.0171	-0.0363
	SVWN	-0.0071	-0.0170	-0.0212	-0.0271	-0.0304	-0.0357
	HF	-0.0137	-0.0126	-0.0250	-0.0209	-0.0355	-0.0276

Molecule	Method	Benzene ($\epsilon = 2.274$)		Chlorobenzene ($\epsilon = 5.62$)		Water ($\epsilon = 78.54$)	
		$\langle r^{-1} \rangle$	$\langle r \rangle$	$\langle r^{-1} \rangle$	$\langle r \rangle$	$\langle r^{-1} \rangle$	$\langle r \rangle$
HF	B3LYP	-0.0131	-0.0006	-0.0154	-0.0095	-0.0178	-0.0171
	B3PW91	0.0608	-0.0582	0.0561	-0.0664	0.0534	-0.0737
	BLYP	-0.0166	0.0033	-0.0180	-0.0062	-0.0194	-0.0144
	BPW91	0.0493	-0.0321	0.0459	-0.0409	0.0440	-0.0486
	SVWN	-0.0029	-0.0128	-0.0079	-0.0216	-0.0109	-0.0293
	HF	-0.0076	-0.0101	-0.0132	-0.0176	-0.0185	-0.0243
PH ₃	B3LYP	0.0555	-0.0027	0.1174	0.0002	0.1641	-0.0101
	B3PW91	0.0642	-0.0016	0.1271	-0.0014	0.1760	-0.0089
	BLYP	0.0564	-0.0035	0.1050	-0.0038	0.1557	-0.0094
	BPW91	0.0598	-0.0058	0.1313	-0.0051	0.1479	-0.0078
	SVWN	0.0558	-0.0075	0.1221	-0.0084	0.1442	-0.0118
	HF	0.0710	-0.0006	0.1216	-0.0059	0.1631	-0.0062
H ₂ S	B3LYP	0.0274	-0.0073	0.0471	-0.0136	0.0630	-0.0182
	B3PW91	0.0292	-0.0083	0.0492	-0.0140	0.0648	-0.0192
	BLYP	0.0274	-0.0083	0.0469	-0.0148	0.0626	-0.0206
	BPW91	0.0286	-0.0090	0.0479	-0.0155	0.0633	-0.0209
	SVWN	0.0269	-0.0095	0.0454	-0.0160	0.0600	-0.0216
	HF	0.0306	-0.0084	0.0518	-0.0145	0.0690	-0.0196
CH ₃ OH	B3LYP	-0.0078	0.0027	-0.0128	0.0039	-0.0164	0.0044
	B3PW91	-0.0071	-0.0065	-0.0137	0.0065	-0.0178	0.0075
	BLYP	-0.0092	0.0023	-0.0151	0.0080	-0.0191	0.0085
	BPW91	-0.0053	0.0006	-0.0100	-0.0014	-0.0129	-0.0021
	SVWN	-0.0076	0.0042	-0.0114	0.0004	-0.0147	0.0006
	HF	-0.0100	0.0075	-0.0164	0.0120	-0.0213	0.0151
CH ₃ SH	B3LYP	0.0010	-0.0096	-0.0024	-0.0019	-0.0021	-0.0060
	B3PW91	-0.0002	-0.0055	-0.0028	-0.0035	-0.0036	-0.0045
	BLYP	-0.0017	-0.0008	-0.0028	-0.0016	-0.0033	-0.0036
	BPW91	-0.0080	0.0287	0.0019	-0.0138	0.0028	-0.0210
	SVWN	-0.0386	0.2647	-0.0388	0.2660	-0.0368	0.2427
	HF	-0.0020	0.0006	-0.0033	-0.0002	-0.0043	0.0006

Table 6.6: The difference between the solvated and gas phase r^2 and r^3 moments as calculated at the centre of mass using the 6-311G(2df,p) basis set and the SCI-PCM solvation model.

Molecule	Method	Benzene ($\epsilon = 2.274$)		Chlorobenzene ($\epsilon = 5.62$)		Water ($\epsilon = 78.54$)	
		$\langle r^2 \rangle$	$\langle r^3 \rangle$	$\langle r^2 \rangle$	$\langle r^3 \rangle$	$\langle r^2 \rangle$	$\langle r^3 \rangle$
N ₂	B3LYP	0.0060	0.0318	0.0103	0.0547	0.0137	0.0724
	B3PW91	0.0048	0.0295	0.0091	0.0516	0.0120	0.0673
	BLYP	0.0067	0.0355	0.0102	0.0569	0.0137	0.0751
	BPW91	0.0068	0.0349	0.0107	0.0562	0.0143	0.0757
	SVWN	0.0063	0.0347	0.0108	0.0582	0.0143	0.0769
	HF	0.0049	0.0255	0.0079	0.0428	0.0105	0.0573
CO	B3LYP	0.0102	0.0522	0.0152	0.0807	0.0238	0.1234
	B3PW91	0.0107	0.0542	0.0185	0.0947	0.0247	0.1276
	BLYP	0.0108	0.0612	0.0194	0.1094	0.0233	0.1364
	BPW91	0.0117	0.0649	0.0195	0.1097	0.0259	0.1462
	SVWN	0.0117	0.0673	0.0090	0.0592	0.0273	0.1559
	HF	0.0099	0.0307	0.0165	0.0515	0.0223	0.0706
CH ₄	B3LYP	-0.0116	-0.0596	-0.0179	-0.0930	-0.0312	-0.1553
	B3PW91	-0.0130	-0.0659	-0.0247	-0.1301	-0.0246	-0.1329
	BLYP	-0.0094	-0.0510	-0.0174	-0.0914	-0.0234	-0.1232
	BPW91	-0.0123	-0.0624	-0.0191	-0.1005	-0.0250	-0.1325
	SVWN	-0.0124	-0.0664	-0.0229	-0.1204	-0.0301	-0.1600
	HF	-0.0071	-0.0366	-0.0130	-0.0685	-0.0189	-0.0974
NH ₃	B3LYP	-0.0510	-0.2561	-0.0904	-0.4472	-0.1210	-0.5958
	B3PW91	-0.0495	-0.2452	-0.0880	-0.4288	-0.1181	-0.5727
	BLYP	-0.0648	-0.3191	-0.1102	-0.5398	-0.1459	-0.7143
	BPW91	-0.0632	-0.3051	-0.1059	-0.5107	-0.1393	-0.6714
	SVWN	-0.0563	-0.2830	-0.0956	-0.4785	-0.1256	-0.6295
	HF	-0.0426	-0.2072	-0.0724	-0.3490	-0.0956	-0.4599
H ₂ O	B3LYP	-0.0014	-0.0786	-0.1342	-0.5802	-0.1768	-0.7632
	B3PW91	-0.0760	-0.3257	-0.1268	-0.5436	-0.1674	-0.7160
	BLYP	-0.0908	-0.3968	-0.1513	-0.6605	-0.1992	-0.8695
	BPW91	-0.0838	-0.3618	-0.1400	-0.6043	-0.1843	-0.7949
	SVWN	-0.0864	-0.3755	-0.1405	-0.6142	-0.1851	-0.8076
	HF	-0.0622	-0.2605	-0.1038	-0.4345	-0.1370	-0.5732

Molecule	Method	Benzene ($\epsilon = 2.274$)		Chlorobenzene ($\epsilon = 5.62$)		Water ($\epsilon = 78.54$)	
		$\langle r^2 \rangle$	$\langle r^3 \rangle$	$\langle r^2 \rangle$	$\langle r^3 \rangle$	$\langle r^2 \rangle$	$\langle r^3 \rangle$
HF							
	B3LYP	0.0002	-0.0081	-0.0399	-0.1619	-0.0736	-0.2896
	B3PW91	-0.2478	-0.8772	-0.2845	-1.0175	-0.3170	-1.1395
	BLYP	0.0175	0.0548	-0.0256	-0.1134	-0.0625	-0.2556
	BPW91	-0.1188	-0.3877	-0.1586	-0.5414	-0.1933	-0.6736
	SVWN	-0.0582	-0.2264	-0.0982	-0.3818	-0.1333	-0.5161
	HF	-0.0442	-0.1654	-0.0768	-0.2857	-0.1059	-0.3920
PH ₃							
	B3LYP	-0.0068	-0.0234	0.0202	0.1128	-0.0315	-0.1273
	B3PW91	0.0005	0.0073	0.0116	0.0648	-0.0239	-0.1009
	BLYP	-0.0103	-0.0391	-0.0027	0.0064	-0.0267	-0.1022
	BPW91	-0.0239	-0.1093	-0.0089	-0.0337	-0.0222	-0.0980
	SVWN	-0.0341	-0.1598	-0.0280	-0.1273	-0.0460	-0.2162
	HF	0.0082	0.0499	-0.0152	-0.0541	-0.0105	-0.0266
H ₂ S							
	B3LYP	-0.0419	-0.2087	-0.0763	-0.3752	-0.1019	-0.4985
	B3PW91	-0.0473	-0.2346	-0.0800	-0.3963	-0.1084	-0.5338
	BLYP	-0.0470	-0.2313	-0.0828	-0.4056	-0.1156	-0.5665
	BPW91	-0.0511	-0.2536	-0.0882	-0.4362	-0.1181	-0.5828
	SVWN	-0.0546	-0.2730	-0.0926	-0.4641	-0.1249	-0.6240
	HF	-0.0468	-0.2250	-0.0796	-0.3811	-0.1068	-0.5088
CH ₃ OH							
	B3LYP	-0.0405	-0.3744	-0.0696	-0.6277	-0.0932	-0.8244
	B3PW91	-0.1016	-0.6992	-0.0578	-0.5749	-0.0795	-0.7637
	BLYP	-0.0574	-0.5022	-0.0636	-0.6572	-0.0895	-0.8753
	BPW91	-0.0376	-0.3106	-0.0894	-0.6944	-0.1182	-0.9106
	SVWN	-0.0235	-0.2770	-0.0839	-0.6842	-0.1103	-0.8960
	HF	-0.0193	-0.2780	-0.0332	-0.4621	-0.0457	-0.6093
CH ₃ SH							
	B3LYP	-0.0902	-0.6171	-0.0720	-0.6507	-0.1062	-0.8744
	B3PW91	-0.0646	-0.4869	-0.0878	-0.7577	-0.1127	-0.9708
	BLYP	-0.0420	-0.3925	-0.0725	-0.6663	-0.1007	-0.8875
	BPW91	0.1636	0.8217	-0.1252	-0.8699	-0.1873	-1.2792
	SVWN	1.5488	7.3136	1.5529	7.3095	1.3748	6.2062
	HF	-0.0349	-0.3492	-0.0622	-0.5940	-0.0787	-0.7703

except CO, HF gives the same trends as the DFT functionals but the changes induced are much smaller than anything produced using DFT. The difference between the HF and DFT results for CO is not unexpected since HF is known to give the incorrect sign for the CO dipole. This behaviour, the decreasing value of some of the CO moments, is also evidence that the electron density is shifting so as to make the molecule more polar.

6.5 Conclusions

The radial moments for N₂ and H₂O were calculated with MP2 and QCISD to investigate the basis set dependence of the moments. The addition of polarisation functions show a definite convergence of the moments to specific values while the addition of diffuse functions gives an increase in the $\langle r \rangle$, $\langle r^2 \rangle$ and $\langle r^3 \rangle$ values. This investigation indicated that the 6-311G(2df,p) basis set was sufficiently accurate for the calculation of the radial moments. Using this basis set the radial moments of a set of molecules were calculated.

Comparison of the calculated moments to experimental results showed that both DFT results and conventional *ab initio* results gave good agreement. For moments which could not be compared to experiment the DFT values gave reasonable agreement with QCISD results while MP2 and CISD values were the closest to QCISD results. The DFT values, though, were generally slightly smaller for $\langle r \rangle$, $\langle r^2 \rangle$ and $\langle r^3 \rangle$ and slightly larger for $\langle r^{-1} \rangle$

Dissolution of the molecules in a variety solvents had only a small effect on most of the calculated moments. The SCI-PCM model, though, did indicate that the solvents had a more significant impact on the moments than was indicated when using the Onsager model. General trends were seen in both solvation models, such as

a general shrinking of the electron cloud for polar molecules which increased as the polarity of the solvent increased. Comparison of the different functionals shows that the B3PW91 and B3LYP functionals gave slightly smaller differences in the moments than BPW91 and BLYP.

Although the radial moments add to the information about the DFT electron densities obtained with the density difference index and the spin-polarisation index, they do not present direct ways to improve these densities. Uses for these tools must still be devised and tested so as to obtain better electron densities. One simple way of utilising the density difference index is given in the next chapter which will hopefully show that these tools can be very useful in designing a new and better exchange-correlation functional.

References

- [1] D. W. Davies, *The Theory of the Electric and Magnetic Properties of Molecules*, John Wiley & Sons, London, 1967.
- [2] J. H. V. Vleck, editor, *The Theory of Electric and Magnetic Susceptibilities*, Oxford University Press, New York, 1932.
- [3] W. E. Lamb, *Phys. Rev.* **60**, 817 (1941).
- [4] W. H. Flygare, *Rec. Chem. Prog* **28**, 63 (1967).
- [5] H. Basch, *Chem. Phys. Lett.* **5**, 337 (1970).
- [6] S. R. Gadre and R. K. Pathak, *J. Chem. Phys.* **92**, 4327 (1990).
- [7] R. A. Bonham and M. Fink, *Phys. Rev. A.* **33**, 1569 (1986).

- [8] G. P. Arrighini, C. Guidotti, M. Maestro, R. Moccia, and O. Salvetti, *J. Chem. Phys.* **49**, 2224 (1968).
- [9] D. Feller, C. M. Boyle, and E. R. Davidson, *J. Chem. Phys.* **86**, 3424 (1987).
- [10] J. Wang and V. H. Smith, Jr., *J. Phys. B:At. Mol. Opt. Phys* **27**, 5159 (1994).
- [11] C. Sarasola, J. Elorza, and J. M. Ugalde, *J. Math. Chem.* **23**, 405 (1998).
- [12] V. R. Saunders, *Computational Techniques in Quantum Chemistry and Molecular Physics*, Reidel, Dordrecht, 1975.
- [13] J. M. Ugalde, C. Sarasola, L. Domínguez, and R. J. Boyd, *J. Math. Chem.* **6**, 51 (1991).
- [14] M. J. Frisch, G. W. Trucks, H. B. Schlegel, P. M. W. Gill, B. G. Johnson, M. A. Robb, J. R. Cheeseman, T. A. Keith, G. A. Petersson, J. A. Montgomery, K. Raghavachari, M. A. Al-Laham, V. G. Zakrzewski, J. V. Ortiz, J. B. Foresman, J. Cioslowski, B. B. Stefanov, A. Nanayakkara, M. Challacombe, C. Peng, P. Y. Ayala, W. Chen, M. W. Wong, J. L. Andres, E. S. Repogle, R. Gomperts, R. L. Martin, D. J. Fox, J. S. Binkley, D. J. DeFrees, J. Baker, J. P. P. Stewart, M. Head-Gordon, C. Gonzalez, and J. A. Pople, *Gaussian 94*, Gaussian, Inc.: Pittsburgh PA, 1995.
- [15] C. Moller and M. S. Plesset, *Phys. Rev.* **46**, 618 (1934).
- [16] J. A. Pople, R. Seeger, and R. Krishnan, *Int. J. Quant. Chem. Symp.* **11**, 149 (1977).
- [17] R. Krishnan and J. A. Pople, *Int. J. Quant. Chem.* **14**, 91 (1978).
- [18] R. Krishnan and J. A. Pople, *J. Chem. Phys.* **72**, 4244 (1980).

-
- [19] J. A. Pople, M. Head-Gordon, and K. Raghavachari, *J. Chem. Phys.* **87**, 5968 (1987).
- [20] P. A. M. Dirac, *Proc. Cambridge Phil. Soc.* **36**, 376 (1930).
- [21] S. H. Vosko, L. Wilk, and M. Nusair, *Can. J. Phys.* **58**, 1200 (1980).
- [22] A. D. Becke, *J. Chem. Phys.* **96**, 2155 (1992).
- [23] J. P. Perdew, J. A. Chevary, S. H. Vosko, K. A. Jackson, M. R. Pederson, D. J. Singh, and C. Fiolhais, *Phys. Rev. B* **46**, 6671 (1992).
- [24] C. Lee, W. Yang, and R. G. Parr, *Phys. Rev. B* **37**, 785 (1988).
- [25] A. D. Becke, *J. Chem. Phys.* **98**, 5648 (1993).
- [26] A. D. McLean and G. S. Chandler, *J. Chem. Phys.* **72**, 5639 (1980).
- [27] R. Krishnan, J. S. Binkley, R. Seeger, and J. A. Pople, *J. Chem. Phys.* **72**, 650 (1980).
- [28] R. A. Kendall and T. H. Dunning, Jr., *J. Chem. Phys.* **96**, 6796 (1992).
- [29] M. Fink and J. Kessler, *J. Chem. Phys.* **47**, 1780 (1967).
- [30] S. N. Ketkar and R. A. Bonham, *Int. J. Quantum Chem.* **20**, 627 (1986).
- [31] Y. Zhong, A. W. Ross, and M. Fink, *Z. Phys. D* **18**, 163 (1991).
- [32] J. F. Harrison, *J. Chem. Phys.* **47**, 2990 (1967).
- [33] A. Gupta and R. J. Boyd, *J. Chem. Phys.* **68**, 1951 (1977).
- [34] R. J. Boyd, *Chem. Phys. Lett.* **44**, 363 (1976).

-
- [35] J. Wang, Z. Shi, R. J. Boyd, and C. A. Gonzalez, *J. Phys. Chem.* **98**, 6988 (1994).
- [36] C. H. Anderson and N. F. Ramsey, *Phys. Rev.* **149**, 14 (1966).
- [37] L.-C. Wang and R. J. Boyd, *J. Chem. Phys.* **90**, 1083 (1989).
- [38] J. Mestres, M. Solà, R. Carbó, F. J. Luque, and M. Orozco, *J. Phys. Chem.* **100**, 606 (1996).
- [39] F. J. Luque, M. Orozco, P. K. Bhadane, and S. R. Gadre. *J. Phys. Chem.* **97**, 9380 (1993).
- [40] J. Gao, F. J. Luque, and M. Orozco, *J. Phys. Chem.* **98**, 2975 (1993).

7. Reoptimisation of the Becke Three-Parameter Hybrid Functional

The molecular properties calculated with density functional theory (DFT) using recent approximate exchange-correlation functionals are approaching experimental and high-level *ab initio* results.¹ Since these properties are inextricably related to the calculated electron density,² these results imply that the calculated electron densities should be of comparable accuracy. The techniques explored in the previous chapters have indicated that the DFT densities are accurate but they have also pointed out some qualitative and quantitative differences between the densities obtained with current approximate functionals and those calculated using high level methods such as second-order Møller-Plesset perturbation theory (MP2)³⁻⁶ or the quadratic configuration interaction method using single and double excitations (QCISD).⁷ Thus, one method for improving existing functionals is to focus on improving calculated electron densities which should in turn improve the calculated molecular properties.

Most exchange-correlation functionals have at least one parameter which must be determined. Although it is advantageous to determine these parameters through first principles,⁸ this cannot be achieved in most cases. Thus, to obtain values for these parameters fitting schemes are employed to find the optimal results.⁹⁻¹³ Currently most

parameters are fitted to the electron affinities, atomisation energies and ionisation energies found in the Gaussian 2 (G2)¹⁴ data set.⁹⁻¹¹ However, this technique only gives an indirect improvement in the calculated electron density which can produce inaccuracies in the electron densities and lead to poor results for properties not used in the fitting procedures.¹⁵ An optimisation scheme which fits the parameters directly to an accurate electron density should produce a functional which is not biased to a particular set of molecular properties. Moreover, the electron density, as calculated with the new functional, should closely approximate the electron density to which it was fitted. Therefore, the accuracy of the molecular properties calculated with the new functional should also approach the accuracy of the method with which the fitting density was calculated.

This chapter will focus on the use of the density difference index (DDI)¹⁶ to directly fit a hybrid functional to an accurate reference density. This should produce functionals with electron densities and molecular properties which are similar to those calculated using the reference methods. To investigate the practicality of these new functionals the molecular properties of a small set of molecules will be investigated and compared to the results obtained using the methods used to calculate the reference density and also to another similar exchange-correlation energy functional.

7.1 Details of Optimisation

The functional which was used in this study was the Becke three-parameter hybrid functional.¹¹

$$E_{xc} = E_{xc}^{LSDA} + a_0(E_x^{HF} - E_x^{LSDA}) + a_x \Delta E_x^{B88} + a_c \Delta E_c^{PW91} \quad (7.1)$$

The above expression mixes the Becke 1988 gradient-corrected exchange energy¹⁰ and the Perdew and Wang 1991 gradient-corrected correlation energy⁸ with the local spin density approximation exchange-correlation energy and the Hartree-Fock exchange energy. Fitting to the G2 data set Becke found that the optimum values were $a_0 = 0.20$, $a_x = 0.81$ and $a_c = 0.72$ and the functional using these parameters will be referred to as B3PW91.

To simplify comparison of functionals the three parameters, a_0 , a_x , and a_c will be optimised using a subset of the molecules in the G2 data set (see table 7.2). Also, all calculations will be done at the G2 geometries, calculated using an all electron MP2 geometry optimisation with the 6-31G(d) basis set, as was used by Becke. Electron densities for all methods were then calculated at these geometries using the 6-311G(df,p)^{17,18} basis set and the DDIs were calculated between the new functional and a reference method for all molecules. To give equal weighting to all molecules each DDI was divided by the number of electrons in each molecule and the results summed. The optimal parameters were then found by minimising this sum.

The two different reference densities used in the DDI calculations were MP2 and QCISD and lead to two different sets of optimised parameters. Density difference plots were then examined for four molecules to visualise the changes in the electron density induced by the new parameters as compared to the B3PW91 functional. To test the accuracy of the new functional various molecular properties, including the radial moments of the electron density, the spin-polarisation index and optimised geometrical structures, are compared to the results obtained with B3PW91, MP2, QCISD and where available experimental data. All electron densities and geometries were calculated using the Gaussian 94 computational chemistry package.¹⁹

7.2 Results and Discussion

Using the MP2 electron density as the reference density in the DDI calculations yielded optimal values of $a_0 = 0.41$, $a_x = 0.61$ and $a_c = 1.00$ and the functional using these values will be referred to as B3P[MP2]. A comparison of these values to those found by Becke for the B3PW91 functional reveals that it has about two times the amount of exact exchange energy and approximately 40% more gradient-corrected correlation energy but only 75% of the amount of gradient-corrected exchange energy. Moving to the QCISD as the DDI reference electron density gave a functional, which will be referred to as B3P[QCI], with similar parameters, $a_0 = 0.47$, $a_x = 0.67$ and $a_c = 0.92$, but with noticeable changes. The shift in the gradient-corrected values

Table 7.1: The DDI/electron for all molecules given by B3PW91 and the optimised functionals and the differences between these two values.

Molecule	MP2-DFT (DDI/electron)			QCISD-DFT (DDI/electron)		
	B3PW91	B3P[MP2]	Relative Change(%)	B3PW91	B3P[QCI]	Relative Change(%)
BeH	0.0192	0.0139	28	0.018	0.0144	20
C ₂ H ₂	0.0198	0.0193	3	0.0229	0.0207	10
C ₂ H ₄	0.015	0.0135	10	0.0189	0.0161	15
C ₂ H ₆	0.0122	0.0105	14	0.0151	0.0119	21
CH	0.012	0.0086	28	0.0175	0.0153	13
CH ₂ (¹ A ₁)	0.0122	0.0093	24	0.0186	0.0166	11
CH ₂ (³ B ₁)	0.009	0.007	22	0.0108	0.0086	20
CH ₃	0.0092	0.0078	15	0.0116	0.0095	18
CH ₃ Cl	0.0057	0.005	12	0.0068	0.0056	18
CH ₃ OH	0.0079	0.0067	15	0.0095	0.0072	24
CH ₃ SH	0.0064	0.0053	17	0.0075	0.0058	23
CH ₄	0.01	0.0087	13	0.0128	0.0101	21
Cl ₂	0.0044	0.0039	11	0.0053	0.0044	17
ClF	0.0054	0.0047	13	0.0067	0.0053	21
ClO	0.0081	0.0046	43	0.0083	0.0065	22
CN	0.0245	0.02	18	0.0144	0.0166	-15

Molecule	MP2-DFT (DDI/electron)			QCISD-DFT (DDI/electron)		
	B3PW91	B3P[MP2]	Relative	B3PW91	B3P[QCI]	Relative
			Change(%)			Change(%)
CO	0.0105	0.0119	-13	0.012	0.0105	13
CO ₂	0.0078	0.0083	-6	0.0101	0.0073	28
CS	0.0092	0.0103	-12	0.0098	0.0089	9
F ₂	0.0079	0.0081	-3	0.0096	0.0089	7
H ₂	0.0162	0.0111	31	0.0239	0.0204	15
H ₂ O	0.0085	0.0078	8	0.0096	0.0081	16
H ₂ O ₂	0.0078	0.0076	3	0.009	0.0079	12
H ₂ S	0.0067	0.0057	15	0.0082	0.0067	18
HCl	0.0054	0.0048	11	0.0064	0.0055	14
HCN	0.012	0.0122	-2	0.0131	0.0118	10
HCO	0.0101	0.0108	-7	0.0113	0.0099	12
HF	0.0072	0.0062	14	0.0079	0.0063	20
HOCl	0.0059	0.0054	8	0.0068	0.0057	16
Li ₂	0.0194	0.0176	9	0.0366	0.0354	3
LiF	0.0078	0.0078	0	0.0107	0.0066	38
LiH	0.0177	0.0117	34	0.0199	0.024	-21
N ₂	0.0122	0.0126	-3	0.0125	0.0115	8
N ₂ H ₄	0.0079	0.007	11	0.0092	0.0076	17
Na ₂	0.0108	0.0076	30	0.0128	0.0102	20
NaCl	0.0058	0.0042	28	0.0064	0.0041	36
NH	0.0083	0.0061	27	0.0102	0.008	22
NH ₂	0.009	0.0074	18	0.0109	0.0089	18
NH ₃	0.0091	0.0085	7	0.0109	0.0093	15
NO	0.035	0.0349	0	0.0108	0.0099	8
O ₂	0.0076	0.0076	0	0.0081	0.007	14
OH	0.0077	0.0062	19	0.0089	0.0072	19
P ₂	0.0076	0.0075	1	0.0086	0.0077	10
PH ₂	0.0077	0.0058	25	0.0091	0.0067	26
PH ₃	0.0085	0.0064	25	0.0102	0.0074	27
S ₂	0.0047	0.0044	6	0.0055	0.0047	15
Si ₂	0.0503	0.0559	-11	0.0531	0.0127	76
Si ₂ H ₆	0.0075	0.0052	31	0.0085	0.0054	36
SiH ₂ (¹ A ₁)	0.0104	0.0073	30	0.0122	0.0092	25
SiH ₂ (³ B ₁)	0.0089	0.0062	30	0.009	0.006	33
SiH ₃	0.0096	0.0068	29	0.0103	0.0066	36
SiH ₄	0.0107	0.0075	30	0.0115	0.0071	38
SiO	0.0086	0.0106	-23	0.0104	0.0085	18
SO	0.0078	0.0073	6	0.0066	0.0054	18
SO ₂	0.0075	0.0092	-23	0.0085	0.0068	20

corresponds better with Becke's parameters while the exact-exchange results continue to diverge from Becke's value of 0.20.

Table 7.2 shows the various differences in the DDI/electron values between B3PW91 and the two new sets of parameters. The B3P[MP2] parameters produced an overall mean relative improvement of 12% and an absolute mean relative difference of 16% in the DDI/electron values when compared to B3PW91. Also, the maximum absolute relative difference in the DDI/electron values was 34% for LiH. The average differences in the DDI/electron values between the B3P[QCI] functional and the B3PW91 functional increased to an overall mean absolute improvement of 19% and a mean absolute relative difference of 20% while the maximum absolute difference increased to 76% for Si₂. The standard deviation of the absolute relative differences were 11% for both the B3P[MP2] and B3P[QCI] functionals, respectively. These deviations indicate that most of the DDI values only have a 10 to 30% reduction.

Figures 7.1 - 7.7 compare the B3P[MP2] and the B3P[QCI] densities with their reference densities through density difference plots. Also presented are MP2-B3PW91 and QCISD-B3PW91 density difference plots to indicate where improvements have been made in the electron densities calculated with the B3P[MP2] and B3P[QCI] functionals. Although this is a relatively small subset of molecules, they give enough information to assess the two new electron densities. Two different features are immediately apparent in the density difference plots of B3P[MP2] and B3P[QCI] when compared to the respective B3PW91 plots. The first is observed near the atomic centres of all of the atoms excluding hydrogen. In the B3PW91 plots the atomic centres have substantial negative density differences which are then followed by large spikes of positive density differences moving towards the valence region. The two new functionals substantially decrease the magnitudes of the large spikes of positive

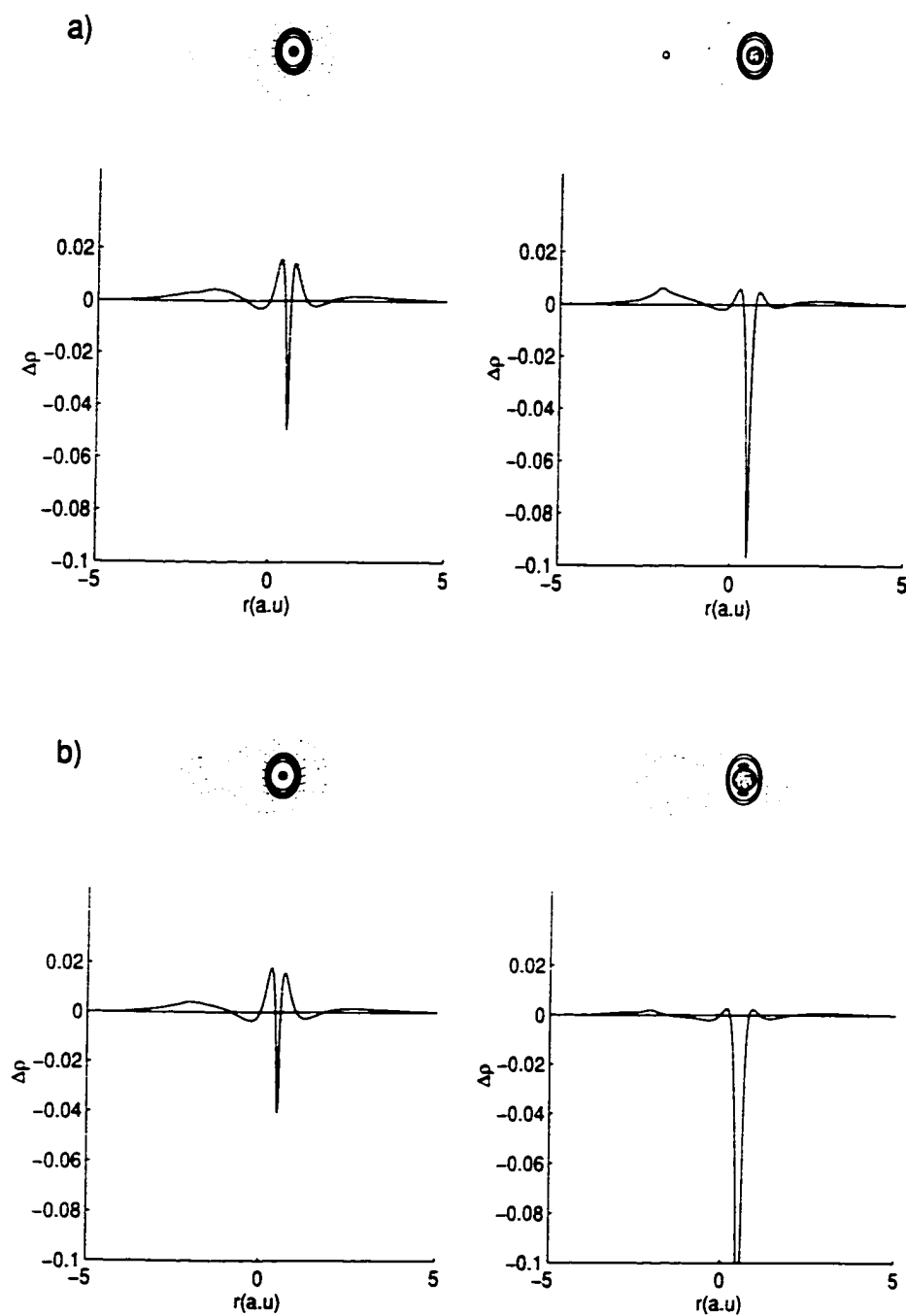


Figure 7.1: Density difference plot for BeH. a) MP2-B3PW91 and MP2-B3P[MP2] b) QCISD-B3PW91 and QCISD-B3P[QCI]

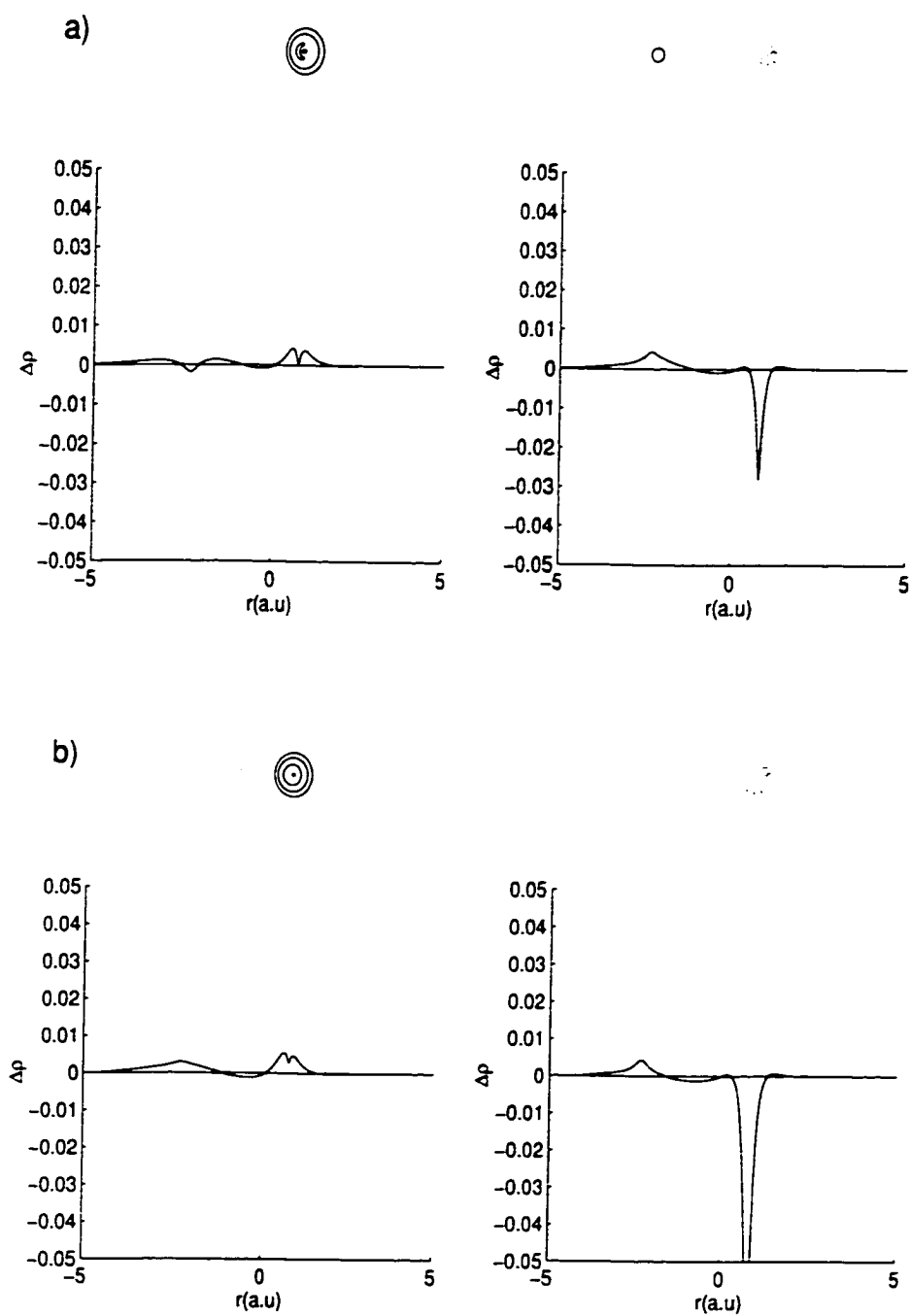


Figure 7.2: Density difference plot for LiH. a) MP2-B3PW91 and MP2-B3P[MP2] b) QCISD-B3PW91 and QCISD-B3P[QCI]

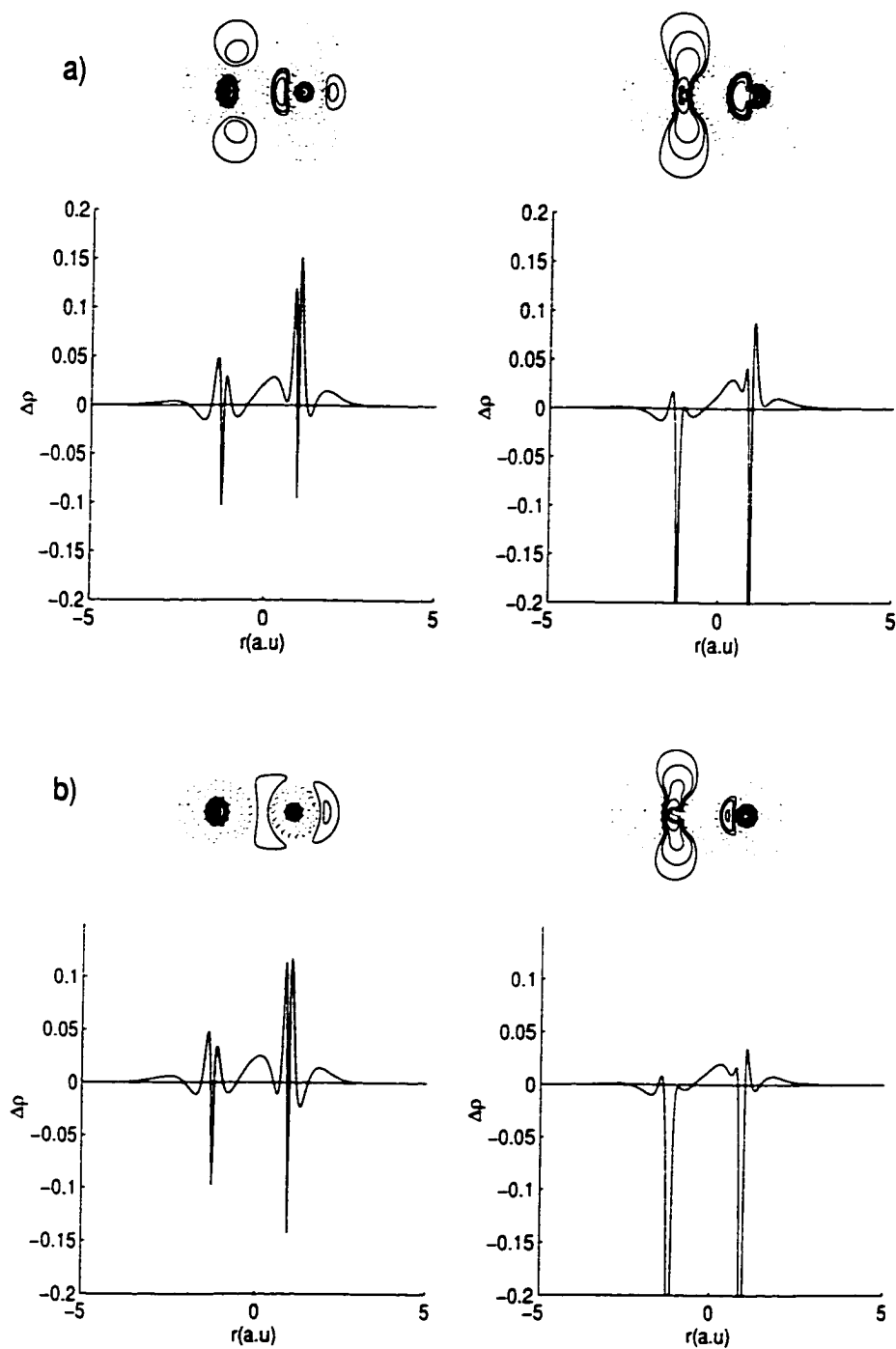


Figure 7.3: Density difference plot for CO. a) MP2-B3PW91 and MP2-B3P[MP2] b) QCISD-B3PW91 and QCISD-B3P[QCI]

density difference but move too much electron density towards the atomic centres increasing the negative density differences there by up to eight times. The second feature is the size of the areas where non-zero density differences are observed. For the B3PW91 plots small areas or relatively large density differences are observed while the B3P[MP2] and B3P[QCI] have much larger areas of relatively small density differences. Overall the B3P[MP2] and B3P[QCI] functionals have an almost uniform distribution of absolute density differences over the whole molecule. This may be an indication that the new functionals' electron density are converging towards the reference density but there may not be enough flexibility in parameters for full convergence. Also, the uniform differences in the electron density may also lead to poor electronic properties since the electron density is slightly inaccurate over most of the molecule.

Two different sets of molecular properties are used to assess the accuracy and practicality of the new functionals. The radial moments of the electron density, explored in chapter 6, can give a comparison of the spatial properties of the different electron densities. The analytical method²⁰ outlined in chapter 6 was used to calculate radial moments for fourteen different molecules and the results are presented in table 7.2. A simple statistical analysis of these results shows that the average absolute difference between the MP2 and B3PW91 moments is, 0.0061, 0.0281, 0.1314 and 0.7933 for the r^{-1} , r , r^2 and r^3 moments, respectively. Between the MP2 and B3P[MP2] moments the average absolute differences increase to 0.0082, 0.0359, 0.1999, and 1.1876 for the r^{-1} , r , r^2 and r^3 moments, respectively. This indicates that the B3P[MP2] results are slightly worse than the B3PW91 values. However, for some molecules, Si₂ and H₂ for example, the B3P[MP2] functional outperforms the B3PW91 functional slightly. Comparison of B3PW91 moments to B3P[MP2] mo-

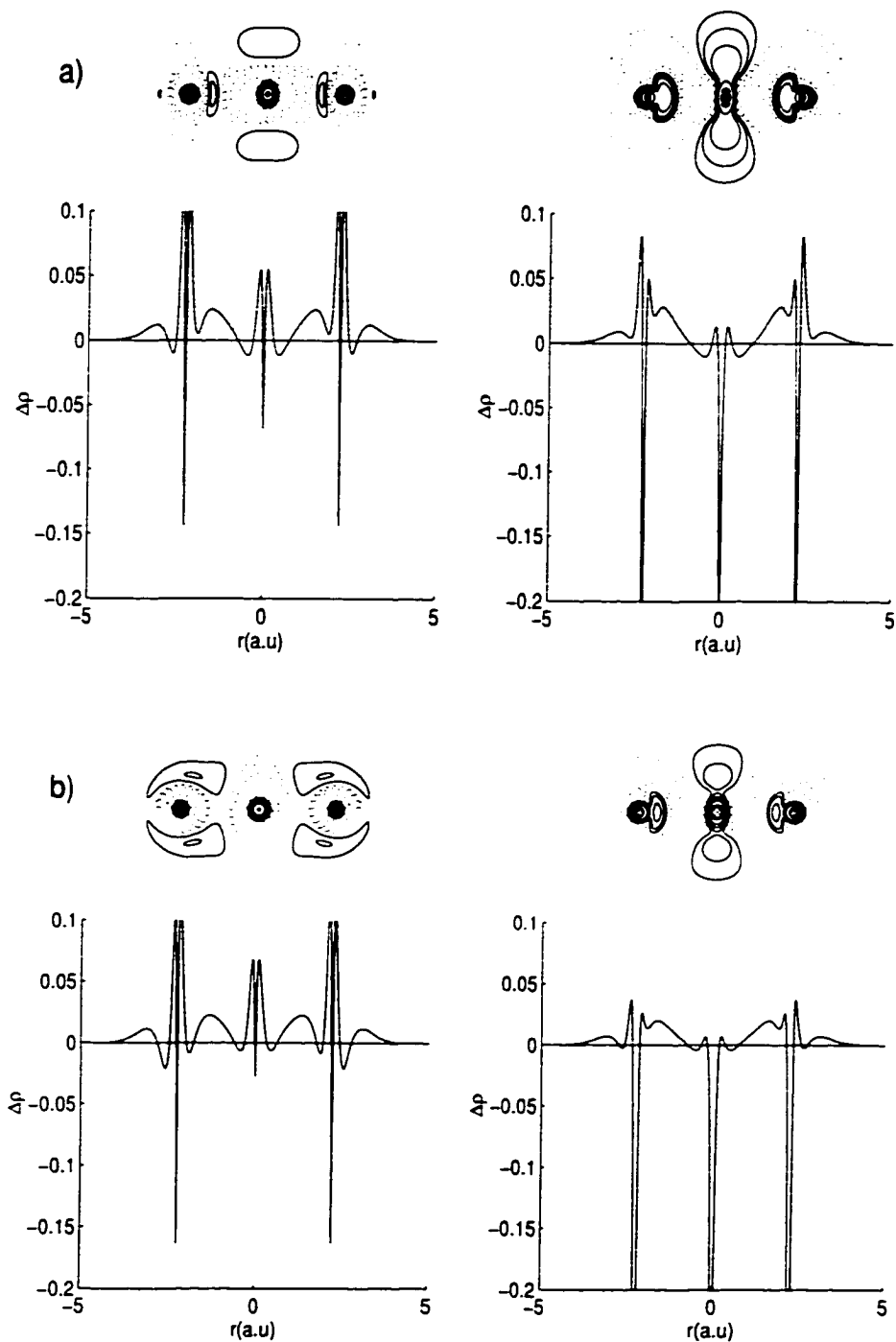


Figure 7.4: Density difference plot for CO₂. a) MP2-B3PW91 and MP2-B3P[MP2] b) QCISD-B3PW91 and QCISD-B3P[QCI]

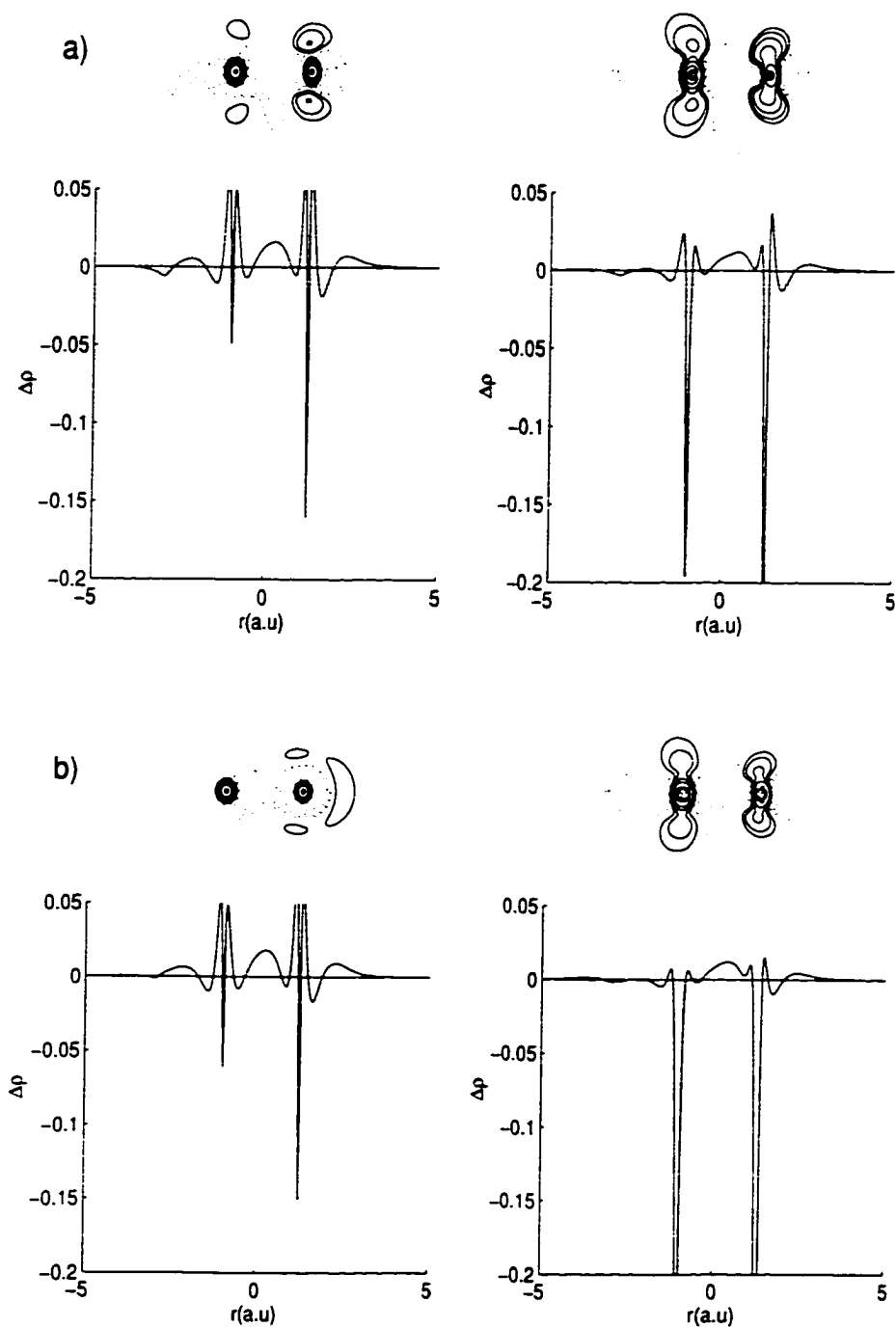


Figure 7.5: Density difference plot for HCN. a) MP2-B3PW91 and MP2-B3P[MP2]
b) QCISD-B3PW91 and QCISD-B3P[QCI]

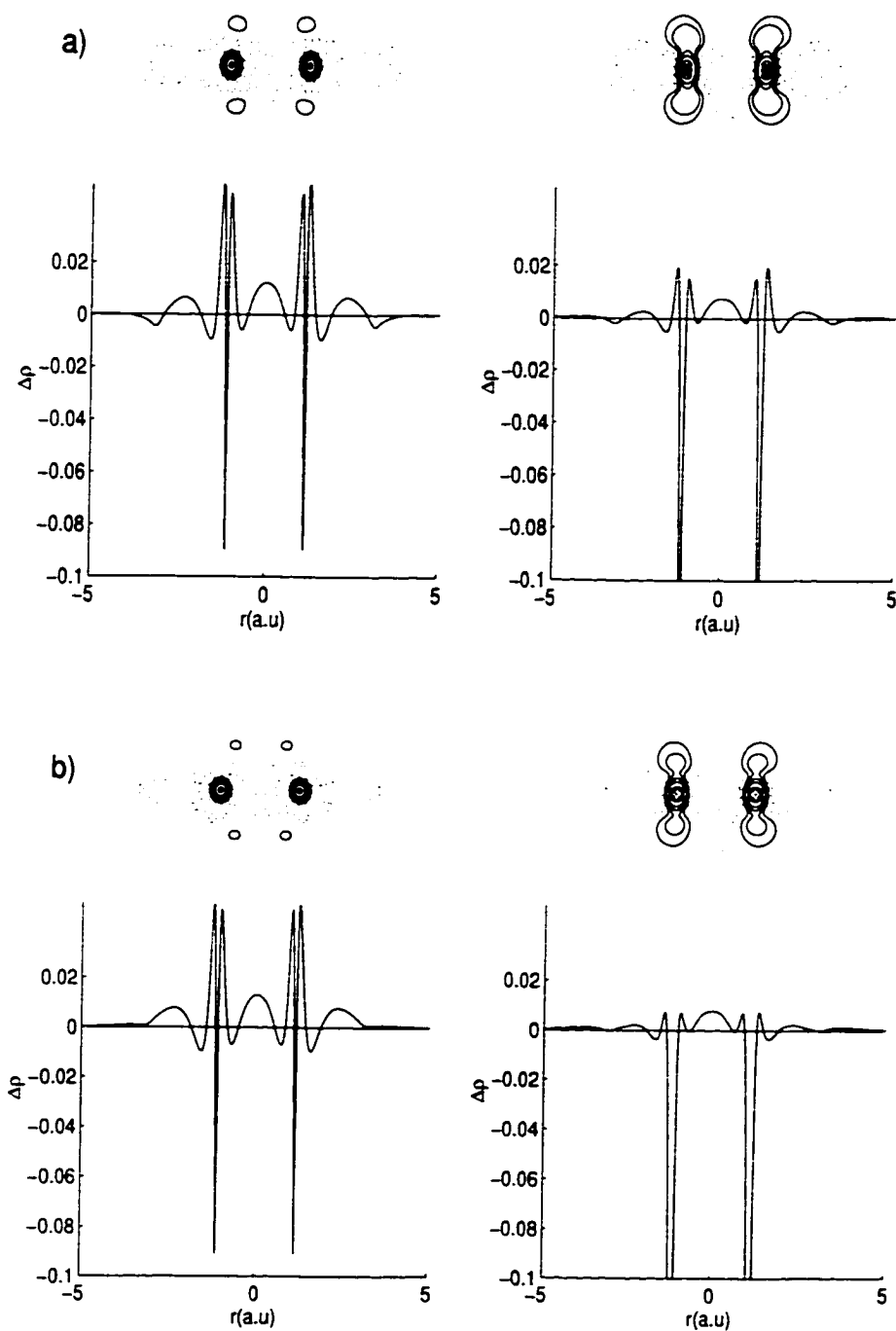


Figure 7.6: Density difference plot for C_2H_2 . a) MP2-B3PW91 and MP2-B3P[MP2]
b) QCISD-B3PW91 and QCISD-B3P[QCI]

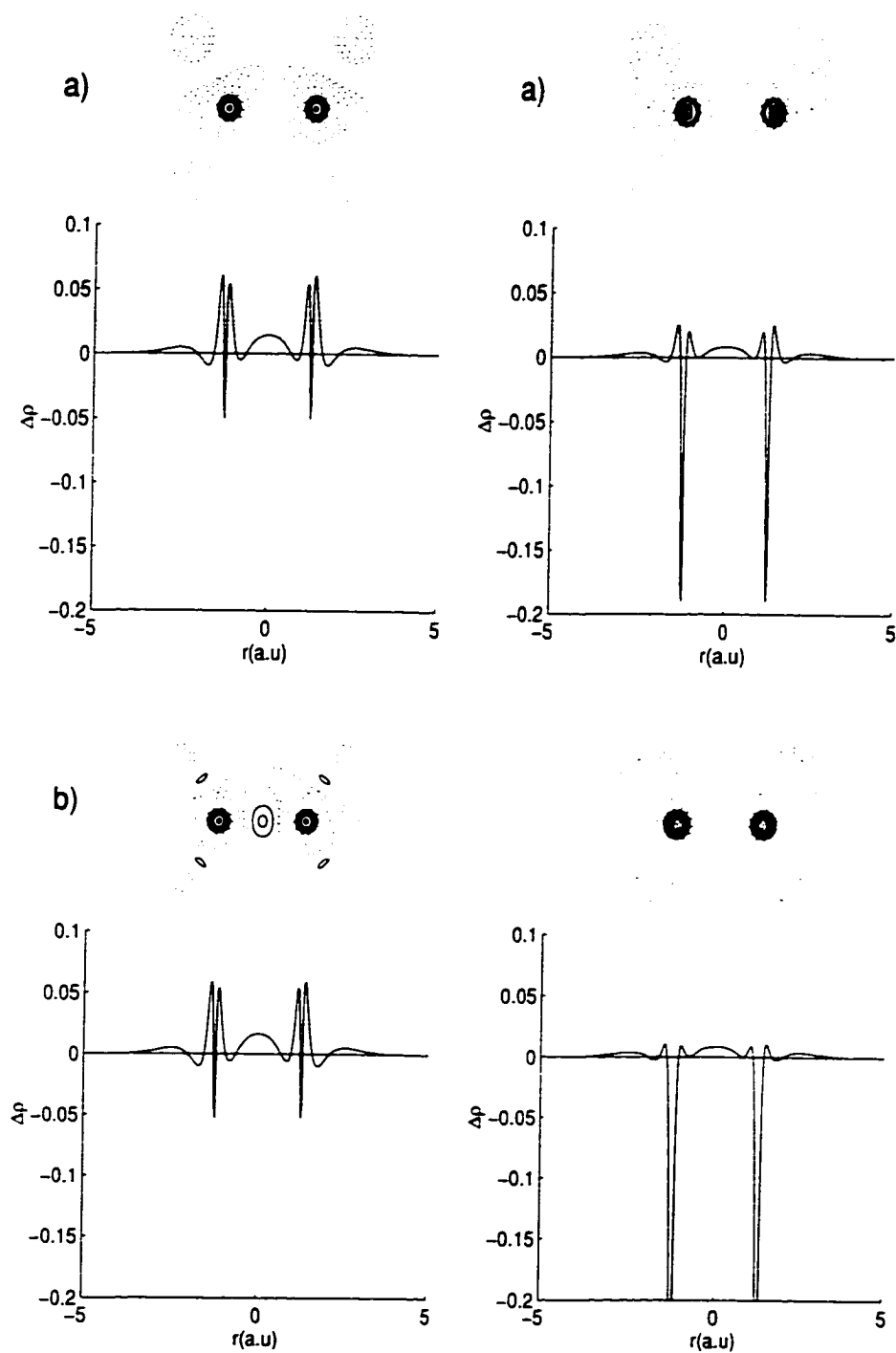


Figure 7.7: Density difference plot for C_2H_4 . a) MP2-B3PW91 and MP2-B3P[MP2]
b) QCISD-B3PW91 and QCISD-B3P[QCI]

ments shows that for most molecules the B3P[MP2] functional gives slightly larger $\langle r^{-1} \rangle$ values and slightly smaller $\langle r \rangle$, $\langle r^2 \rangle$ and $\langle r^3 \rangle$ values. The QCISD and B3PW91 moments yield average absolute differences of 0.0060, 0.0280, 0.1305 and 0.5885 for the r^{-1} , r , r^2 and r^3 moments, respectively. This shows a slight improvement in the performance of the B3PW91 functional when compared to QCISD than when compared to MP2. The average absolute differences between the B3P[QCI] and QCISD moments, 0.0109, 0.0438, 0.2668 and 1.4273 for the r^{-1} , r , r^2 and r^3 moments, respectively, is much larger than those observed with the B3PW91 functional. The B3P[QCI] functional again shows increased values and decreased $\langle r \rangle$, $\langle r^2 \rangle$ and

Table 7.2: Comparison of molecular properties for fourteen different molecules.

Molecule	B3PW91	B3P[MP2]	B3P[QCI]	MP2	QCISD
BeH					
$\langle r^{-1} \rangle$	6.9280	6.9321	6.9381	6.9275	6.9299
$\langle r \rangle$	8.6226	8.6153	8.6041	8.6614	8.6507
$\langle r^2 \rangle$	23.4421	23.3745	23.2982	23.6774	23.6105
$\langle r^3 \rangle$	79.1023	78.6145	78.1584	80.2921	79.9324
C ₂ H ₄					
$\langle r^{-1} \rangle$	9.9078	9.9085	9.9107	9.8976	9.8988
$\langle r \rangle$	32.9338	32.9220	32.9165	32.9927	32.9877
$\langle r^2 \rangle$	82.6728	82.5340	82.4894	83.0315	82.9669
$\langle r^3 \rangle$	243.2201	242.2012	241.9025	245.0698	244.5513
CH					
$\langle r^{-1} \rangle$	12.2834	12.2828	12.2900	12.2769	12.2820
$\langle r \rangle$	9.4227	9.4151	9.4051	9.4375	9.4228
$\langle r^2 \rangle$	19.1770	19.1136	19.0642	19.2140	19.1533
$\langle r^3 \rangle$	48.2395	47.8990	47.6913	48.2888	48.0705
CH ₃ OH					
$\langle r^{-1} \rangle$	11.1106	11.1155	11.1175	11.1028	11.1068
$\langle r \rangle$	35.6955	35.6690	35.6604	35.7485	35.7371
$\langle r^2 \rangle$	84.2634	84.0581	83.9967	84.5646	84.4741
$\langle r^3 \rangle$	231.8359	230.5870	230.2301	233.2596	232.6723
CH ₄					
$\langle r^{-1} \rangle$	16.7321	16.7319	16.7410	16.7248	16.7218
$\langle r \rangle$	15.9384	15.9246	15.9187	15.9841	15.9780
$\langle r^2 \rangle$	35.5862	35.4534	35.4079	35.8052	35.7408
$\langle r^3 \rangle$	94.0096	93.2321	92.9889	94.9410	94.5346

Molecule	B3PW91	B3P[MP2]	B3P[QCI]	MP2	QCISD
CN					
$\langle r^{-1} \rangle$	10.5036	10.5101	10.5143	10.4889	10.4954
$\langle r \rangle$	20.1602	20.1471	20.1376	20.1701	20.1775
$\langle r^2 \rangle$	38.5461	38.4696	38.4247	38.5717	38.6104
$\langle r^3 \rangle$	89.4985	89.1150	88.9264	89.5355	89.7006
CO					
$\langle r^{-1} \rangle$	11.6232	11.6256	11.6292	11.6127	11.6179
$\langle r \rangle$	21.3407	21.3313	21.3220	21.3827	21.3574
$\langle r^2 \rangle$	40.2791	40.2211	40.1754	40.4890	40.3503
$\langle r^3 \rangle$	92.6086	92.3205	92.1265	93.4906	92.8688
H ₂					
$\langle r^{-1} \rangle$	1.9546	1.9579	1.9633	1.9540	1.9534
$\langle r \rangle$	2.8268	2.8169	2.8079	2.8210	2.8193
$\langle r^2 \rangle$	5.1639	5.1170	5.0827	5.1293	5.1194
$\langle r^3 \rangle$	11.7098	11.5172	11.3989	11.5507	11.5080
H ₂ O					
$\langle r^{-1} \rangle$	19.3442	19.3415	19.3489	19.3386	19.3339
$\langle r \rangle$	11.4373	11.4185	11.4093	11.4563	11.4505
$\langle r^2 \rangle$	19.1406	19.0357	18.9979	19.2123	19.1723
$\langle r^3 \rangle$	39.6816	39.2451	39.1134	39.9175	39.7346
LiH					
$\langle r^{-1} \rangle$	4.5510	4.5551	4.5595	4.5520	4.5517
$\langle r \rangle$	7.5906	7.5707	7.5595	7.5962	7.6030
$\langle r^2 \rangle$	23.0714	22.8979	22.8093	23.0862	23.1516
$\langle r^3 \rangle$	88.1590	86.8059	86.1788	88.0190	88.5516
N ₂					
$\langle r^{-1} \rangle$	11.3976	11.3968	11.3991	11.3913	11.3903
$\langle r \rangle$	21.4096	21.4148	21.4090	21.4213	21.4304
$\langle r^2 \rangle$	39.8176	39.8288	39.8014	39.8754	39.9092
$\langle r^3 \rangle$	88.5342	88.5247	88.4128	88.7891	88.8856
O ₂					
$\langle r^{-1} \rangle$	12.2825	12.2851	12.2877	12.2773	12.2792
$\langle r \rangle$	24.7832	24.7793	24.7710	24.7896	24.7960
$\langle r^2 \rangle$	44.6934	44.6654	44.6267	44.7223	44.7456
$\langle r^3 \rangle$	93.2139	93.0682	92.9210	93.3223	93.3855
Si ₂					
$\langle r^{-1} \rangle$	14.0292	14.0248	14.0491	14.0333	14.0356
$\langle r \rangle$	62.6775	62.6948	62.5269	62.6293	62.6203
$\langle r^2 \rangle$	160.4743	160.5629	159.6836	160.4818	160.3335
$\langle r^3 \rangle$	484.8195	485.0841	481.8326	487.2823	485.8494
SO ₂					
$\langle r^{-1} \rangle$	23.9385	23.9263	23.9229	23.9340	23.9237
$\langle r \rangle$	63.6712	63.7059	63.7125	63.7051	63.7427
$\langle r^2 \rangle$	161.3489	161.4789	161.4929	161.5859	161.7477
$\langle r^3 \rangle$	468.1479	468.4477	468.4141	469.5300	470.0323

$\langle r^3 \rangle$ values for most molecules. These changes, though, are much larger than was observed in the B3P[MP2] values and thus, the B3P[QCI] functional is outperformed by B3PW91 for all molecules studied.

The optimised geometries for the same fourteen molecules are given in table 7.3 along with the frequencies of the diatomic molecules. Comparison of these values shows that the performance of the new functionals is mixed but produces some discernible trends. The bond lengths calculated by the B3P[MP2] and B3P[QCI] functionals are quite a bit smaller than the B3PW91 and as expected this leads to higher calculated diatomic frequencies than observed for B3PW91. Although the performance between the functionals is important, of more interest is how the new functionals perform when compared to the reference methods. Table 7.4 shows the mean of the absolute differences for the various properties when the DFT results are compared to QCISD, MP2 and experimental results. The B3PW91 functional continues to outperform the other two functionals when compared to experimental results while the B3P[MP2] functional is only slightly worse. However, the B3P[MP2] functional performs as well if not slightly better than B3PW91 when compared to the MP2 results while B3P[QCI] continues give worse results than B3PW91 when compared to QCISD. Focussing on the diatomic frequencies shows that for some molecules the B3P[MP2] and even the B3P[QCI] functional yield more accurate frequencies than B3PW91. The continued poor performance of B3P[QCI] is discouraging but a look at the maximum absolute differences shows that there has been some convergence of the B3P[QCI] density towards the QCISD density.

Many of the molecules used for the optimisation of these functionals have open-shell ground states. In chapter 5 some DFT functionals were shown to exhibit very low spin polarisation within some molecules. To examine how well the new func-

Table 7.3: Calculated geometric parameters and frequencies. Bond lengths are in Å and frequencies are in cm^{-1} .

Property	B3PW91	B3P[MP2]	B3P[QCI]	MP2	QCISD	Experiment ^{21,22}
BeH						
r_e	1.348	1.344	1.340	1.343	1.348	1.343
ν	2049	2064	2082	2107	2062	2059
C ₂ H ₄						
$r_e(CC)$	1.325	1.318	1.318	1.332	1.333	1.339
$r_e(CH)$	1.086	1.080	1.078	1.085	1.087	1.085
$\angle CCH$	121.7	121.7	121.7	121.4	121.6	121.1
CH						
r_e	1.130	1.120	1.116	1.120	1.127	1.120
ν	2815	2892	2927	2946	2862	2858
CH ₃ OH						
$r_e(CO)$	1.411	1.400	1.402	1.411	1.410	1.421
$r_e(OH)$	0.958	0.950	0.947	0.956	0.955	0.963
$r_e(CH')$	1.092	1.086	1.084	1.091	1.093	1.093
$r_e(CH'')$	1.100	1.093	1.091	1.098	1.100	1.093
$\angle COH$	107.8	108.3	108.4	106.5	106.8	108.0
$\angle OCH'$	107.1	107.3	107.3	107.0	107.1	107.0
$\angle OCH''$	112.8	112.6	112.5	112.6	112.5	
CH ₄						
r_e	1.090	1.086	1.083	1.090	1.093	1.086
CN						
r_e	1.163	1.152	1.150	1.127	1.170	1.172
ν	2170	2251	2269	2887	2181	2069
CO						
r_e	1.125	1.116	1.115	1.135	1.129	1.128
ν	2239	2308	2320	2156	2215	2170
H ₂						
r_e	0.745	0.741	0.736	0.738	0.743	0.741
ν	4418	4485	4552	4533	4423	4401
H ₂ O						
r_e	0.959	0.950	0.948	0.956	0.956	0.959
$\angle HOH$	104.0	104.6	104.8	102.7	102.9	103.9
LiH						
r_e	1.600	1.596	1.592	1.601	1.603	1.595
ν	1398	1407	1417	1431	1407	1406
N ₂						
r_e	1.094	1.084	1.082	1.117	1.101	1.098
ν	2459	2542	2560	2190	2410	2360
O ₂						
r_e	1.199	1.181	1.179	1.222	1.200	1.207
ν	1678	1791	1802	1469	1676	1580
Si ₂						
r_e	2.159	2.142	1.967	2.005	2.018	2.246
ν	553	573	806	714	683	511
SO ₂						
r_e	1.448	1.429	1.427	1.454	1.438	
$\angle OSO$	118.8	118.8	118.8	119.9	119.2	

Table 7.4: Mean of the absolute differences between DFT and high-level *ab initio* or experimental geometric parameters. Maximum absolute differences are given in the brackets.

	Experiment-			MP2-		QCISD-	
	B3PW91	B3P[MP2]	B3P[QCI]	B3PW91	B3P[MP2]	B3PW91	B3P[QCI]
r_e	0.010 (0.087)	0.015 (0.104)	0.027 (0.279)	0.016 (0.154)	0.015 (0.043)	0.011 (0.141)	0.014 (0.051)
ν	54 (101)	100 (211)	147 (295)	197 (717)	184 (618)	32 (130)	91 (150)
\angle	0.3 (0.6)	0.5 (0.7)	0.6 (0.9)	0.7 (1.3)	1.0 (2.1)	0.5 (1.1)	0.7 (1.9)

tionals handle the spin-polarisation of open-shell molecules the spin polarisation index (SPI)²³ has been calculated for a series of doublet and triplet ground state molecules.(see table 7.5) No discernible trends are observed in the calculated SPIs using any of the three functionals with some values being larger than the MP2 and QCISD values and others being smaller. The B3PW91 yields good SPIs for all of the molecules except for O₂ where it gives a value which is much lower than would be expected. The B3P[MP2] functional improves the SPIs of B3PW91 for all molecules when compared to the MP2 results. The same is not true for the B3P[QCI] functional which only gives more accurate SPIs than B3PW91 for a few molecules when compared to QCISD.

Overall performance of the new functionals is fair to poor. The B3P[QCI] functional performed rather poorly for most calculated properties when compared to the QCISD results. However, there were some signs that the new parameters yielded electron densities that gave a reasonable qualitative approximation of the QCISD density. The B3P[MP2] functional fared much better even sometimes outperforming the B3PW91 functional when compared to MP2 results. Again the B3P[MP2] results

Table 7.5: Calculated SPIs for molecules in doublet or triplet states.

Molecule	B3PW91	B3P[MP2]	B3P[QCI]	MP2	QCISD
Doublet States					
BeH	0.1799	0.1832	0.1855	0.1878	0.1867
CH	0.4260	0.4254	0.4273	0.4207	0.4187
CH ₃	0.4003	0.3997	0.4017	0.3890	0.3896
OH	0.7245	0.7252	0.7264	0.7180	0.7181
NH ₂	0.5604	0.5573	0.5583	0.5438	0.5441
CN	0.2365	0.2516	0.2552	0.3339	0.2574
Triplet States					
CH ₂ (³ B ₁)	0.6273	0.6188	0.6194	0.6049	0.6065
NH	0.9084	0.9041	0.9053	0.8966	0.8956
O ₂	0.2228	0.2907	0.3099	0.2513	0.3521
SiH ₂ (³ B ₁)	0.4014	0.3948	0.3975	0.3829	0.3833

show that its calculated electron density gives a good qualitative approximation of the MP2 density and gives a reasonable quantitative approximation of the MP2 density. Results from this fitting technique could be limited by the parameters which can be optimised and improved results could probably be obtained by fitting more parameters.

7.3 Conclusion

The parameters for a hybrid functional were determined through fitting the DFT electron density directly to a high-level *ab initio* electron density. This fitting was achieved by using the DDI to give a quantitative difference between the DFT and high-level *ab initio* electron densities. The optimal parameters $a_0 = 0.41$, $a_x = 0.61$ and $a_c = 1.00$ were obtained using the MP2 electron density as a reference with the resulting functional being called B3P[MP2]. Using the MP2 molecular properties as a reference showed that the performance of the B3P[MP2] was only fair when compared

to B3PW91. Switching to the QCISD electron density for the DDI calculations yielded the optimal parameters $a_0 = 0.47$, $a_x = 0.67$ and $a_c = 0.92$, with the functional using these parameters being identified as B3P[QCI]. These parameters only gave a small decrease in the DDIs giving only a relative change between 10 and 30% for most molecules which may not be a significant increase. Like the B3P[MP2] functional the comparison of the B3P[QCI] and B3PW91 results used the reference method, that is QCISD, molecular properties as a reference. This time the performance of the new functional, B3P[QCI], dropped off giving relatively poor values. A close look at the results, though, shows some encouraging signs that both the B3P[QCI] and B3P[MP2], electron densities give at least a reasonable qualitative description of their reference densities QCISD and MP2, respectively.

Although the results from these two functionals were relatively poor, it should be remembered that this is just the first attempt to reoptimise parameters through the use of DDI. Improvements can be made in both the fitting technique and also to the functional that is being fitted to allow for more flexibility and hence a better fit of the electron densities. Also, the other properties presented in the previous chapters should help to provide some of the framework for further attempts at functional design. Increasing the use of electron densities in functional design should lead to functionals with increased accuracy.

References

- [1] B. G. Johnson, P. M. W. Gill, and J. A. Pople, *J. Chem. Phys.* **98**, 5612 (1993).
- [2] R. G. Parr and W. Yang, *Density-Functional Theory of Atoms and Molecules*, Oxford University Press, 1989.

-
- [3] C. Møller and M. S. Plesset, *Phys. Rev.* **46**, 618 (1934).
- [4] J. A. Pople, R. Seeger, and R. Krishnan, *Int. J. Quant. Chem. Symp.* **11**, 149 (1977).
- [5] R. Krishnan and J. A. Pople, *Int. J. Quant. Chem.* **14**, 91 (1978).
- [6] R. Krishnan and J. A. Pople, *J. Chem. Phys.* **72**, 4244 (1980).
- [7] J. A. Pople, M. Head-Gordon, and K. Raghavachari, *J. Chem. Phys.* **87**, 5968 (1987).
- [8] J. P. Perdew, J. A. Chevary, S. H. Vosko, K. A. Jackson, M. R. Pederson, D. J. Singh, and C. Fiolhais, *Phys. Rev. B* **46**, 6671 (1992).
- [9] A. D. Becke, *J. Chem. Phys.* **107**, 8554 (1997).
- [10] A. D. Becke, *Phys. Rev. A* **38**, 3098 (1988).
- [11] A. D. Becke, *J. Chem. Phys.* **98**, 5648 (1993).
- [12] C. Lee, W. Yang, and R. G. Parr, *Phys. Rev. B* **37**, 785 (1988).
- [13] J. P. Perdew, *Phys. Rev. B* **33**, 8822 (1986).
- [14] L. A. Curtiss, K. Taghavachari, G. W. Trucks, and J. A. Pople, *J. Chem. Phys.* **94**, 7221 (1991).
- [15] S. D. Wetmore, R. J. Boyd, and L. A. Eriksson, *J. Chem. Phys.* **106**, 7738 (1997).
- [16] S. K. Worsnop, J. Wang, and R. J. Boyd, *J. Chem. Phys.* **107**, 17 (1997).
- [17] A. D. McLean and G. S. Chandler, *J. Chem. Phys.* **72**, 5639 (1980).

- [18] R. Krishnan, J. S. Binkley, R. Seeger, and J. A. Pople. *J. Chem. Phys.* **72**, 650 (1980).
- [19] M. J. Frisch, G. W. Trucks, H. B. Schlegel, P. M. W. Gill, B. G. Johnson, M. A. Robb, J. R. Cheeseman, T. A. Keith, G. A. Petersson, J. A. Montgomery, K. Raghavachari, M. A. Al-Laham, V. G. Zakrzewski, J. V. Ortiz, J. B. Foresman, J. Cioslowski, B. B. Stefanov, A. Nanayakkara, M. Challacombe, C. Peng, P. Y. Ayala, W. Chen, M. W. Wong, J. L. Andres, E. S. Repogle, R. Gomperts, R. L. Martin, D. J. Fox, J. S. Binkley, D. J. DeFrees, J. Baker, J. P. P. Stewart, M. Head-Gordon, C. Gonzalez, and J. A. Pople, *Gaussian 94*, Gaussian, Inc.: Pittsburgh PA, 1995.
- [20] C. Sarasola, J. Elorza, and J. M. Ugalde, *J. Math. Chem.* **23**, 405 (1998).
- [21] G. Herzberg and K. P. Huber, *Molecular Spectra and Molecular Structure IV Constants of Diatomic Molecules*, Van Nostrand Reinhold Company, New York, 1979.
- [22] D. J. Defrees, B. A. Levi, S. K. Pollack, W. J. Hehre, J. S. Binkley, and J. A. Pople, *J. Am. Chem. Soc.* **101**, 4085 (1979).
- [23] S. K. Worsnop, R. J. Boyd, C. Sarasola, and J. M. Ugalde, *J. Chem. Phys.* **108**, 2824 (1997).

8. Conclusion and Future Work

This work has presented an indepth analysis of the electron densities calculated using many different methods. Three different methods were employed to measure many different aspects of these densities focussing, in particular, on the accuracy of the electron densities from density functional theory (DFT) calculated using several different approximate exchange-correlation functionals. The first method, the density difference index (DDI), gave a difference between the DFT densities and high-level electron densities. The spin polarisation index was the second method and was used to measure the difference between the α and β electron densities within an open-shell molecule. The final method yielded the radial moments of the electron density giving spatial information about the calculated electron densities. The observed results gave insights into many aspects of the electron density which led to the reoptimisation of a hybrid functional to try and increase the accuracy of its calculated electron density.

The results from the density difference index (DDI) indicate that it gives a semi-quantitative measure of the differences between two electron densities. The electron densities from many different functionals were reasonably close to the second order Møller-Plesset perturbation (MP2) theory electron density with Becke's three-parameter hybrids having the best results. When these electron densities were com-

pared to the the quadratic configuration interaction method including single and double excitations (QCISD) electron density the DDIs were slightly larger. Comparison of the DFT DDIs to the QCISD-MP2 DDIs indicates that there is not only a quantitative difference between DFT densities and MP2 or QCISD densities but there is a qualitative one as well.

The indication of a qualitative difference between the electron densities as calculated using DFT and those calculated using methods based on the Hartree-Fock (HF) ground state wavefunction led to the investigation of other properties of the electron density. One aspect of the electron density, the spin-polarisation, has proven to be difficult to quantify yet is important in open-shell species. A new method was outlined to try to solve the problem of quantifying this important property, termed the spin-polarisation index (SPI). The SPI results calculated using DFT yield very low values for a small number of open-shell molecules indicating that they did not calculate the spin-polarisation properly for these molecules. For the rest of the molecules the DFT SPIs were in reasonably good agreement with QCISD results. O₂ was one of the molecules where the DFT functionals performed poorly and a further investigation of O₂ electron density was carried out. The radially averaged α - and β -electron densities of O₂ were plotted and two interesting features were observed. The first, exhibited by all methods, was that the β -electron density went through a minimum between the bond midpoint and the oxygen atoms which was not mirrored in the α -electron distribution. The second feature revealed a qualitative difference between the DFT and wavefunction-based electron densities at the bond midpoint. For the former methods the electron densities revealed an excess amount of α -electron density at the bond midpoint, while the latter methods revealed an excess amount of β -electron density is at the bond midpoint.

The observations of the radially averaged α - and β -electron densities of O₂ led to the investigation of other radially averaged properties, specifically the radially averaged moments of the electron density. Obtained from the results of these calculations were insights into the spatial distribution of the electron densities for several methods. Also, by using experimental results the accuracy of electron density distributions could be assessed. The DFT radial moments calculated with several exchange-correlation functionals showed good agreement with the experimental data available and for values which were not available comparison to QCISD results also showed good agreement. Usually, though, the DFT radial moments were too large for all moments which indicates a more expanded electron cloud.¹ Results were also obtained for approximating the effects of solvation with two different methods. Again, the DFT results gave differences which were in very good agreement with the changes in the QCISD moments. The results from the HF based methods which included correlation effects were all quite similar as is expected.

The results from the DDI, SPI and radial moments of the electron density calculations are good indicators of the accuracy of electron densities but should also be of use in improving DFT electron densities. An attempt at using one of these tools, the DDI, in reoptimising the parameters of the Becke three-parameter functional was performed. Fitting the parameters by minimising the DDI values of a series of molecules should produce a functional with an electron density that approximates the reference density used in the DDI calculations. The two functionals found using this method were obtained by fitting the parameters to the MP2 and QCISD densities. Comparing the molecular properties calculated with these two functionals to those calculated with B3PW91 gave poor to fair results. However, there were some encouraging indications that the calculated densities from the two new functionals gave at least a

reasonable qualitative description of the reference densities.

Although the results from the new functionals were discouraging, there were some signs of qualitative similarities between the reference and DFT densities. Further optimisations using more flexible functionals or a more refined fitting technique should yield even more accurate functionals. However, with the information that can be obtained with only these three tools about the qualitative and quantitative differences between electron densities a fitting procedure which utilises two or three of these methods may yield even better fit parameters. This procedure should then produce a functional with an accurate electron density that gives not only correct spin properties but also spatial properties. Ultimately though any new fitting procedure should balance many properties including energetics, geometrical properties, and electron densities.

Fitting techniques, though, are limited to reoptimising preexisting functionals or to being applied to methods such as Becke's systematic optimisation scheme.² To get the most improvement in calculated electron densities functionals must be designed from first principles. With many new methods, such as the Zhao, Morrison and Parr method,³ being proposed there are many opportunities to incorporate the tools presented in this thesis into the design of new functionals.

References

- [1] P. Duffy, D. P. Chong, and M. Dupuis, *J. Chem. Phys.* **102**, 3312 (1995).
- [2] A. D. Becke, *J. Chem. Phys.* **107**, 8554 (1997).
- [3] Q. Zhao, R. C. Morrison, and R. G. Parr, *Phys. Rev. A* **50**, 2138 (1994).